TUNABLE AND DUAL-WAVELENGTH PASSIVE Q-SWITCHED PULSE GENERATION WITH FIBER-OPTIC INTERFEROMETERS

SITI FAZILAH BINTI SHAIK MOHD NOOR

FACULTY OF SCIENCE
UNIVERSITI MALAYA
KUALA LUMPUR

2024

TUNABLE AND DUAL-WAVELENGTH PASSIVE Q-SWITCHED PULSE GENERATION WITH FIBER-OPTIC INTERFEROMETERS

SITI FAZILAH BINTI SHAIK MOHD NOOR

THESIS SUBMITTED IN FULFILMENT OF THE REQUIREMENTS FOR THE DOCTOR OF PHILOSOPHY

DEPARTMENT OF PHYSICS
FACULTY OF SCIENCE
UNIVERSITI MALAYA
KUALA LUMPUR

2024

UNIVERSITY OF MALAYA

ORIGINAL LITERARY WORK DECLARATION

Name of Candidate: **SITI FAZILAH BINTI SHAIK MOHD NOOR**

Matric No: **SVA 17006748**

Name of Degree: **DOCTOR OF PHILOSOPHY**

Title of Project Paper/Research Report/Dissertation/Thesis ("this Work"):

TUNABLE AND DUAL-WAVELENGTH PASSIVE Q-SWITCHED PULSE GENERATION WITH FIBER-OPTIC INTERFEROMETERS

Field of Study: **PHOTONICS**

I do solemnly and sincerely declare that:

1) I am the sole author/writer of this Work;
2) This Work is original;
3) Any use of any work in which copyright exists was done by way of fair dealing and for permitted purposes and any excerpt or extract from, or reference to or reproduction of any copyright work has been disclosed expressly and sufficiently and the title of the Work and its authorship have been acknowledged in this Work;
4) I do not have any actual knowledge nor do I ought reasonably to know that the making of this work constitutes an infringement of any copyright work;
5) I hereby assign all and every rights in the copyright to this Work to the University of Malaya ("UM"), who henceforth shall be owner of the copyright in this Work and that any reproduction or use in any form or by any means whatsoever is prohibited without the written consent of UM having been first had and obtained;
6) I am fully aware that if in the course of making this Work I have infringed any copyright whether intentionally or otherwise, I may be subject to legal action or any other action as may be determined by UM.

Candidate's Signature Date: 28 January 2024

Subscribed and solemnly declared before,

Witness's Signature Date: 28 January 2024

Name:

Designation:

TUNABLE AND DUAL-WAVELENGTH PASSIVE Q-SWITCHED PULSE GENERATION WITH FIBER-OPTIC INTERFEROMETER

ABSTRACT

Tunable and multi-wavelength Q-switched Erbium doped fiber laser (EDFLs) operating in 1.5-micron region have gained tremendous interests in recent years due to their important applications in many areas including material processing, optical communication and biomedical. These lasers are normally realized by using an interference filter in conjunction with saturable absorber (SA). The filter functions to enable tunability and multi-wavelength operation while SA functions to initiate pulses by passive means. Up to date, plenty of works have been reported on developing new SA devices which have a good optical characteristic to produce high performance pulse lasers and on finding new applications for various interference filters. This work was aimed to explore the use of two types of fiber-optic interferometer: sagnac loop mirror (SLM) and single-mode fiber (SMF) – multimode fiber (MMF) – single-mode fiber (SMF) or SMS structure for demonstrating a tunable or dual-wavelength Q-switched EDFL using graphene oxide (GO) and aluminum oxide (Al_2O_3) thin film as SA. Both GO and Al_2O_3, thin films have been successfully fabricated by embedding in PVA thin film and characterized with modulation depths of 24.1% and 3.5 %, respectively. Wavelength tunable Q-switched EDFLs have been successfully demonstrated using the SLM in figure-of-eight laser cavity as a tunable filter and GO or Al_2O_3, thin film as SA. For instance, a stable passively Q-switched EDFL tunable by Sagnac interferometer operation was realized with a GO. By tuning the temperature of SLM from 30°C to 70 °C, the central wavelength of the Q-switched EDFL could be tuned continuously from 1566.3 nm to 1559.3 nm. At 1566.3 nm operation, the maximum repetition rate and minimum pulse width was recorded at 41.5 kHz and 7.3 μs, respectively. A dual-wavelength Q-switched

pulse generation has been successfully demonstrated in an EDFL cavity using GO SA and SMS filter to operate at wavelengths of 1549.6 nm and 1558.6 nm. The maximum pulse repetition rate and the shortest pulse width are obtained at 65.27 kHz and 2.9 μs, respectively. At 225.1 mW pump power, the maximum output power and pulse energy were obtained at 0.99 mW and 15.17 nJ, respectively. This study revealed the promising potential of GO and Al_2O_3 based SA to be used in pulse generation. Both SLM and SMS could also be used as filters for tunable or multi-wavelength laser generation. The fabrication of the SAs and filters are simple, hence reducing the cost of the laser itself. Simple and low-cost fiber lasers are required in various applications including medical diagnostics and environmental sensing.

Keywords: Q-switching, Erbium-doped fiber laser, Sagnac loop mirror, multimode interference, passive saturable absorber

JANAAN LASER DWI PANJANG GELOMBANG DAN LASER SUIS Q PASIF BOLEH LARAS MENGGUNAKAN INTERFEROMETER GENTIAN OPTIK

ABSTRAK

Laser gentian doped Erbium (EDFL) yang boleh ditala dan berbilang panjang gelombang yang beroperasi di rantau 1.5 mikron telah mendapat minat yang luar biasa sejak beberapa tahun kebelakangan ini kerana aplikasi pentingnya dalam banyak bidang termasuk pemprosesan bahan, komunikasi optik dan bioperubatan. Laser ini biasanya direalisasikan dengan menggunakan penapis gangguan bersama-sama dengan penyerap tepu (SA). Penapis berfungsi untuk membolehkan kebolehtalakan dan operasi berbilang panjang gelombang manakala SA berfungsi untuk memulakan denyutan dengan cara pasif. Sehingga kini, banyak kerja telah dilaporkan untuk membangunkan peranti SA baharu yang mempunyai ciri optik yang baik untuk menghasilkan laser nadi berprestasi tinggi dan mencari aplikasi baharu untuk pelbagai penapis gangguan. Kerja ini bertujuan untuk meneroka penggunaan dua jenis interferometer gentian optik: cermin gelung sagnac (SLM) dan gentian mod tunggal (SMF) - gentian mod berbilang (MMF) - gentian mod tunggal (SMF) atau struktur SMS untuk menunjukkan EDFL boleh talar atau dwi-panjang gelombang Q-suis menggunakan filem nipis graphene oxide (GO) dan aluminium oksida (Al_2O_3) sebagai SA. Kedua-dua GO dan Al_2O_3, filem nipis telah berjaya dibuat dengan membenamkan dalam filem nipis PVA dan dicirikan dengan kedalaman modulasi masing-masing 24.1% dan 3.5%. EDFLs suis Q boleh tala panjang gelombang telah berjaya ditunjukkan menggunakan SLM dalam rongga laser angka lapan sebagai penapis boleh tala dan filem nipis GO atau Al_2O_3 sebagai SA. Sebagai contoh, EDFL pasif Q-switched stabil yang boleh ditala oleh operasi interferometer Sagnac telah direalisasikan dengan GO. Dengan menala suhu SLM daripada 30ºC kepada 70ºC, panjang gelombang pusat EDFL yang ditukar-Q boleh ditala secara berterusan daripada

1566.3 nm kepada 1559.3 nm. Pada operasi 1566.3 nm, kadar pengulangan maksimum dan lebar nadi minimum direkodkan pada 41.5 kHz dan 7.3 μs, masing-masing. Penjanaan nadi Q-switched dwi-panjang gelombang telah berjaya ditunjukkan dalam rongga EDFL menggunakan penapis GO SA dan SMS untuk beroperasi pada panjang gelombang 1549.6 nm dan 1558.6 nm. Kadar pengulangan nadi maksimum dan lebar nadi terpendek diperoleh pada 65.27 kHz dan 2.9 μs, masing-masing. Pada kuasa pam 225.1 mW, kuasa keluaran maksimum dan tenaga nadi diperolehi pada 0.99 mW dan 15.17 nJ, masing-masing. Kajian ini mendedahkan potensi menjanjikan SA berasaskan GO dan Al_2O_3 untuk digunakan dalam penjanaan nadi. Kedua-dua SLM dan SMS juga boleh digunakan sebagai penapis untuk penjanaan laser boleh tala atau berbilang panjang gelombang. Pembuatan SA dan penapis adalah mudah, oleh itu mengurangkan kos laser itu sendiri. Laser gentian mudah dan kos rendah diperlukan dalam pelbagai aplikasi termasuk diagnostik perubatan dan penderiaan alam sekitar.

Kata kunci: Q-switching, laser gentian doped Erbium, cermin gelung Sagnac, gangguan pelbagai mod, penyerap tepu pasif

ACKNOWLEDGEMENTS

In the name of Allah, the Most Gracious, the Most Merciful.

Highest praise be to Allah the almighty that I finally able to submit my PhD thesis. As the saying goes, the higher the position, the bigger the challenges. I went through the pandemic season when Covid-19 strikes, something I could have never imagined happening while doing my PhD.

It occurs to me that PhD is not just a process to gain in depth knowledge of the subject matter but also to take into account the management process, working with all levels of people and competency plus making sure that the study process become fruitful in the end.

I would like to take this opportunity to express my appreciation to the first supervisor Professor Ulung Datuk Dr. Harith Ahmad for paving the way for me to be where I am now with all your invaluable knowledge and experience in this field. To another supervisor, Professor Sulaiman wadi Harun, I just cannot thank you enough for being the pillar of strength to all the students when we thought we cannot go on. To my family especially ma and abah, I know how proud you are and I am glad. Love and thank you for everything and for being with me in this beautiful journey called life.

Not forgetting friends and staffs that I encounter along the way and have been very helpful, thank you.

Alhamdulillah..

TABLE OF CONTENT

ABSTRACT…….. iii

ABSTRAK…… v

AKNOWLEDGEMENTS……. vii

TABLE OF CONTENT…… viii

LIST OF FIGURES…….. xi

LIST OF TABLES…… xiv

LIST OF SYMBOLS AND ABBREVIATIONS……. xv

LIST OF APPENDICES..... xix

CHAPTER 1 : INTRODUCTION

1.1 Background of Study…… 20

1.2 Research motivation……. 23

1.3 Problem Statement……... 25

1.4 Research Objectives……. 28

1.5 Scope of Study……. 28

1.6 Significance of study…… 30

1.7 Thesis outline……... 30

CHAPTER 2: LITERATURE REVIEW

2.1 Introduction…….. 32

2.2 Fundamental of Optical Fiber…….. 33

2.3 Fiber Laser……... 36

2.4 Erbium-doped Fiber Laser……... 40

2.5 Q-switching Technique…… 43

2.6 Fiber-optic interferometer…… 48

2.6.1 Sagnac interferometer ……. 48

2.6.2 Singlemode multimode singlemode (SMS) fiber structure-based interferometer…….. 50

2.7 Saturable absorber……... 53

CHAPTER 3: PREPARATION AND CHARACTERIZATION OF FIBER INTERFEROMETER AND SATURABLE ABSORBER

3.1 Introduction…….. 57

3.2 Fiber-optic interferometer…… 58

3.2.1 All-fiber Sagnac Loop Mirror (SLM)…….. 59

3.2.2 Single mode-multimode-single mode (SMS) fiber structure….. 62

3.3 Preparation of saturable absorber (SA)…… 67

3.3.1 Preparation of GO SA…….. 68

3.3.2 Preparation of Al_2O_3 thin film……. 71

3.4 Optical linear and nonlinear characteristics of the prepared SA device.. 73

3.5 Summary…….. 77

CHAPTER 4: Q-SWITCHED TUNABLE FIBER LASER WITH SAGNAC LOOP MIRROR

4.1 Introduction…….. 79

4.2 Passively Q-switched EDFL with Graphene Oxide SA……... 80

4.2.1 Laser configuration……... 81

4.2.2. Q-switched laser performance…….. 83

4.3 Q-switched Tunable Fiber Laser with Aluminum Oxide SA……... 90

4.3.1 Laser Configuration…….. 91

4.3.2 Result and discussion…… 93

4.4 Summary……..100

CHAPTER 5: DUAL-WAVELENGTH Q-SWITCHED ERBIUM-DOPED FIBER LASER USING A SMF–MMF–SMF STRUCTURE AND GRAPHENE OXIDE

5.1 Introduction…….. 101

5.2 Preparation of laser setup……. 102

5.3 Laser performances…….. 105

5.4 Summary…….. 109

CHAPTER 6: CONCLUSION AND FUTURE WORK

6.1 Conclusion..... 110

6.2 Recommendation for future work…….. 113

REFERENCE……..... 116

LIST OF PUBLICATIONS AND PAPERS PRESENTED…….…..... 133

APPENDIX……..... 134

LIST OF FIGURES

Figure 2.1 : (a) The drawing of an optical fiber with its cross-section comprises a core, cladding and polymer jacket. (b) Illustration of TIR in an optical fiber core…….. 34

Figure 2.2 : Light propagation in multimode and single-mode fiber…….. 36

Figure 2.3 : Basic elements of a laser……... 37

Figure 2.4 : Energy level diagram illustrates (a) absorption (b) spontaneous emission and (c) stimulated emission processes……... 39

Figure 2.5 : The energy diagram of Erbium ion, which explain the pumping mechanism and stimulated emission……. 41

Figure 2.6 : Absorption and emission cross sections of Er^{3+} ions ($^4I_{15/2} \rightarrow {}^4I_{13/2}$ and $^4I_{13/2} \rightarrow {}^4I_{15/2}$ transitions) in silica host glass (Babu, P., 2007) …… 42

Figure 2.7 : Evolution of loss, gain, and power on the time scale of pulse width plotted from the numerical integration of the rate equation (Spühler, G.J., 1999)…….. 44

Figure 2.8 : The captured oscilloscope trace from Q-switched fiber laser…… 45

Figure 2.9 : The captured RF spectrum of a Q-switched fiber laser…….. 46

Figure 2.10 : The schematic diagram of an optical fiber Sagnac interferometer ……. 50

Figure 2.11 : (a) Schematic diagram of a traditional SMS fiber structure (Wang, Q., G. Farrell, and W. Yan, 2008 (b) mode distribution along an MMF within a length of 30 mm as calculated by using Eq. (2.21)…….. 53

Figure 2.12 : The illustration of saturable absorption mechanism based on the two-level electronic model (Milani, A., 2019)……..... 55

Figure 2.13 : The illustration of how SA affects light intensity…… 56

Figure 3.1 : Schematic diagram of the proposed SLM……... 60

Figure 3.2 : Experimental setup of the SLM with a PMF as a sensing fiber ……..... 61

Figure 3.3 : The measured input ASE spectrum and transmission spectrum of the SLM…… 61

Figure 3.4 : The measured transmission spectrum at different temperature …….. 62

Figure 3.5 : Schematic diagram of a SMS structure…… 63

Figure 3.6 : The mode distribution along an MMF, which was calculated utilizing Equation (3.5)…… 65

Figure 3.7 : The measured input ASE spectrum and transmission spectrum of the SMS structure…… 66

Figure 3.8 : Transmission spectra of the SMS structure at various temperatures…… 67

Figure 3.9 : Dip wavelength shift vs temperature…….. 67

Figure 3.10 : Illustrations of the electrochemical exfoliation of graphene from graphite rods. (a) providing 20V potential using a DC power supply, (b) graphite rods as cathode and anode immerse in electrolyte, (c) After several minutes where bubbles were observed at the cathode due to the formation of hydrogen gas (d) after two hours of exfoliation process (e) The graphene suspension obtained after the electrochemical process …… 69

Figure 3.11 : (a) The GO PVA thin film obtained after let dry at room temperature (b) EDX profile (c) Raman spectrum (d) The thin film was sandwiched between two ferrules to form a fiber compatible SA device…….. 71

Figure 3.12 : Preparation of Al_2O_3 PVA film…… 72

Figure 3.13 : (a) FESEM image of the Al_2O_3 PVA film, and (b) The image of fabricated film as it was attached onto a fiber ferrule…….. 73

Figure 3.14 : The experimental setup for (a) linear absorption and (b) nonlinear absorption measurement…… 75

Figure 3.15 : Optical properties of the GO PVA film. (a) linear transmission and (b) nonlinear transmission profile……... 76

Figure 3.16 : Optical properties of the Al_2O_3 PVA film. (a) linear absorption (b) nonlinear transmission profile……..... 77

Figure 4.1 : Schematic diagram of the Q-switched EDFL with figure-of-eight cavity and GO SA……. 82

Figure 4.2 : Output spectra of the Q-switched EDFL at various temperature applied to PMF……. 85

Figure 4.3 : Temporal characteristics of the Q-switched laser at operating wavelength of 1566.3 nm (a) typical pulse train (b) enlarged pulse train (c) RF spectrum. Inset of (c) shows the enlarged RF spectrum at the fundamental frequency……. 85

Figure 4.4 : Temporal characteristics of the Q-switched laser at operating wavelength of 1561.4 nm. (a) typical pulse train (b) enlarged pulse train (c) RF spectrum. Inset of (c) shows the enlarged RF spectrum at the fundamental frequency…… 87

Figure 4.5 : Pulse repetition rate and pulse width of the GO based Q-switched EDFL against pump…….. 89

Figure 4.6 : Average output power and pulse energy of the GO based Q-switched EDFL against pump…….. 90

Figure 4.7 : Experimental setup of the tunable Q-switched EDFL with Al_2O_3-PVA SA based on a figure-of-eight cavity arrangement... 92

Figure 4.8 : Output spectrum of the Q-switched laser at different temperature settings for the SLM……. 94

Figure 4.9 : Temporal characteristics at operating wavelength of 1556 nm And pump power of 176 mW (a) typical oscilloscope trace. Inset shows the enlarged pulse train (b) RF spectrum with the inset showing the fundamental frequency in the enlarged RF spectrum…… 95

Figure 4.10 : Temporal and frequency characteristics of the Q-switched laser operating at wavelength of 1568 nm when the pump power was 87 mW (a) typical pulse train. Inset shows the enlarged pulse train (b) RF spectrum within 600 kHz span. Inset shows the fundamental frequency at 26.25 kHz in the enlarged spectrum…… 97

Figure 4.11 : The repetition rate and pulse width performance with the change of pump power for the proposed Al2O3 based laser…… 98

Figure 4.12 : The output power and pulse energy agaist pump power for the proposed Al_2O_3 based laser…….. 99

Figure 5.1 : (a) SMF–MMF–SMF structure and (b) its transmission spectrum …….. 103

Figure 5.2 : Configuration of the dual-wavelength Q-switched laser with GO SA and SMF–MMF–SMF structure…….. 105

Figure 5.3 : Output spectrum of the dual-wavelength Q-switched laser at 225.1 mW pump power…… 106

Figure 5.4 : Typical pulse train at 225.1 mW pump power. The inset shows the enlarged dual-pulse envelop……... 107

Figure 5.5 : RF spectrum at 225.1 mW pump power. The inset shows the fundamental frequency……. 107

Figure 5.6 : Pulse rate and pulse width obtained at different pumping powers …….. 108

Figure 5.7 : Output power and pulse energy obtained at different pumping powers……... 109

LIST OF TABLES

Table 3.1 : Characteristics of both SA thin films…… 78

Table 6.1 : Performance Comparison of passively Q-switched fiber lasers with various SAs…….. 114

LIST OF SYMBOLS AND ABBREVIATIONS

λ	: Operating wavelength
A_{21}	: Probability coefficient of spontaneous emission
AL_G	: Volume of pumped gain medium
B_{12}	: Probability coefficient of absorption
B_m	: Propagation constant of each eigenmode within MMF
ΔT	: Saturable absorption
Er^{3+}	: Erbium ion
F	: Repetition rate
f_1	: Number of electrons in the ground
$g(t)$	: Gain
l	: Total cavity loss per round trip
M	: Total number of eigenmodes LP_{0m}
n_1	: Refractive index (optical fiber)
n_2	: Refractive index (cladding)
Θ_c	: Critical angle
P_p	: Peak power
P_{avg}	: Average laser power
$P(t)$	: Intracavity power
$\rho(h\upsilon)$	: Number of protons with adequate energy
β_m	: Propagation constant of each eigenmode within the multimode fiber
R_{abs}	: Absorption rate
R_{spon}	: Spontaneous emission rate
R_{stim}	: Stimulated emission rate
τ_p	: Pulse width
S_p	: Pulse shape factor

ASE : Amplified spontaneous emission

BBS : Broadband light source

BP : Black phosphorus

CNT : Carbon Nanotubes

CW : Continuous Wave

DI : Deionized water

E : Energy

EDF : Erbium doped fiber

EDFA : Erbium doped fiber amplifiers

EDFL : Erbium doped fiber laser

EDX : Energy Dispersive X-Ray Analysis

E_S (r) : Fundamental guided mode

FESEM : Field Emission Scanning Electron Microscope

FSR : Free spectral range

FWHM : Full width at half maximum

g(t) : Gain

GO : Graphene Oxide

GOSA : Graphene oxide saturable absorber

HiBi : High birefringent

HBF : High birefringent fiber

hν : Photon energy

I : Ion

I : Input intensity

Isat : Saturating intensity

LASER : Light Amplification by Stimulated Emission of Radiation

LIDAR : Light detection and ranging

MIR : Mid-infrared

MMF : Multimode fiber

MMI : Multimode interference

NA : Numerical aperture

NPR : Non-linear polarizing rotating technique

OPM : Optical power meter

OSA : Optical spectrum analyzer

PC : Polarization controller

PCF : Photonic crystal fiber

PD : Photodetector

PVA : Polyvinyl Alcohol

PMF : Polarization maintaining fiber

q_0 : Saturable absorber with bleach '0' unbleached conditions

$q(t)$: Saturable absorber loss coefficient

RFSA : Radio frequency spectrum analyzer

SA : Saturable absorber

SDS : Sodium Dodecyl Sulphate

SESAM : Semiconductor saturable absorber mirror

SLM : Sagnac loop mirror

SMF : Single mode fiber

SMF–MMF–SMF : Single mode fiber–multimode fiber–single mode fiber

SNR : Signal-to-noise ratio

SMS : Singlemode-multimode-singlemode

SPM :

SWCNT : Single-walled carbon nanotubes

T : Optical intensity transmission

T(I) : Transmission rate

TDFL : Thulium-doped fiber laser

TI : Topological insulator

TIR : Total internal reflection

TMD : Transition metal dichalcogenides

TMO : Transition metal oxides

Tns : Non-saturable absorbance

VOA : Variable optical attenuator

WDM : Wavelength division multiplexer

WLS : White light source

YDF : Ytterbium-doped fiber

LIST OF APPENDICES

Appendix A : https://icc.com..... Figure 2.1(a)

Appendix B : https://www.gophotonics.com..... Figure 2.1(b)

Appendix C : https://www.quora.com..... Figure 2.2

Appendix D : https://www.researchgate.net..... Figure 2.3

Appendix E : https://link.springer.com..... Figure 2.4

Appendix F : https://www.researchgate.net..... Figure 2.5

Appendix G : https://www.researchgate.net..... Figure 2.10

Appendix H : https://www.researchgate.net..... Figure 2.11

CHAPTER 1: INTRODUCTION

1.1 Background of Study

Albert Einstein postulates stimulated emission in a centuries-old paper, The Quantum Theory of Radiation (Einstein, 1917). His math suggests an atom in the Planck's oscillator can absorb and spontaneously emit photon so that it can remain at its equilibrium state for a certain amount of time. According to the paper, a stray of photon energy may also stimulate an atom to emit another photon with the same frequency as the first one, the emission of a coherent photon was called stimulated emission. He confirmed the equilibrium state between absorption, spontaneous emission, stimulated emission, and Planck's radiation law in the published manuscript. Hence, upgraded our understanding about the nature of light and revolutionized the field of laser physics, which makes a multitude of technological applications possible such as laser printing, communication, laser nuclear fusion, spectroscopy, optical discs, heat treatment, barcode scanners, and laser cooling. The field of laser physics started when the first practical laser was ignited by Theodore Maiman (1960) . Since then, the development of laser has progressed immensely and the lasers have been used for numerous areas of applications, such as range finder, LIDAR systems (Mizuno, 2017), eye surgery (Sakimoto, 2006), and skin treatment (Goldberg, 1993), to mention just a few. The list of applications is close to endless, but many of them have requirements on whether the laser should be operating in continuous-wave or pulsed regime.

On the other hand, optical fiber is a stable, low-cost, durable, and practical medium for transmitting optical signals. The use of optical fiber for communication was firstly proposed by Charles Kao in 1960s. Due to this great contribution, he received the Nobel Prize in physics in the year of 2009 (Hecht, 2019). As the optical fiber can confine the light propagation along a core area, the optical signals can be transmitted via a total

internal reflection for communication applications. It can travel a long distance with a loss as small as 0.15 dB/km and thus it lay a foundation in the development of fiber laser in 1970s (Shi, 2014). Fiber lasers advanced dramatically in the 1980s, owing primarily to the availability of powerful and dependable laser diodes as well as the advancement of diode-pumped laser technology. They have the advantages of small-weight, compact-structure, and no need for spatial alignment. Therefore, fiber lasers are expected to be new generation of lasers to replace solid-state lasers. They have also been applied in wide areas of applications including materials processing, nonlinear optics, fast medical diagnosis, biomedicine, communication etc (Shi, 2014; Sugioka; Cheng, 2014 & Liu, 2011). The mode operation of fiber laser can be continuous wave (CW) or pulse. A continuous wave (CW) laser light runs continuously with time. The phase and amplitude of the CW laser oscillate randomly which makes it preferable in laser cutting, welding, and manufacturing (Shiner, 2016).

Q-switching is an effective method to produce short pulses. It can be used to produce pulses with pulse duration from microsecond to nanosecond level and repetition rate in kHz regime through the modulation of the Q-factor or loss in the laser cavity. The pulse could be used to promote the interaction between matter and light for various applications including LIDAR, rang finder, laser beauty, and holography (Liu et al., 2011; Goel, 2008). Q-switched fiber lasers can be realized by either active or passive techniques. The active technique uses an acousto-optic or electro-optic modulator to generate pulses by modulating the resonator loss or changing the resonator round-trip phase (Nikodem, 2008).

It necessitates frequent alignments and has significant signal loss between components. On the other hand, the passive technique is based on saturable absorber (SA) device, which is inserted in the laser cavity to generate pulses. The passive techniques are also capable to modulate the resonator loss quicker than the modulator to generate shorter

pulses (Zhang, 2021). Compared to the active Q-switching, the passive approaches are preferable due to their many advantages in terms of cost, simplicity, flexibility, and compactness (Zulkipli, 2020). With a lower cavity loss, this approach also improves the quality of the output pulses. Furthermore, it does not require any alignment.

Up to now, a variety of materials have been proposed and employed as SA such as semiconductor saturable absorber mirror (SESAM) (Okhotnikov et al., 2004), carbon nanotubes (CNT) (Ahmed, 2015), black phosphorus (Chu, 2016), topological insulators (Haris, 2017), and transition metal dichalcogenides (TMDs) (Ahmad et al., 2019). These materials exhibit intensity-dependent transmission and are explored to generate Q-switched pulses at different operating wavelengths in different synthesis methods. SESAMs were the dominant material for Q-switching pulses generation. However, SESAMs have a limited operational bandwidth and complicated fabrication process. A simpler and cost-effective alternative relies on CNTs. However, SWCNTs have a low damage threshold and their operating wavelength depends on the diameters of the nanotube (Choi, 2009). 2D materials such as black phosphorus, topological insulators, and TMDs commonly suffer from low damage threshold and short-term stability that are induced by thermal damage of high optical-power and oxidation, respectively. Therefore, the surge for a new SA material is still ongoing due to certain drawbacks of these materials.

Recently transition metal oxides (TMOs) have been fabricated and investigated as the alternative SAs. TMO nanomaterials such as Fe_3O_4 (Bai, 2016), ZnO (Ahmad, 2016), TiO_2 (Ahmad, 2019) show great advantages for SA applications for having distinguished optical properties such as high optical damage threshold, fast recovery time, wide absorption band and large nonlinearity. Previously, Ahmad et al. produced Q-switching pulses train using zinc oxide (ZnO) nanoparticles based SA in Erbium doped fiber laser (EDFL) cavity (Ahmad, 2016).

On the other hand, the phenomenon of interference of light is employed in many applications including, high precision measuring systems, lasers, and sensors. The optical path can be controlled by optical waveguides and optical fibers. The use of optical fibers allows making such devices extremely compact and economic. To date, different structures of optical fiber interferometers have been reported for various applications. Herein, this work investigated two types of fiber-optic interferometer: sagnac loop mirror (SLM) and SMF–MMF–SMF (SMS) fiber structure. Two new SA devices based on graphene oxide (GO) and aluminum oxide (Al_2O_3) thin film are also fabricated and investigated. In this thesis, new Q-switched EDFLs with tunable output wavelength and dual-wavelength operations are demonstrated using the fiber-optic interferometer as a filter and the newly developed passive SA as a Q-switcher.

1.2 Research Motivation

Q-switched fiber lasers operating at 1.5 μm have attracted huge interest in recent years due to their ability to produce high pulses energy through the modulation of optical losses in the laser cavity. In contrast to mode-locked fiber lasers, the Q-switched fiber lasers are typically able to generate much higher energy. This type of laser is also more favorable from the efficiency, cost, and ease of construction perspectives. Furthermore, dispersion and nonlinearity characteristics need to be balanced in the mode-locked fiber lasers. This can only be achieved by the optimization and careful design of the cavity parameters.

The Q-switched lasers have many potential applications in various fields especially in areas where high pulses duration are important or ultrashort pulses are not required, such as environmental sensing, LIDAR, medical fields, material processing and optical time domain reflectometers (Liu, 2011; Goel, 2008; Adachi et al., 2002). They can be realized by using various approaches including the passive techniques based on saturable

absorbers (SAs). These SAs can be developed for laser generation by using several types of materials and construction techniques.

Throughout the past decades, many types of nanomaterial such as carbon nanotubes (CNTs) (Ahmed, 2015), graphene (Ismail, 2013), transition metal dichalcogenide (TMD) (Ahmad et al., 2019), topological, insulators (TIs) (Chen, 2013), and recently oxides materials have been fabricated and investigated as the alternative SAs. Previously, Aziz et al., (2017) demonstrated a Q-switched EDFL using a ZnO based SA, which was fabricated by embedding a ZnO powder into a poly (vinyl alcohol) film. A small piece of the film is then sandwiched between two fiber ferrules and is incorporated in an EDFL cavity for generating a stable Q-switching pulse train. GO and Al_2O_3 also show great potentials for SA applications due to their distinguished optical properties such as high optical damage threshold, fast recovery time, wide absorption band and large nonlinearity.

The ability to tune the operating wavelength is also important for the Q-switched lasers especially in sensing and communication applications. Tunable lasers are normally realized through a manipulation of the cavity loss and deployment of tunable bandpass filter (Chen, 2003). For instance, wavelength tunable EDFL was reported by controlling the output coupling ratio (Lin, 2006). Recently, a tunable Q-switched EDFL was also reported by using a tunable filter (Wang, 2015). Because of the large insertion losses of this narrow bandwidth filter, the Q-switched pulse was only obtained at the relatively high pump threshold power of 132.4 mW. On the other hand, dual-wavelength fiber lasers have also gained tremendous attentions in recent years for their application in various areas including the generation of Terahertz (THz) signal (Majkić, 2014). The THz radiations bring significant value in various applications such as imaging, sensing, manufacturing, military, spectroscopy, and communication (Bogue, 2018; Mittleman,

2017). The tunable and dual-wavelength laser operation can be realized using an interference filter.

Recently, the fiber Sagnac loop mirror (SLM) and single mode fiber–multimode fiber–single mode fiber (SMF–MMF–SMF) structure have also attracted a great interest due to its promising applications in sensing, fiber lasers and many other areas. For instance, a highly sensitive temperature sensor was demonstrated using an all-fiber Sagnac loop interferometer combined with metal-filled side-hole photonic crystal fiber (PCF) (Reyes et al., 2017). In another work, an optical fiber curvature sensor was demonstrated using a SMF–MMF–SMF (SMS) structure as a sensor probe (Tian, 2017). Compared to other filters, the SLM and SMS structure-based filter have larger thermal damage threshold, simpler structure, and it also opens a promising way for high energy pulse fiber laser generation.

1.3 Problem Statement

Tunable lasers are important in various applications due to their ability to adjust the output wavelength or frequency of the emitted light. This tunability provides several advantages and makes them versatile for different purposes. They allow users to select specific wavelengths, making them valuable in applications where precise control over the spectral characteristics of the light is essential.

This is particularly crucial in fields such as spectroscopy, where different materials or molecules absorb and emit light at specific wavelengths. In optical communication systems, tunable lasers are used to match the wavelength of the transmitted signal with the characteristics of the optical fiber being used. This helps in optimizing data transmission, reducing signal loss, and enhancing overall system performance. In medical applications, tunable lasers are utilized in techniques such as optical coherence tomography (OCT) and fluorescence spectroscopy.

The ability to tune the laser allows for improved imaging resolution and the ability to target specific biological tissues or molecules. In short, the tunability of lasers allows for flexibility and adaptability in addressing the specific requirements of different applications, making them a crucial tool in various scientific, industrial, and medical fields.

On the other hand, numerous multi-wavelength source implementations have been proposed, each presenting its unique set of advantages and drawbacks. In broad terms, practicality, reliability, and precision emerge as paramount considerations. This entails not only stability concerning peak powers and emission wavelengths but also simplicity in terms of implementation or design. Ultimately, as these sources are typically geared towards commercial availability, a preference is given to solutions that offer cost-effectiveness.

Previous implementations have explored a range of technologies, including both incoherent spectra sliced broadband sources, such as light-emitting diodes (LEDs) and amplified spontaneous emissions (ASE), as well as coherent Raman lasers, Erbium-doped fiber (EDF) lasers, and semiconductor fiber lasers (SFL). EDF amplifiers stand out for their cost-effectiveness, yet their limitations in achieving multi-wavelength lasing, especially when used as a gain medium in a fiber laser, can pose challenges.

Numerous articles highlight the issues associated with the homogeneous broadening of the EDF gain medium, hindering or complicating the attainment of multi-wavelength lasing. On the other hand, Raman and semiconductor optical amplifiers (SOA) serve as compelling gain media due to their broader bandwidths and the flexibility to emit in various bands, not confined to C- or L-bands.

Semiconductor amplifiers, being more compact, offer advantages, while their inhomogeneous broadened gain spectrum allows multiple wavelengths to emit concurrently within a laser cavity at room temperature, akin to Raman amplifiers.

However, SOAs may exhibit slightly greater susceptibility to power fluctuations. To address this, the use of linear optical amplifiers (LOAs) has been proposed for dynamic wavelength-division multiplexing (WDM) systems, paving the way for potential future advancements.

Whether opting for a coherent laser or an incoherent source implementation, a mechanism for generating multiple wavelength peaks is imperative. Broadband sources can be spectrum-sliced using various techniques, while gain mediums like amplifiers positioned within a fiber ring configuration, for instance, can coherently emit at multiple wavelengths with the insertion of a multi-wavelength comb filter inside the ring cavity. A diverse array of spectrum-slicing methods and comb filters has been proposed, all functioning similarly and relying on technologies such as fiber Fabry-Perot filters, Michelson and delayed interferometers, arrayed waveguide gratings, fiber Bragg gratings (FBG), and high birefringence fiber loop mirrors (HiBi-FLM).

Regardless of the chosen method, the resulting source must exhibit high contrasts and output powers, a flat or well-apodised emission spectrum if desired, be minimally susceptible to environmental perturbations, and provide the maximum number of peak wavelengths to ensure the multi-wavelength source is compelling for future applications.

Various techniques have been proposed to dynamically alter the output spectrum of the source, encompassing adjustments to individual wavelengths, their corresponding powers, and the capability to uniformly control the wavelength separation between peaks. Tunability can manifest as continuous or discrete, with a preference for a uniform, equispaced change in wavelength spacing, coupled with low complexity and user-friendly operation. In the case of interferometer-based filtering, for instance, the capacity to vary the induced phase shift in one arm facilitates changes in the phase difference, thereby adjusting the wavelength spacing of the generated comb filter.

Consequently, each filtering implementation can be endowed with tunability. In general, the greater the tunability of the source, the more compelling the technique becomes for future applications requiring diverse sets of output spectra.

1.4 Research Objectives

This thesis aims to demonstrate a tunable and dual-wavelength Q-switched fiber laser using a fiber-optic interferometer as a filter and passive saturable absorber (SA) as a Q-switcher. Two types of fiber-optic interferometer are explored in this study: sagnac loop mirror (SLM) and SMF–MMF–SMF (SMS) fiber structure. This work also unveils the optical properties of the newly fabricated SAs based on GO and Al_2O_3 thin film. The objectives of this work are stated, as follows.

1. To develop comb filter for laser tuning. Two fiber optic interferometers: SLM and a SMS fiber structure are evaluated in this work.
2. To fabricate and characterize SA device for Q-switching. Two types of SA based on GO and Al_2O_3 thin film are explored in this work.
3. To demonstrate tunable Q-switched EDFL based on temperature tuning of SLM in figure-of-eight laser configuration.
4. To demonstrate a dual-wavelength Q-switched fiber laser operation by using a SMS structure and graphene oxide as filter and SA, respectively.

1.5 Scope of Study

This thesis aims to demonstrate a tunable and dual-wavelength Q-switched fiber laser using a fiber-optic interferometer as a filter and passive saturable absorber (SA) as a Q-switcher. The laser cavity is constructed using an Erbium-doped fiber (EDF) as the gain medium and thus it operates in 1550 nm region. At first, CW laser is obtained in this work by a ring cavity of EDFL without the implementation of the SA device. The developed

EDFL cavity is shown to be able to generate a stable CW laser, which is workable in the 1.55-μm region.

Two fiber optic interferometers: SLM and SMS fiber structure are explored in this study to function as an interference filter. SLM was fabricated by using a 3dB fiber coupler and a fiber loop with PMF. It allows two beams to propagate in counter directions with different polarization states to produce interference, which is sensitive to the change in surrounding temperature. A SMS fiber structure consists of a short section of MMF, which was fusion- spliced between two SMFs. The mechanism underpinning the operation of an SMS fiber structure is multimode interference and associated self-imaging. SMS structure is also tested for temperature sensing.

Up-to-date, various SA materials are implements in the EDFL, all aimed to improve its optical properties and pulse laser performance. However, most of the SA undergone a tedious preparation procedure. Thus, two SAs based on GO and Al_2O_3 PVA thin films are explored in this work. Both SAs have favorable optical properties, and simple preparation procedure. The thin films are fabricated using a simple drop and dry approach and characterized to investigate both linear and nonlinear characteristics. The optical characterization results indicate the potentiality of these SAs to be used in pulse generation. The fabrication cost of both SAs is cheap due to the simplicity of the fabrication process, hence reducing the cost of the laser itself.

A tunable Q-switched EDFL is then demonstrated based on temperature tuning of SLM in figure-of-eight laser configuration. using the newly developed passive SA film as a Q-switcher. A dual-wavelength Q-switched pulse generation is also demonstrated in an EDFL cavity using a SMF–MMF–SMF structure-based filter and GO SA. The SA functions to modulate the cavity loss for Q-switching while the MMI filter responsible for dual-wavelength operation.

1.6 Significance of study

Development of pulsed fiber laser utilizing passive saturable absorbers have given many contributions in occupying the demands of low-cost compact fiber laser with simple design of laser cavity, high repetition rate and narrow pulse width. This study would be beneficial to other researcher in understanding the construction of passively Q-switched fiber lasers-based nanomaterial saturable absorbers. Dual-wavelength fiber lasers have gained tremendous attentions in recent years for their application in various areas including the generation of Terahertz (THz) signal. The THz radiations bring significant value in various applications such as imaging, sensing, manufacturing, military, spectroscopy, and communication. Step by step with detailed explanations were briefly discussed in this whole thesis structured. Researcher may vary the type of material used in their research work by improvising the use of our techniques.

1.7 Thesis outline

This thesis is structured in six chapters including this introductory chapter and conclusion. Chapter 1 briefly describes the background of this study and explains why it is worth to expand the current work on this field. The motivation of this thesis is also elaborated, together with the important of the Q-switched fiber laser for various applications. This section also states the significance and scope of the study.

The thorough literature review is presented in Chapter 2. At first, optical fiber and fiber lasers are introduced, and their working principles are explained. The working principle of EDFL, the basic concept of Q-switching technique, and saturable absorber are discussed in this chapter. The working principle and application of various interference filters are also discussed in this chapter.

In Chapter 3, the construction method and operating principles of SLM and SMS structure are described. The fabrication and characterization of two types of SA are also

presented in this chapter. Two types of SA are explored in this study: graphene oxide and aluminum oxide (Al_2O_3) thin film.

In Chapter 4, a tunable Q-switched EDFL is proposed and demonstrated based on temperature tuning of SLM in figure-of-eight laser configuration. using the newly developed passive SA film as a Q-switcher.

Chapter 5 reports on a dual-wavelength Q-switched fiber laser operation using a SMS structure and GO as filter and SA, respectively. The SA functions to modulate the cavity loss for Q-switching while the SMS filter responsible for dual-wavelength operation.

Chapter 6 summarizes and concludes the finding of this study. Future works are also suggested in this chapter.

CHAPTER 2: LITERATURE REVIEW

2.1 Introduction

Optical fiber serves as a device for signal channeling due to its ability to transmit light over a long distance. When a group of photons travels along its cylindrical waveguide, the light propagated through the fiber with almost negligible loss based on so-called total internal reflection (TIR) principle. This makes the optical fiber useful for many device applications including fiber laser, optical sensor, optical modulator, etc. In this regard, the potential of optical fiber doped with erbium ion (Er^{3+}) as an active gain medium is investigated. This quasi-three-level laser system provides emission at the telecom band, which is essential for a multitude of research and industrial applications. Erbium-doped fiber lasers (EDFLs) have been the focal point of significant research efforts due to their potential to be deployed in many scientific and industrial fields, occupying a large share of the commercial laser market. Fiber lasers can be divided into two types depending on the mode of operation: continuous and pulsed.

The pulsed fiber laser has high pulse energy and short pulse width, greatly expanding the application of lasers in fiber optic communication, automotive manufacturing, laser cutting, medical devices, and other fields. Q-switching is one of the techniques enabling pulsed laser, which can be implemented actively or passively. The passive approach has gained increasing interest in the last few years due to its simplicity, flexibility, compactness, and low manufacturing cost. Unlike the active approach, the passive one does not rely on bulky and complex optical modulators and electronic drivers, which can achieve laser pulse output simply by placing a saturable absorber (SA) in the resonant cavity. Therefore, the SA plays a crucial role in the passive Q-switched lasers. It is worth mentioned that the Q-switching performance is comparable to the previous work mostly on fixed wavelength and not much literature on tunable laser.

This thesis aims to demonstrate a tunable and dual-wavelength Q-switched fiber laser using a fiber-optic interferometer as a filter and passive saturable absorber (SA) as a Q-switcher. This chapter presents a thorough literature review on fiber lasers. The fundamental principle of optical fiber, the working principle of Erbium-doped fiber laser, the basic concept of Q-switching technique, and saturable absorber are discussed in this chapter. The working principle and application of various interference filters are also discussed in this chapter.

2.2 Fundamental of Optical Fiber

An optical fiber is a silica-based cylindrical waveguide, which has considerably high advantages over the conventional metallic conductor as a medium for signal transmission. It has a transmission loss of less than 0.2 dB/km (Csencsits, 1988), which equivalent to more than 98 % transmission efficiency, making it the most powerful tool for signal transmission. Furthermore, an optical fiber system is immune to the external radiation or electromagnetic interference. Optical fiber guided the light in a small core surrounded by the silica-made cladding, and a plastic protective layer, as depicted in Figure 2.1 (a). The diameter and dimensions of the three main compositions of fiber vary according to optical fiber types. A physical phenomenon known as a total internal reflection (TIR) allows the light to propagate through the waveguide effectively. The bizarre mechanism of TIR is established based on the refractive index difference between the cladding and core. As the light passes from a denser (core) to a less dense medium (cladding) at an angle greater than the critical angle, it allows nearly 100% of light to reflect inside the fiber. Normally, the optical fiber core owns a refractive index of n_1=1.4492, while the cladding has a refractive index of n_2=1.4440.

The TIR mechanism can be explained based on illustration in Figure 2.1 (b). A critical angle (Θ_c) is an angle of incidence with a 90° angle of refraction, which is derived based on the Snell-Descartes' law. First, let the refractive index of the core be n_1, and its

incidence angle be Θ_1. Then, the refractive index of the cladding is n_2 with Θ_2 as its angle of refraction, as shown in Figure 2.2. The derivation is as follows:

$$n_1 \sin\theta_1 = n_2 \sin\theta_2 \quad (2.1)$$

By substituting Θ_2 with 90°, the angle of incidence is the critical angle ($\Theta_1 = \Theta_c$). Thus Equation (2.1) becomes

$$n_1 \sin\theta_c = n_2 \sin(90°) \quad (2.2)$$

$$\sin\theta_c = \frac{n_2}{n_1} \quad (2.3)$$

Finally, n_1 and n_2 are substituted with the refractive index of core and cladding, respectively. The value of Θ_c is calculated as follows:

$$\theta_c = \sin^{-1}\frac{1.4440}{1.4492} \quad (2.4)$$

$$\theta_c = 85.14^\circ \quad (2.5)$$

Therefore, to establish the so-called TIR conditions, the angle of incidence must be greater than the calculated value of Θ_c, allowing the light to totally reflects from the cladding even if it is transparent.

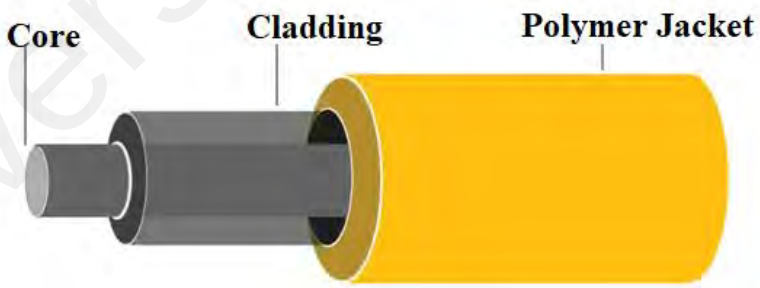

(a)

Figure 2.1, continued.

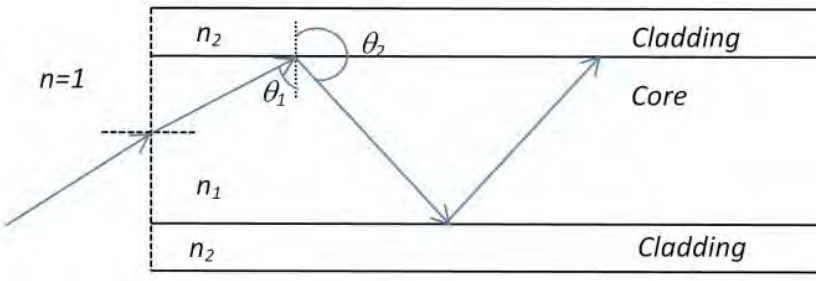

(b)

Figure 2.1: (a) The drawing of an optical fiber with its cross-section comprises a core, cladding and polymer jacket. (b) Illustration of TIR in an optical fiber core.

Optical fibers are classified based on the way light propagates through it, which is related to the diameter of its two main components (cladding and core). Figure 2.2 compares the light propagation in single mode and multimode fiber. A multimode fiber allows signals to transmit along different paths of multiple modes, while only one mode of light travels inside a single-mode fiber. This is attributed to size of the core, which is significantly larger in multimode fiber compared with the single-mode fiber. Compared to the multimode fiber, the single-mode fiber provides significantly higher bandwidth and lower attenuation. The structure of its reduced core diameter (around 9 μm) makes light propagate in one mode of propagation and eliminates the modal dispersion; this makes the single mode fiber favorable in the communication system. This fiber's ability to carry signals in its core is as high as 100 Gbit/s, the introduction of a dispersion compensating device has allowed a long-distance signal channeling in its core (Chraplyvy & R. Tkach, 1993). The optical fiber capacity may be enhanced by injecting multiple signals with different wavelengths into one fiber, by using wavelength division multiplexer.

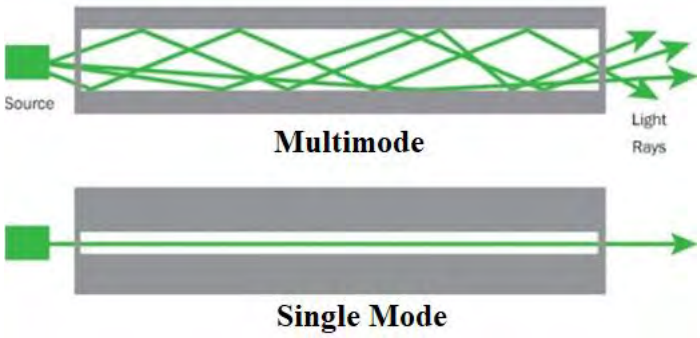

Figure 2.2: Light propagation in multimode and single-mode fiber

2.3 Fiber Laser

The laser was firstly proposed by Schawlow and Townes in 1958 when they described the principle of "Optical Maser'. The laser is essentially an optical amplifier with optical feedback. The word of LASER stands for Light Amplification by Stimulated Emission of Radiation (Tünnermann et al., 2010).

It works based on the principle of stimulated emission. It is the process by which an incoming photon of a specific wavelength or energy can interact with an excited atomic electron (or other excited molecular state), causing it to drop to a lower energy level and generate two identical photons. Towards better understand how fiber lasers work, it is convenient to explain the basic of a basic laser structure. Lasers are come in a great variety of forms by using many different of materials, many different of atomic system and many different kind of excitation techniques (pumping source). Nevertheless, every laser comprises three essential elements: active medium (the medium of the laser), energy source (pumping) and optical feedback (resonator) as shown in Figure 2.3.

The active medium could be gas (such as HeNe or CO_2), liquid (such as dye), solid crystal (such as Nd:YAG and Ruby) or semiconductor (such as InGaAs and GaAs). It contains atoms which can absorb light to excite atoms to higher energy levels to allow population inversion and provides amplification via stimulated emission. The choice of medium materials affects the emission wavelength. The second component is the energy source, which pumps the active atoms from ground state to excited state to achieve

population inversion. Pumping can be performed either electrically or optically depending on the active medium. The third element is the resonator that provides feedback for the light generated inside the medium. At each end of the active medium there is a mirror. At least one must be partially reflective to allow the coherent light to be emitted.

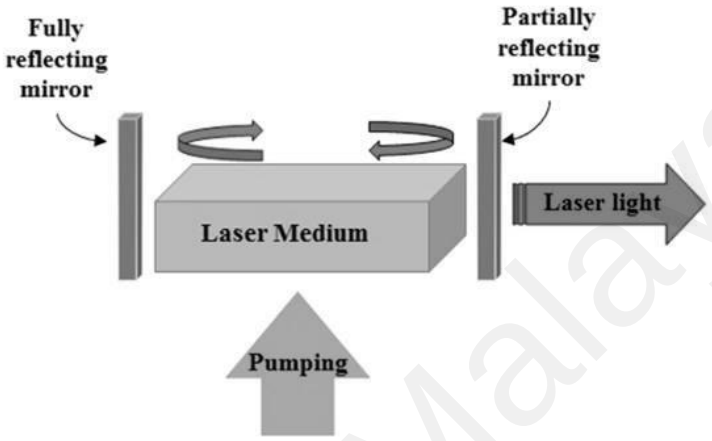

Figure 2.3: Basic elements of a laser

The first fiber laser was invented by Elias Snitzer in 1963 (Snitzer, 1966). However, it took almost another two decades of development before the fiber lasers are ready for commercial production. The first fiber laser devices appeared in market in the late 1980s and these lasers use a single mode fiber as a pumping source that can produce output power at a few tens of milliwats (Tünnermann at al., 2010). Currently, many developments have been focused on fiber lasers due to their advantages over other class of lasers in term of performance, functionality, and practically. It is also interesting to see that the advances in fiber-optic technology have revolutionized the laser technology especially in communication and medical fields. Optical fiber technology was conceived as a superior alternative to conventional copper cables in telecommunications applications.

The operation and configuration of the laser is much more stable by utilizing a fiber laser. The revolution of fiber laser continued with the variation of rare earth elements such as erbium, ytterbium, and neodymium. The function of rare earth elements in laser cavity act as an active ion which is provide the energy level in the laser system. For instance, Erbium is one of the rare earth elements that have attracted many researchers to develop a practical fiber laser operating at 1.5-micron region. Other rare-earth elements that also attracted researcher are Ytterbium and Thulium which can operate at 1 micron and 2-micron region, respectively (Sotor, 2015 & Soltanian, 2015).

Figure 2.4 shows three possible processes that can occur between a two-level system (ground and excited state) when there is an interaction between a photon and matter. The processes are absorption, spontaneous emission, and stimulated emission. In the case of absorption, an electron occupying a ground state (E_1) absorbs a photon that has an energy equal to (E_2-E_1= hν); hence, the electron will move to an empty state in the upper energy level (E_2). The absorption rate (R_{abs}) depends on the number of photons with adequate energy ρ (hν), number of electrons in the ground f_1 and the number of empty states in the upper energy level $(1 - f_2)$. It can be presented by the following equation:

$$R_{abs} = B_{12} f_1 (1 - f_2) \rho (h\nu) \tag{2.6}$$

where B_{12} is a probability coefficient of absorption. A spontaneous emission occurs when an electron occupying an energy state in the upper-level falls to the ground level spontaneously and releases a photon with energy equal to (E_2-E_1= hν). The phase and the direction of the photons that are produced in this process are random. The spontaneous emission rate (R_{spon}) is only controlled by the number of electrons in the upper energy level f_2 and the available empty states in the lower energy level $(1 - f_1)$, as given in the equation below:

$$R_{spon} = A_{21} f_2 (1 - f_1) \tag{2.7}$$

where A_{21} is a probability coefficient of the spontaneous emission. It is important here to mention that electrons can fall to a lower energy state via non-radiative processes.

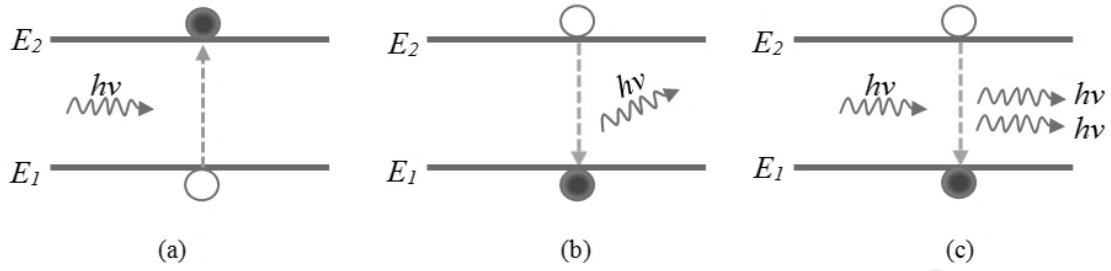

Figure 2.4: Energy level diagram illustrates (a) absorption (b) spontaneous emission and (c) stimulated emission processes.

Stimulated emission occurs when an incoming photon with energy equal to (E_2-E_1= hν*)* disturbs an electron occupying an energy state in the upper level and releases another photon with the same energy (E_2-E_1= hν); moreover, the produced photon has the same phase as the incident photon and travels in the same direction. The stimulated emission rate (R_{stim}*)* is therefore controlled by the number of electrons in the upper energy level f_2, the available empty states in the lower energy level (1 - f_1) and the photon density, as given below:

$$R_{stim} = B_{21}(1 - f_1) f_2 \rho(h\nu) \tag{2.8}$$

where B_{21} is a probability coefficient of the stimulated emission. In equilibrium conditions the absorption rate must balance the emission rates, so:

$$R_{abs} = R_{spon} + R_{stim} \tag{2.9}$$

The rate of downward transitions is equal to the rate of the upward transitions. And it can be shown that $B_{21} = B_{12}$. The laser produces a coherent ray by allowing stimulated emission to dominate over absorption and spontaneous emission. Consequently, this means there must be more populations in the upper state than the ground state and this condition in referred to “population inversion”.

2.4 Erbium-doped Fiber Laser

Erbium-doped fiber lasers (EDFLs) are contemporary sources of coherent radiation which operate in the telecommunication regions covering a wide wavelength range from 1520 nm to 1620 nm. They used an Erbium-doped fiber (EDF), which can be pumped with compact, efficient, and inexpensive 980 nm or 1480 nm laser diodes as the gain medium. EDFs are the fundamental building elements of fiber-optic amplifiers, specifically Erbium-doped fiber amplifiers (EDFAs), which are utilised in long-haul communication systems. When the EDFs are optically pumped with 980 nm or 1480 nm laser diode, they can produce laser amplification via stimulated emission process. By integrating the feedback element into the EDFA, the device can be transformed to a laser device (EDFL) for generating laser at 1.55 μm wavelength region. EDFLs have many benefits including broad wavelength tunability, superior beam quality, small size and low cost.

This thesis focuses on EDFL generation operating in 1.5-micron region whereby the erbium ion, E_r^{3+} is used as an active-dopant for the gain medium. The EDF uses silicate glass as a host material. 980 nm laser diode is used as pumping source in this work because of its efficiency, which is higher compared to other pumping wavelengths. It can reduce the power consumption and the generation of heat thus the cooling system can be eliminated. The beam quality also improved due to weaker of thermal effect.

The working principle of the EDF laser (EDFL) can be explained by using the energy diagram of erbium ions as shown in Figure 2.5. The manifolds of E_1, E_2, and E_3 are corresponded to the energy at ground level, metastable state, and excited state, respectively. As seen, the Er^{3+} ions are excited to a short lifetime excited state as the EDF is pumped by 980 nm laser diode. Then, the Er^{3+} ions are non-radiatively decayed to the long lifetime intermediate state or metastable state, E_2 by emitting the phonons due to the lattice vibration. The Er^{3+} ions at E_2 have a long lifetime ~ 10 ms. Thus, more E^{3+} ions

are accumulated at E_2 which eventually lead a population inversion between E_2 and E_1. Then, the E^{3+} ion spontaneously decayed from E_2 to E_1 by emitting a random photon within the 1525-1565nm band via spontaneous emission (Ngo, 2018). If the light energy already exists within the 1525-1565 nm band, for example due to a signal channel passing through the EDF, then this stimulates the decay process (so called stimulated emission), resulting in additional light energy. Thus, if a pump wavelength and a signal wavelength are simultaneously propagating through an EDF, energy transfer will occur via the erbium from the pump wavelength to the signal wavelength, resulting in signal amplification. In a laser cavity, the amplified spontaneous emission (ASE) light is forced to oscillate and generate laser at 1550 nm region.

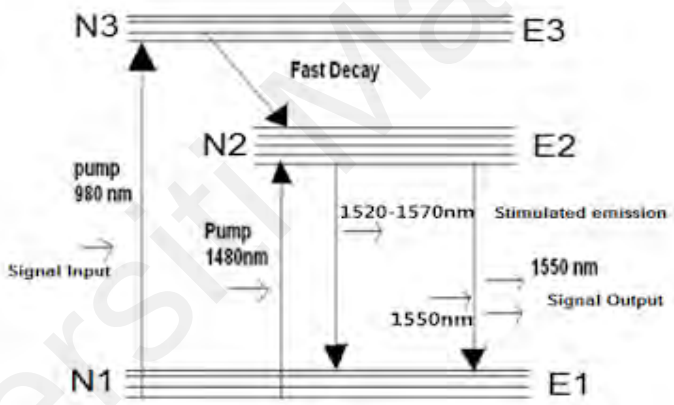

Figure 2.5: The energy diagram of Erbium ion, which explain the pumping mechanism and stimulated emission.

Figure 2.6 illustrates the emission and absorption spectra of Er^{3+} ions at the $^4I_{13/2} \rightarrow {}^4I_{15/2}$ transition, which represents the strong line for zero-phonon vibration. The luminescence span from 1450 to 1650 nm. EDFLs are attractive for numerous applications requiring both continuous-wave (CW) and pulsed operations. Pulsed operation, presenting big interest for practice, can be accomplished in EDFLs by using either active or passive Q-switching and mode-locking techniques. For instance, Q-switching technique can enforce a laser to generate short pulses with durations ranged from microsecond to nanosecond regime.

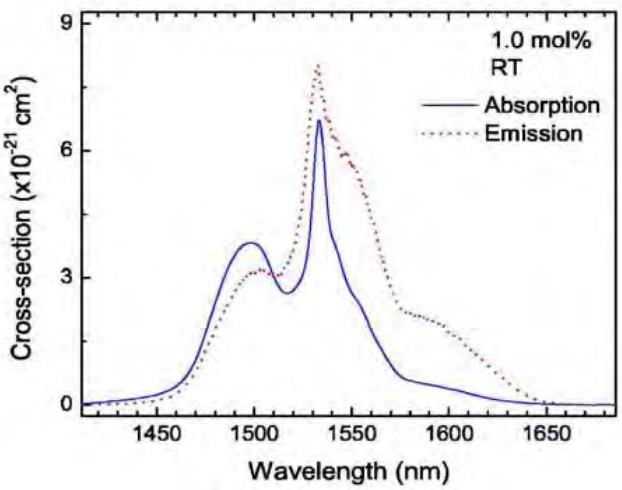

Figure 2.6: Absorption and emission cross sections of Er^{3+} ions ($^4I_{15/2} \rightarrow {}^4I_{13/2}$ and $^4I_{13/2} \rightarrow {}^4I_{15/2}$ transitions) in silica host glass (Babu, 2007).

Over the years, numerous efforts have been made by scientists around the world to produce reliable and powerful pulsed lasers for a multitude of industrial and scientific applications (Addanki et al., 2018 & Dubey et al., 2008). In the past few decades, the pulsed laser produced is mainly based on a bulk solid-state gain medium (Keller, 2003). However, the limitations of this laser bring the research on another type of laser based on rare-earth doped fiber such as EDF as the gain medium.

The fiber laser employs a passive saturable absorber (SA) for generating pulses train. The problem of bulky, alignment-dependent set up, and expensive maintenance operation has been successfully overcome by the deployment of the fiber laser with passive SA. Conventionally, the pulse generation in fiber laser is normally achieved using semiconductor saturable absorber mirrors (SESAMs) as the SA (Keller, 1996), (Bonaccorso et al., 2014). In addition, the fiber laser is proven better than the conventional bulk laser as it covers a wider operating bandwidth (ranging from 1 to mid-infrared wavelength region). An EDFL is the most widely investigated fiber laser. It operates at a 1.55 μm regime and thus is suitable for telecommunication applications.

2.5 Q-switching Technique

Pulse generation in the nanosecond to microsecond time domain is realized by controlling the intracavity losses in a laser resonator. This method is also known as a Q-factor modulation or Q-switching technique with the production of a few hundred nanojoule energy. Q-factor generally refers to the strength of the resonator modes damping while in the energy storage term, it is the ratio between energy stored and dissipated energy in one complete oscillation (Paschotta, 2008). However, the term became slightly different in lasing with two significant characteristics, which are the round-trip losses and a laser gain to compensate for the loss during continuous-wave operation.

The mechanism of Q-switching starts by pumping the gain medium to keep the resonator losses high (low Q-factor), this simultaneously avoids the energy to be extracted from the resonator. Then, the Q-factor is increased which is the result of a higher gain compared to resonator losses. As such, the intracavity power rises exponentially until the power drops and the gain saturates. The generated light energy produced from this process originates from the energy stored in a gain medium. Therefore, gain medium plays a significant role in producing a Q-switched laser with high pulse energy. A few factors that needed attention when selecting a gain medium are high laser-active ions population, slow upper-state lifetime, and moderate gain efficiency. This is important, since a high-efficiency gain medium may trigger an excessive amplified spontaneous emission which in turn limits the initial loss and energy stored of Q-switch laser.

For a better understanding of Q-switched laser operation, let consider the following mechanism. Figure 2.7 shows the single pulse energy of Q-switched laser. First, consider a saturable absorber with bleach '0', unbleached conditions 'q_0', saturable absorber loss coefficient ‘q(t)’, and total cavity loss per round trip ‘l’. Refer to phase 1 of Figure 2.4, when the total cavity loss (low Q) and gain are the same, the pulse will emerge at the

saturable absorber unbleached conditions. Then, as the laser intensity increase, the gain starts to bleach the absorber. This instantly promotes the increment of intracavity power P(t) when the gain g(t) becomes similar to l, thus saturates the absorber and allowing it to grow significantly.

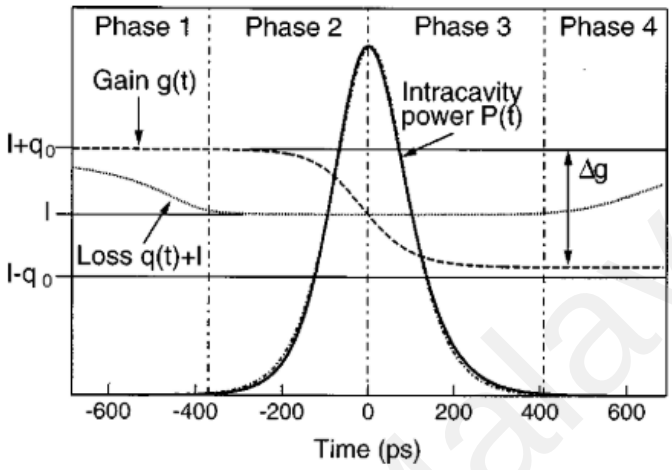

Figure 2.7: Evolution of loss, gain, and power on the time scale of pulse width plotted from the numerical integration of the rate equation (Spühler, 1999).

At phase 2, upon increasing the pump power, the absorber becomes fully bleach when the gain is kept at high Q. Further, the gain is depleted to the loss level of q(t) + l. When the gain g(t) is equal to the total cavity loss l at the bleach condition, the maximum pulse is obtained. Later at phase 3, the gain continues to decrease and eventually reaches the negative value, this leads to the decrease in the intracavity power P(t). In the last phase, which is phase 4, the absorber is restored to its unbleached states attributed to the shorter recovery time of the absorber in comparison to the gain. Then, the pumped gain medium will continue to provide gain to the laser, which allows the next cycle of pulse to starts. The gain medium stored the source of energy for the entire lasing operation, which is expressed by the following expression,

$$E_{stored} = AL_G N_2 h\nu_1 \tag{2.10}$$

where hv_1 is a photon energy at the pumping wavelength, N_2 is the excitation energy in the gain medium, and AL_G is the volume of pumped gain medium.

Repetition rate is defined as how many pulses are formed per second or simply an inverse of pulses' time interval. In a passively Q-switched fiber laser, the repetition rate is usually in the range of 1 to 100 kHz. However, a few works have successfully achieved Q-switched with a repetition rate of more than 100 kHz (Sobon, 2012 & Wang, 2019). This leads to the formation of a pulsed laser that produces a high pulse energy operation. The repetition rate is a laser parameter that depends on the optical intensity of the laser diode pump. Upon increasing the pump power, the repetition rate increase, however, it is limited to the maximum value that the laser diode can achieve. This limit varies according to the laser diode pump and controller. Figure 2.8 shows the method to measure the pulse's repetition rate of a passively Q-switched laser.

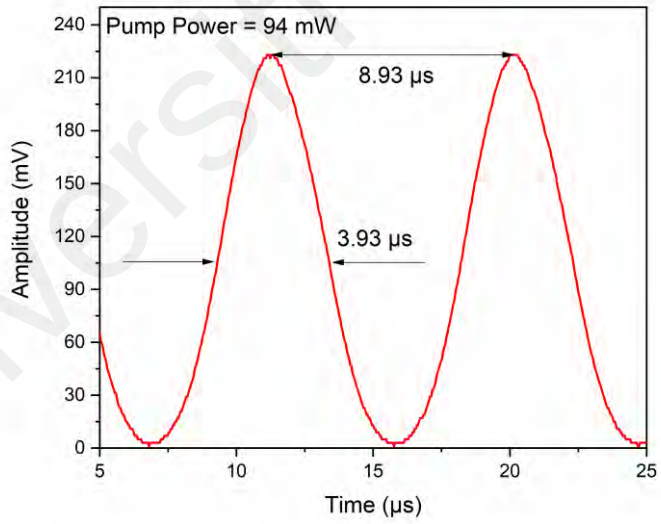

Figure 2.8: The captured oscilloscope trace from Q-switched fiber laser.

The pulse period or interval between two consecutive pulses (T) measured is 8.93 µs, based on the following expression, the value of repetition rate can be obtained.

$$f = \frac{1}{T} \tag{2.11}$$

The captured series of pulses owns a repetition rate, *f* of 112 kHz. One can verify the stability of the generated pulses by measuring the frequency domain of such a laser using a radio frequency spectrum analyzer. In a Q-switched laser, the spectrum will consist of a series of peaks with different heights as shown in Figure 2.9. As seen in the figure, the peaks become shorter as the frequency span increase. This is typical Q-switching behavior. An important parameter that determines the pulse's stability is a signal-to-noise ratio (SNR). It can be defined as the distance between the peak and the floor of the fundamental peak (the first peak on the spectrum).

For a passively Q-switched operation, the value above 30 dB indicates that the laser is stable. This is closely related to the suppression of noise in a laser cavity and the pulses' resonant relaxation oscillation frequency (Yue, 2013). Note that the repetition rate of the fundamental peak must match the calculated repetition rate from equation (2.11).

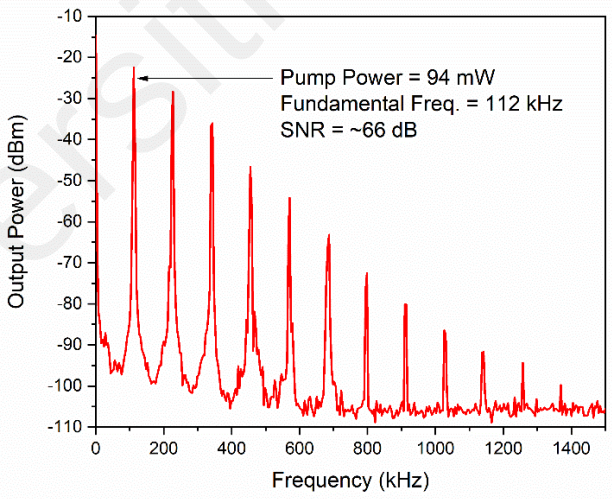

Figure 2.9: The captured RF spectrum of a Q-switched fiber laser.

Pulse width is the measure of how broad a single pulse is, by measuring the width of the pulse at half the intensity. It can also be referred to as a full width at half maximum (FWHM). Refer to Figure 2.8 for the measurement of a pulse width based on a captured oscilloscope trace. Usually, the pulse width is around a few nanoseconds to microseconds

for a Q-switched laser (Salam, 2019). In a typical Q-switched operation, the pulse width decreases with the increase in pump power. The following expression yields the relationship between pulse width (τ_p), laser cavity, and saturable absorption properties,

$$\tau_p = \frac{S_p T_r}{q_0}\left[\frac{\delta(1+\delta)\eta}{\Delta - \ln(1+\delta)}\right] \quad (2.12)$$

where S_p or the pulse shape factor is approximately 0.88, T_r is the cavity's round-trip time, q_o is the cavity loss, Δ is the modulation depth, η is the energy extraction efficiency, and δ is the ratio of saturable to non-saturable loss. Therefore, the following assumptions can be obtained, where the pulse width is proportional to the round-trip time of cavity and inversely proportional to the saturable loss of a material (saturable absorber).

When measuring the power-dependent laser performance of Q-switched, the optical intensity is adjusted from the lowest possible value to the laser diode limit. For every 10^{th} pump intensity, the measurement of average power is obtained with an optical power meter. The pulse energy is defined as average power divided by repetition rate. During Q-switching, the value of pulse energy, E_p is calculated based on the following expression.

$$E_p = \frac{P_{avg}}{f} \quad (2.13)$$

where P_{avg} and f is an average laser power and repetition rate, respectively. Those parameters are related to each other, and they also change with the change in optical intensity. Pulse energy is dependent on the amount of energy stored in the gain medium (Spühler, 1999). Therefore, it is important to ensure that the gain medium used owns a high device efficiency. The two properties that influence pulse energy are the gain medium lifetime and absorber's saturation loss. On the other hand, peak power is defined as the highest attainable optical power of a pulse. Peak power, P_p is related to pulse energy and pulse duration based on the following expression,

$$P_p = \frac{E_p}{\tau} \quad (2.14)$$

where E_P and τ is pulse energy and pulse width at FWHM, respectively. It is shown that if the pulsed laser has a short pulse width, it will consume high peak power. A fiber laser with high peak power has advantageous of low heat affected zone that can produce a good laser ablation procedure. There is a multitude of applications that manipulates a pulsed laser with high peak power such as micromachining of material, optical data storage, and waveguide production (Balling & J. Schou, 2013; Jiang, 2018).

2.6 Fiber-optic interferometer

An interferometer is a device that utilizes the concept of superimposed waves for the purpose of determining certain properties. In this device, a laser beam is split into two beams, a sample beam and reference beam. These beams travel along a path of a particular design and undergo an interaction before combining to produce an interference pattern. The device has many applications in guidance system, holography, telescope, sensing etc. To date, fiber-optic interferometers have been widely investigated for both sensor and laser applications (Eberle et al., 2006). The fiber-optic interferometers can be used for various physical parameters including strain, temperature, refractive index, and pressure. The interferometers can be categorized into many types including Sagnac, Fabry-Perot, Mach-Zehnder and Michelson. In this section, two types of interferometric are reviewed in terms of operating principles, fabrication methods, and application fields.

2.6.1 Sagnac interferometer

Since its first demonstration over 25 years ago, Sagnac interferometers have received substantial research and development investment. They have been applied in many applications ranging from the conventional gyroscopic measurements to unexpected new applications including sensing. For instance, fiber optic based Sagnac interferometers are recently in great interest in various sensing applications due to their advantages of easy fabrication, simple structure, low insertion loss, high anti-noise ability and environmental

robustness (Culshaw, 2005). A schematic diagram of an optical fiber Sagnac interferometer is shown in Figure 2.10. It consists of an optical fiber loop, which is constructed using a 3 dB single-mode fiber coupler and a piece of high birefringent (HiBi) fiber. The 3dB coupler split the laser beam from broadband light source (BBS) into two beams, which are propagating in counter directions with different polarization states. HiBi fiber introduces optical path difference of the two counter-propagating waves and causes an interferential spectrum, which could be employed as the sensing element.

The optical intensity transmission (T) of the Sagnac interferometer or Sagnac loop mirror (SLM) is approximately a periodic function of the wavelength with a spacing between adjacent transmission peaks of $S = \lambda^2 /BL$ (which is named free spectral range (FSR)) and is described by (Dong et al., 2007).

$$T = \frac{1-\cos\varphi}{2} \tag{2.15}$$

where B, L and λ is the birefringence of the HiBi fiber, length of the HiBi fiber and wavelength, respectively. $\varphi = 2\pi BL/\lambda$ is the phase difference between the two counter-propagating beams caused by the birefringence of the fiber. As shown in Eq. (2.15), the transmission function is determined by the product of BL and wavelength. Generally, the wavelength does not change once being established. That means the transmission spectra is only decided by the product of BL. Meanwhile, the value of BL is linearly proportional to the change in temperature, pressure, strain etc. As seen in Fig. 2.10, the phase difference ($\Delta\varphi = |\varphi_0-\varphi_1|$) of the transmission spectra at two different wavelength λ_0 ($\varphi_0 = 2\pi BL/\lambda_0$) and λ_1 ($\varphi_1 = 2\pi BL/\lambda_1$) can be presented as:

$$\Delta\varphi = \frac{2\pi BL(\lambda_1-\lambda_0)}{\lambda_0\lambda_1} \tag{2.16}$$

Therefore, the BL can be calculated through measuring the two wavelengths if the phase difference Δφ is fixed to 2kπ (k is a positive integer). It is worthy to note that, k can be adjusted, and its maximum is restricted by the bandwidth of the optical source (see the Figure 2.10). Eq. (2.16) can also be written as:

$$BL = \frac{k\lambda_0\lambda_1}{(\lambda_1 - \lambda_0)} \tag{2.17}$$

As reported in many literatures (Liu, 2005; Moon, D.S., 2007), BL is linearly proportional to many measurands. Therefore, the SLM can be used in sensor applications for temperature, magnetic field, strain, pressure, ultrasonic, torsion, and biochemical measurement. This is attributed to its distinctive advantages including ease of manufacture, simple design, low insertion loss and higher anti-noise ability in comparison to other types of fiber optic sensors (Zu, 2014; Shao, 2016). The measurable range of this demodulation method is unlimited theoretically. That has a huge advantage over the conventional demodulation method with peak/dip wavelength observation.

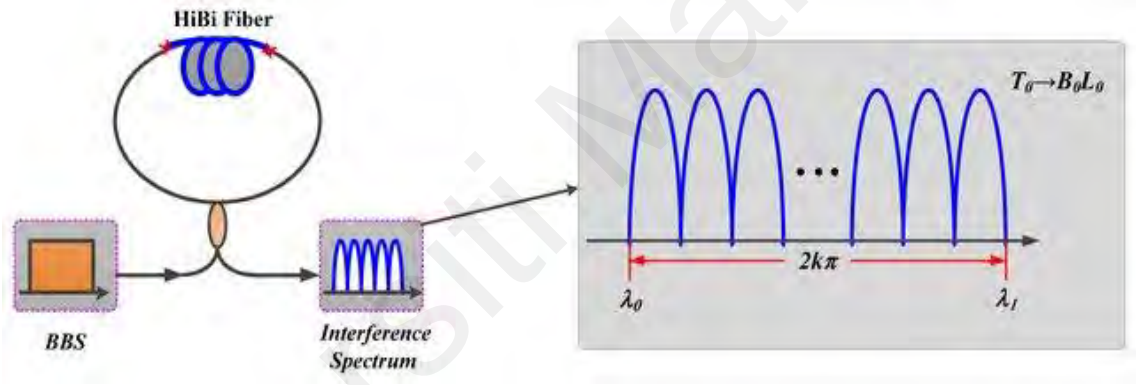

Figure 2.10: The schematic diagram of an optical fiber Sagnac interferometer.

2.6.2 Singlemode multimode singlemode (SMS) fiber structure-based interferometer

A singlemode-multimode-singlemode (SMS) fiber structure consists of a short section of multimode fiber (MMF) fusion- spliced between two single mode fibers (SMFs). Its operation is based on multimode interference and the associated self-imaging mechanism. The SMS structures can be applied in a variety of optical fiber systems but are most employed for sensing a variety of measurands such as temperature, strain, flow rate, vibration, refractive index. They can also be used for sensors in detecting micro-world measurands including pathogens, proteins, DNA, and specific molecules.

Figure 2.11 (a) shows a SMS fiber structure, which is obtained by fusion splicing a short section of MMF between two SMFs. As illustrated in the figure, as light is injected from input SMF into the MMF, multiple modes (including fundamental and higher order modes) will be excited and propagate independently through the MMF section. Multimode interference occurs between these multiple modes within the MMF, and this dictates the transmission spectral response at the output SMF. Let's assume that both SMF and MMF are circularly symmetric and the central axes of SMF and MMF are aligned perfectly, only the LP_{0m} modes can be excited within the MMF when light is launched from the input SMF into the MMF. In both input and output SMFs only the fundamental guided mode E_s (r) can be supported, which can be decomposed into the eigenmodes LP_{0m} in the MMF when the light enters from the input SMF (Wu, 2011). The field profile of LP_{0m} is defined as ϕ_m (r) and the eigenmodes within the MMF are normalized as:

$$\int_0^\infty |E_s(r)|^2 r dr = \int_0^\infty |\varphi_m(r)|^2 r dr = 1, m = 1,2, \ldots. \quad (2.18)$$

The input field at the MMF is equal to that of the SMF E_s (r), which can be expressed as:

$$E_s(r) = \sum_{m=1}^{M} b_m \varphi_m(r) \quad (2.19)$$

where M is the total number of eigenmodes LP_{0m} within MMF and b_m is the excitation coefficient of each eigenmode in the MMF. b_m is defined as the field overlap between the input SMF E_s (r) and the MMF eigenmode of ϕ_m (r) and is given as:

$$b_m = \frac{\int_0^\infty E_s(r)\varphi_m(r) r dr}{\int_0^\infty \varphi_m(r)\varphi_m(r) r dr} \quad (2.20)$$

In the MMF section, the field at a propagation distance *z* is:

$$E_M(r, z) = \sum_{m=1}^{M} b_m \varphi_m(r) \exp(j\beta_m z) \quad (2.21)$$

where β_m is the propagation constant of each eigenmode within the MMF. Assuming the parameters of the output SMF are the same as those of the input SMF, the transmission power of the SMS fiber structure can be determined by using the field overlap integral method between E_M (r, z) and the fundamental mode of the output SMF E_s (r) as:

$$P(z) = 10.\log_{10}\left(\frac{\left|\int_0^\infty E_M(r,z)E_S(r)rdr\right|^2}{\int_0^\infty E_S(r)\varphi_m(r)rdr}\right) = \frac{\int_0^\infty E_S(r)\varphi_m(r)rdr}{\int_0^\infty \varphi_m(r)\varphi_m(r)rdr} \quad (2.22)$$

By using the orthogonal relationship between the eigenmodes of the MMF and substituting Eq. (2.21) into Eq. (2.22), the output of the SMS fiber structure can be simplified as:

$$P(z) = 10.\log_{10}(|\sum_{m=1}^{M} b_m^2 \exp(j\beta_m z)|^2) \quad (2.23)$$

A self-imaging phenomenon also occurs periodically within the MMF due to a multimode interference (Soldano et al., 1995). Figure 2.11 (b) shows an example of simulated mode distribution along the MMF section using Eq. (2.21), where the wavelength is assumed 1550 nm (Wu, 2020). As shown in the figure, the self-imaging length of the SMS fiber structure is obtained at circa of 10.2 mm.

As the surrounding environmental parameters such as temperature, change, several parameters, including the effective refractive index of both the core and the cladding, the length and diameter of the MMF may change, and thus the eigenmodes $\phi_m(r)$ and effective length of the MMF will change, resulting in changes to b_m in Eq. (2.20) and the output of the SMS fiber interferometer.

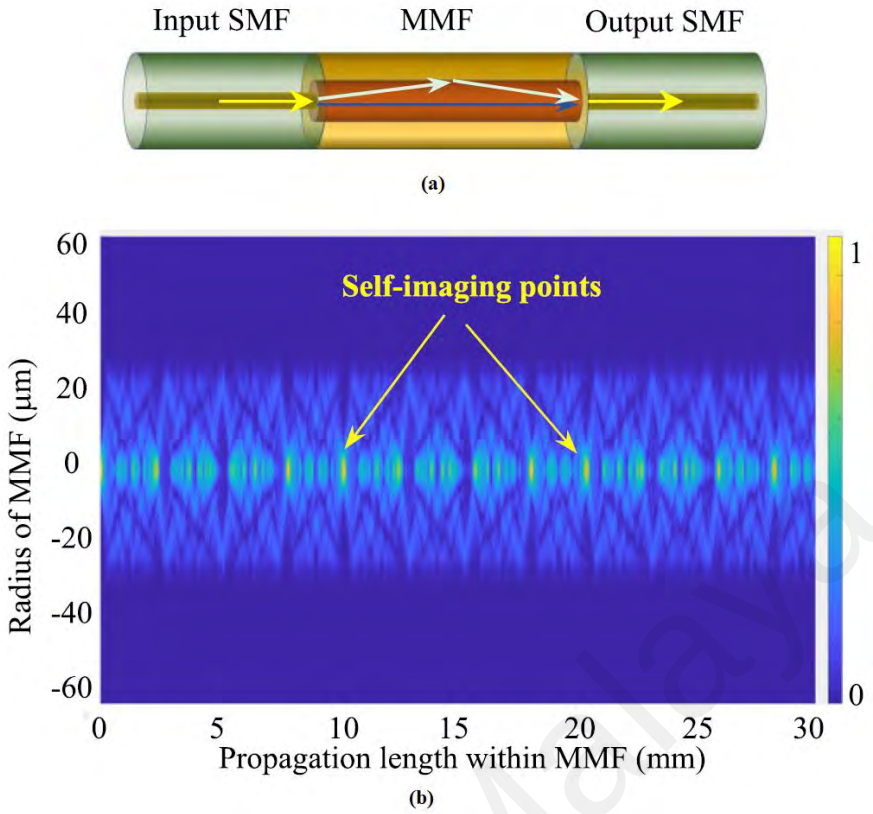

Figure 2.11: (a) Schematic diagram of a traditional SMS fiber structure (Wang et al., 2008), (b) mode distribution along an MMF within a length of 30 mm as calculated by using Eq. (2.21).

2.7 Saturable absorber

A saturable absorber (SA) is a material incorporated inside a laser cavity, which was able to initiate pulsed laser with a short pulse duration. Such-laser is one of the important tools in the scientific and industrial world, as it is used in a variety of applications, including microfabrication of material, high-precision material processing, skin therapy, and corrective eye surgery (Juodkazis et al., 2009 ; Graf, 2015; Shah, & T.S. Alster, 2010). The SA acts as photons absorber as opposed to the high-intensity laser beam.

The phenomenon of saturable absorption can be explained by a simple two-level electronic model, in which the saturable absorption is symmetrical to the gain saturation. Figure 2.12 shows the transition of electrons between two energy states. First, the ground state electron which is located at the valence band (E_1) will absorb energy from the

incoming photons. Assuming that the photon energy of this electron is the same as the energy difference between the energy states, the electron will be ejected to the excited state or conduction band (E_2), provided there is a vacancy at that upper energy state. The difference between these two energy states can also be referred to as a bandgap.

When the optical intensity of laser reaches a certain threshold, the electron populations in the upper energy state is higher than the ground state. The mechanism of saturable absorption obeys a Pauli blocking principle, which states that two or more identical particles cannot occupy the same quantum state within the quantum system at the same time (Travagnin, 2001). Therefore, as the excited states occupied, the SA/material can no longer allow electrons to make a transition between the two energy states. In such a manner, the stimulated emission occurs, releasing a bunch of photons in optical pulses form simultaneously when the electrons decays back to the ground state. At a high enough laser intensity, the material or SA becomes transparent to light, resulting in the saturation of the light absorption and the photon can be transmitted easily through the material without being absorbed. These processes continuously occur as the electrons have a specific lifetime that allows them to revert to the ground state and re-excited back to the upper energy state at high laser intensity. For a material to qualify as SA, it must have a sufficient saturable absorption, a broad linear absorption, and suitable relaxation time, so that it is compatible with any laser configurations (Hussain, 2019).

Current research on SAs such as FIrpic (Salam, 2019), MoS_2 (Ahmed, 2017), WO_3 (Al-Hiti, 2020), NiO (Nady, 2017), Sb_2Te_3 (Bogusławski, 2016), BP (Ahmed, 2016), WTe_2 (Ahmad, 2020), Lu_2O_3 (Baharom, 2019), WSe_2 (Chen, 2016), Ti_2AlC_6 (Lee, 2019), Si (Liu, 2020), P_3HT (Samsamnun, 2020), Eu_2O_3 (Zulkipli, 2020), CuO (Sadeq, 2018) and turmeric (Al-Hiti, 2021) are among SAs that can be used for q-switching and being compared to for this research.

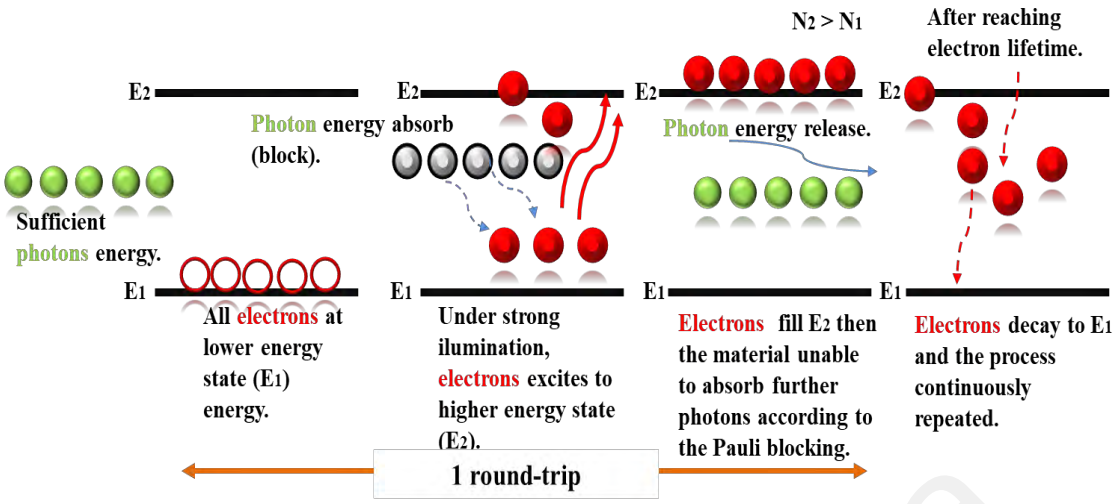

Figure 2.12: The illustration of saturable absorption mechanism based on the two-level electronic model (Milani, 2019).

Figure 2.13 shows the effect of SA, which suppresses weak pulses while amplifying strong pulses, in which the strong pulse becomes shorter and more intense. The SA's performance and pulsed laser performance are governed by the few factors including wavelength range, modulation depth, saturation intensity, non-saturable loss, and recovery time. The wavelength range of SA operation refers to the range of wavelengths over which it can absorb power and exhibiting saturation behaviour. Modulation depth of SA is referred to the maximum change in absorption. Larger modulation depths are required for fibre lasers because the round-trip gain and loss are high, while fibre dispersion and nonlinearity have a significant impact on the pulse formation. Saturation intensity is defined as the intensity of SA necessary to reduce the absorption to half of its unbleached value. The non-saturable loss is the portion of the total loss that cannot be saturated. Although it is an inherent material property, it can be significantly influenced by the fabrication process. The damage threshold represents the SA's upper thermal limit. The recovery time of SA is indicative of its intrinsic response time, which has a significant effect on the pulse duration.

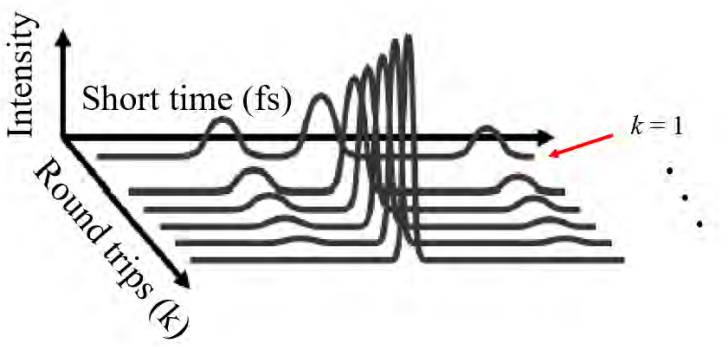

Figure 2.13: The illustration of how SA affects light intensity.

Up to now, a variety of materials have been proposed and demonstrated for SA application. SAs are mostly made of elements and compounds of Carbon and Boron groups. They include nanomaterials such as graphene, carbon nanotube (CNT), black phosphorus (BP), and transition metal dichalcogenides (TMD). Graphene based SAs offer a high absorption spectrum but suffer from a low modulation depth and damage threshold (Dong, 2012). CNT based SAs can be easily fabricated at low cost (Li, 2014; Hasan, 2009), but they have a short spectral band, that is heavily influenced by the diameter of the nanotubes (Wang, 2015). BP based SAs usually have a wide broadband spectrum range but a low nonlinear absorption, low optical threshold and complex fabrication process (Chen, 2015). SAs based on TMD materials such as WS_2 (Yang, 2019; Mao, 2015), SnS_2 (Niu, 2018), and $MoSe_2$ (Liu, 2018) have been shown to have a good absorption property. However, they are affected by a low optical damage threshold and the complex fabrication. Therefore, the search of alternative SAs is still ongoing. The SA could be integrated into a fiber laser cavity by several approaches such as sandwiching the material in between the fiber ferrules or depositing the SA onto the side-polished fiber (Nizamani, 2020).

CHAPTER 3: PREPARATION AND CHARACTERIZATION OF FIBER INTERFEROMETERS AND SATURABLE ABSORBER

3.1 Introduction

Over the last few decades, optical fibers have been commonly used as a transmission medium in telecommunication industries. This is owing to their unique characteristics such as low propagating loss, light weight, high flexibility, low fabrication cost, multiplexing capability, and immunity to electromagnetic interference (Keiser, 2006). In addition, with the advance in photonic technology, optical fibers have also been intensively studied for sensing and laser applications (Boetti et al., 2017). For example, optical fibers have been utilized for sensing of a variety of measurands including strain, temperature, refractive index, rotation, pressure, displacement, etc (Kang et al., 2003). To date, various innovative fiber optic technologies such as fiber Bragg grating (Chiavaioli, et al., 2017), Brillouin/Raman scattering (Muanenda et al., 2019), microfiber (Lou., 2014), surface Plasmon resonance (SPR) (Zhou et al., 2018), specialty fiber couplers (Lee et al., 2010) and fiber optic interferometer (Li et al., 2023) have been utilized to improve their sensing abilities. Among these technologies, fiber optic interferometers have gained tremendous interests in recent years especially for sensing and laser applications.

Likewise, several saturable absorbers (SAs) such as semiconductor saturable absorber mirrors (SESAMs) and carbon nanotubes (CNTs) have been proposed and demonstrated for various pulse generations. SESAMs have been widely employed, particularly in solid state lasers since its first demonstration in 1992 (Keller et al., 1996). This is attributed to their many advantages such as fast recovery time and suitable modulation depth. However, SESAMs have many drawbacks, given its dominance, such as low damage threshold and complex manufacturing process (Popa et al., 2011). In addition, they suffer from a narrow absorption bandwidth and are considerably bulky and relatively costly. On the other hand, the bandwidth and absorption efficiency of CNT based SAs highly depend

on the diameter of the CNTs used. Therefore, there is an ongoing search for alternative materials as candidates for SAs in the past few years. The material should be relatively cheap, easy to prepare and is able to produce stable pulses in various fiber laser cavities (Kang et al., 2018).

This thesis aims to demonstrate a tunable and dual-wavelength Q-switched fiber laser using a fiber-optic interferometer as a filter and passive saturable absorber (SA) as a Q-switcher. In this chapter, the construction method and operating principles of fiber optic interferometer are described. The fabrication and characterization of two types of SA are also presented in this chapter.

3.2 Fiber-optic interferometer

Fiber optic interferometers have been widely investigated for use in sensing of various physical parameters including strain, refractive index, pressure, and temperature (Soares et al., 2021). This is owing to their unique characteristics including remote sensing ability, low fabrication cost, low propagating loss, high flexibility, high accuracy, high sensitivity, simultaneous sensing ability, small form factor, and immunity to electromagnetic interference. Indeed, some fiber optic interferometers have been deployed in sensing applications for real time deformation monitoring of bridges, ships, aircrafts, and constructions (Rao, 2006) as well as in laser applications as an interference filter (Qi et al., 2016). A fiber optic interferometer typically uses the interference between two or more beams that propagating through different optical paths of a single fiber or two different fibers. These beams are transmitted independently but interfere constructively or destructively when the beams combined to produce transmission peaks or dips over a broad wavelength range. In a fiber-optic interferometer, changes in refractive index or effective path lengths for example due to temperature or stress will shift spectral position of the peaks or dips. Therefore, it can be used in various sensors to

determine the unknown measurand by measuring changes in the spectrum (Lee et al., 2012)[101].

The current trend of fiber-optic interferometers is to miniaturize them by deploying all-fiber structure. The all-fiber structure is more compact and offers several advantages including high coupling efficiency, easy alignment, and high stability. Here, two types of fiber-optic interferometers, namely an all-fiber Sagnac Loop Mirror (SLM) and single mode-multimode-single mode (SMS) fiber structures.

3.2.1 All-fiber Sagnac Loop Mirror (SLM)

Recently, SLMs are obtained great interests for various sensor and laser applications due to their advantages of easy fabrication, simple structure, and environmental robustness (Fu et al., 2008). Figure 3.1 shows the structure of all-fiber SLM. It consists of a 3 dB fiber coupler and an optical fiber loop. The coupler split the input light into two beams, which are propagating in counter directions with different polarization states. The two counter-propagating beams are combined again at the same coupler. The output interference pattern is determined by the optical path difference of the SLM, which is depended on the polarization dependent propagating speed of the mode guided along the loop. To maximize the polarization-dependent feature of the interferometer, a high birefringent fiber (HBF) or polarization maintaining fiber (PMF) is typically used in sensing part. The polarizations are adjusted by a polarization controller (PC) attached at the beginning of the sensing fiber. The signal at the output port of the fiber coupler is governed by the interference between the beams polarized along the slow axis and the fast axis. The phase of the interference is simply given as:

$$\delta = \frac{2\pi}{\lambda} BL,\ B = |n_f - n_s| \tag{3.1}$$

where B is the birefringent coefficient of the PMF, L is the length of the PMF while n_f and n_s are the effective refractive index of the fast and slow modes, respectively (Fu et al., 2008).

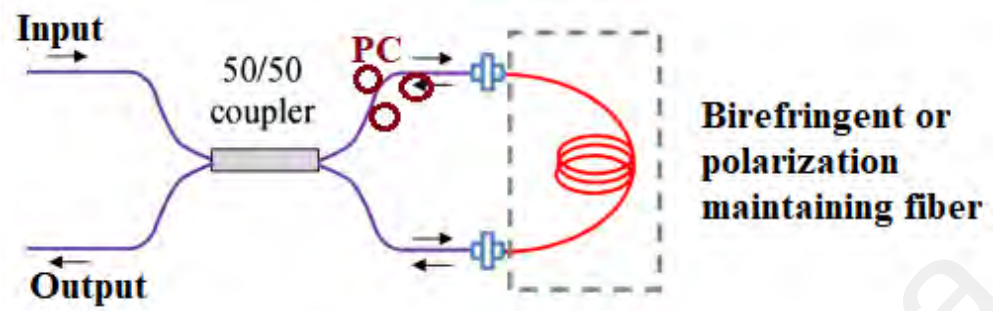

Figure 3.1: Schematic diagram of the proposed SLM.

In general, HBFs or PMFs are incorporated in the SLM to acquire a high phase sensitivity. For instance, a doped fiber with a large thermal expansion coefficient is used to induce high birefringence variation for the temperature sensing application (Shao et al., 2015). In this work, the SLM is constructed based on PMF and the temperature effect on the device performance is characterized as shown in Figure 3.2. A piece of PMF is spliced with ports 3 and 4 of a 3 dB coupler to form a fibre loop. The input port of the SLM (Port 1) is connected to the amplified spontaneous emission (ASE) source while the output (port 2) is connected to optical spectrum analyser (OSA). As shown in Figure 3.2, the fibre was put into an oven for the temperature measurement. Figure 3.3 compares the output spectrum from the SLM with the input ASE spectrum at a fixed temperature of 30^{o}C. It is shown that the interference pattern is obtained with a transmission dip at wavelength of 1543.2 nm.

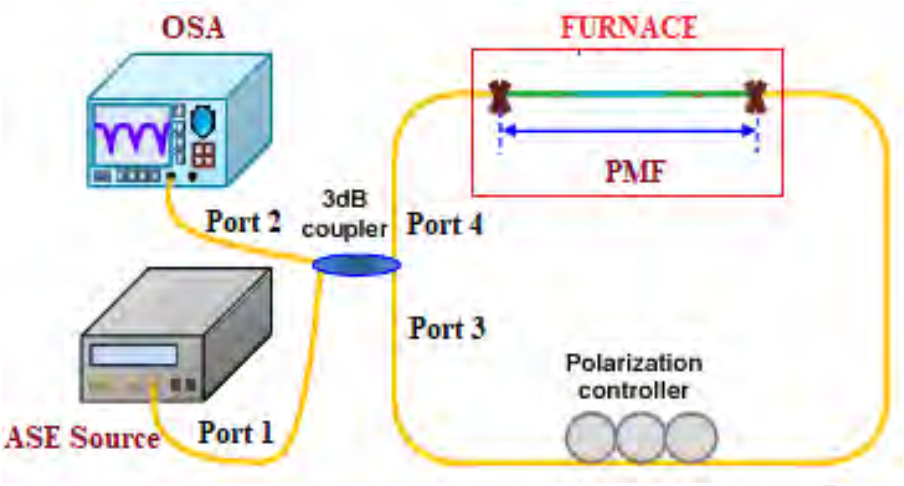

Figure 3.2: Experimental setup of the SLM with a PMF as a sensing fiber.

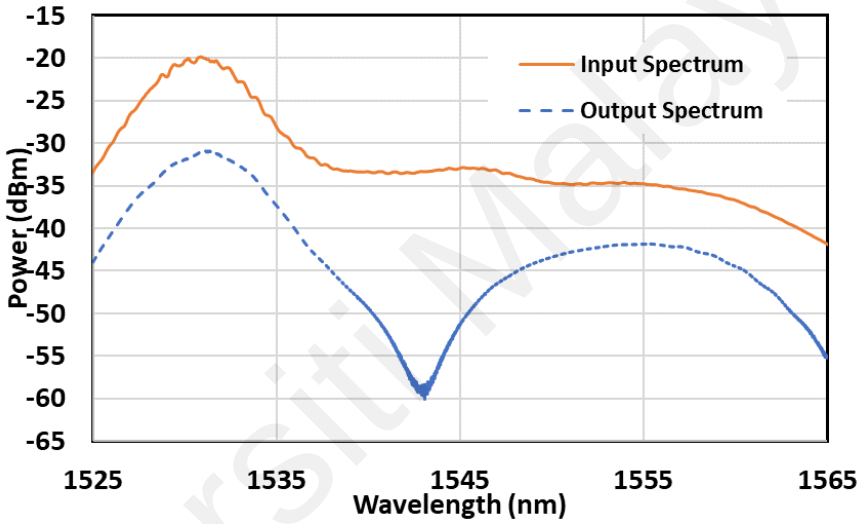

Figure 3.3: The measured input ASE spectrum and transmission spectrum of the SLM.

Figure 3.4 presents the measured transmission spectrum at different temperature. An interference signal with two transmission dips is observed within the interesting wavelength range. This transmission dips are caused by the PMF in the SLM, which is sensitive to temperature change. The polarization modes of the fiber are sensitive to the temperature due to the thermo-optic characteristic of the silica material. As increasing the temperature, the interference signal was shifted to the shorter wavelength direction. The reason for weak transmission spectra shows the effect of various polarization inside the interferometer. The reduction of loop length is expected to improve the spectra.

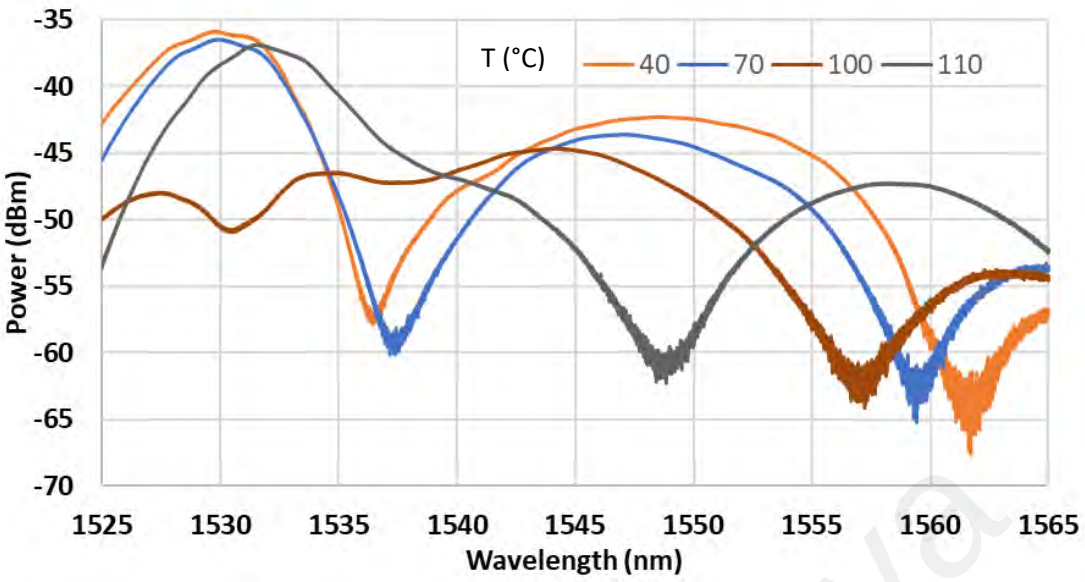

Figure 3.4: The measured transmission spectrum at different temperature.

3.2.2 Single mode-multimode-single mode (SMS) fiber structure

In the previous sub-section, SLM was introduced and demonstrated. It was formed by an optical fibre loop, where a 50/50 fibre coupler was used to divide the input ASE light into two counter-propagating beams and a short length of highly birefringent PMF was placed in the loop. Interference occurs due to the phase difference introduced by transmission along both the slow and fast axes of the PMF. In this sub-section, a single mode-multimode-single mode (SMS) fiber structure is introduced, fabricated, and characterized. It employs a short section of multimode fibre (MMF) spliced between two single-mode fibres (SMFs). This structure is also referred to a fibre heterostructure since it can be formed by combining two different fibre types. The proposed SMS structure has many advantages including low cost, ease of fabrication, high sensitivity, and flexible design, all of which are useful advantages in the development of photonic devices especially optical sensors (Hatta et al., 2013). It can be deployed used in a variety of optical fiber systems but are most used as physical sensors for measuring strain, temperature, vibration, refractive index, flow rate and humidity. It can also be deployed

for biosensors in detecting pathogen, DNA, proteins, and specific molecules (Kaushik et al., 2018).

The mechanism supporting the operation of an SMS fiber structure is multimode interference and associated self-imaging. Figure 3.5 shows the simplest SMS fiber structure, which was fabricated by fusion splicing a short section of MMF between two SMFs. As a light beam is launched from the input SMF into MMF, multiple modes (higher order modes) will be excited and propagate independently through the MMF section. Multimode interference occurs between these multiple modes within the MMF, and this dictates the transmission spectral response at the output SMF.

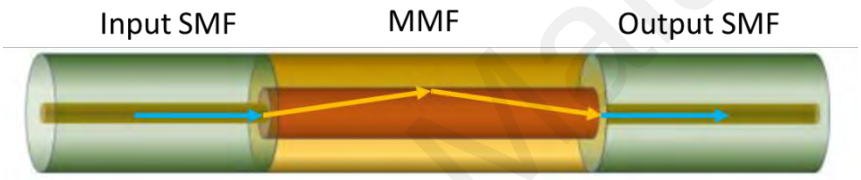

Figure 3.5: Schematic diagram of a SMS structure.

Assuming that the central SMF and MMF axes are perfectly aligned and both SMFs and MMF are circularly symmetric, the MMF can only excite the LP0m modes when light beam is launched from the input SMF into the MMF. Both SMFs can only support the fundamental guided mode E_s (r), which can be decomposed into the eigenmodes LP0m in the MMF when the light enters from the input SMF. The eigenmodes within MMF are normalized as (Wang, Farrell, & Yan, 2008):

$$\int_0^\infty |E_s(r)|^2 rdr = \int_0^\infty |\varphi_m(r)|^2 rdr = 1, m = 1,2, \ldots. \quad (3.2)$$

where the field profile of LP0m is defined as ϕm(r). The input field at the MMF is equal to that of the fundamental guided mode of SMF E_s (r), which can be written as:

$$E_s(r) = \sum_{m=1}^{M} b_m \varphi_m(r) \quad (3.3)$$

where M is the total number of eigenmodes LP0m within MMF and b_m is the excitation coefficient of each eigenmode in the MMF. b_m is the field overlap between the input SMF E_s (r) and the MMF eigenmode of ϕ_m(r) and is given as:

$$b_m = \frac{\int_0^\infty E_S(r)\varphi_m(r)\, rdr}{\int_0^\infty \varphi_m(r)\varphi_m(r)\, rdr} \tag{3.4}$$

In the MMF section, the field at a propagation distance z is:

$$E_M(r,z) = \sum_{m=1}^{M} b_m \varphi_m(r) \exp(j\beta_m z) \tag{3.5}$$

where β_m is the propagation constant of each eigenmode within the multimode fibre. Assuming the parameters of the output SMF are the same as those of the input SMF, the output power at output SMF of the SMS structure can be determined by using the field overlap integral method between E_M (r, z) and the fundamental mode of the output SMF E_s (r) as:

$$P(z) = 10.\log_{10}\left(\frac{\left|\int_0^\infty E_M(r,z)E_s(r)rdr\right|^2}{\int_0^\infty |E_M(r,z)|^2 rdr \int_0^\infty |E_s(r)|^2 rdr}\right) \tag{3.6}$$

By substituting equation (3.5) into equation (3.6) and deploying the orthogonal relationship between the MMF's eigenmodes, the power output from the SMS structure can be simplified as:

$$P(z) = 10.\log_{10}\left(\left|\sum_{m=1}^{M} b_m^2 \exp(j\beta_m z)\right|^2\right) \tag{3.7}$$

Figure 3.6 illustrates an example of simulated mode distribution along the MMF section using Equation (3.5) at the operating wavelength of 1550 nm. As seen, the well-known self-imaging phenomenon occurs periodically within the MMF due to the multimode interference. The SMS structure has a self-imaging length of approximately 1 cm. The output of the proposed SMS structure is defined in Equations (3.6) and (3.7). It changes as the surrounding environmental parameters (strain, temperature, vibration strain, vibration, etc) varies. The variation in these parameters change the effective refractive index of both the core and cladding and the effective length of MMF. This in turn change the eigenmodes ϕ_m(r) and b_m in Equation 3.4. The multimode interference in

the SMS structure is strongly dependent on bm or the excitation coefficient of each eigenmode in the MMF.

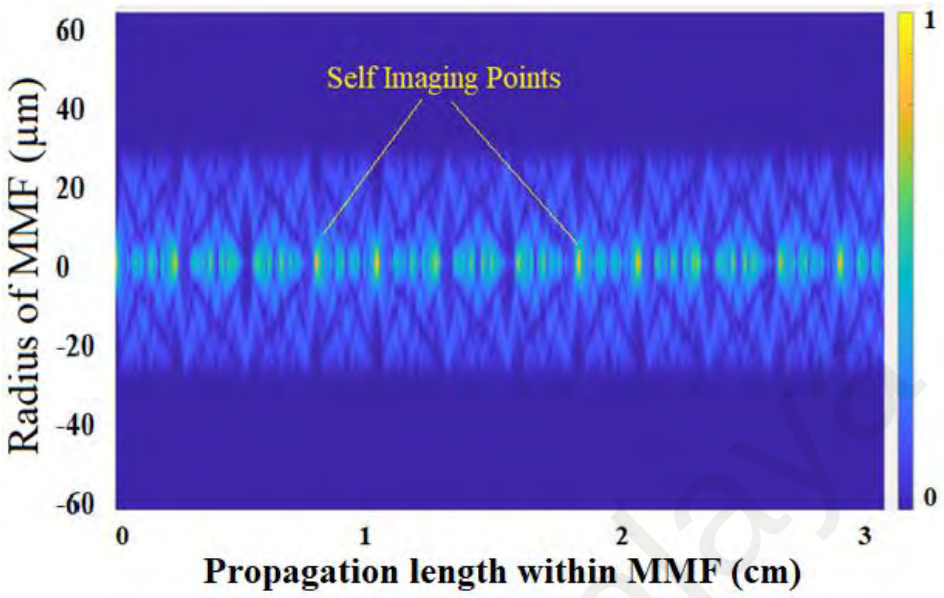

Figure 3.6: The mode distribution along an MMF, which was calculated utilizing Equation (3.5).

In the experiment, the SMS fiber structure was fabricated by sequentially fusion splicing of the SMF, a section of 5.5 cm step index MMF, and the SMF, as shown in Figure 3.5. The SMF has a core/cladding diameter of 9/125 μm while the MMF has a core/cladding diameter of 50/125 μm. The spectral response of the SMS fiber structure at the output SMF was then measured as the ASE light source was injected into the input SMF. Figure 3.7 shows the measured optical spectra before and after transmission through the SMS structure. Several transmission dips were clearly observed at 1537 nm, 1551 nm, and 1565 nm in the latter spectrum due to the multimode interference. The SMS structure can have a variety of applications but the two most common are as an interference filter or as a sensing probe.

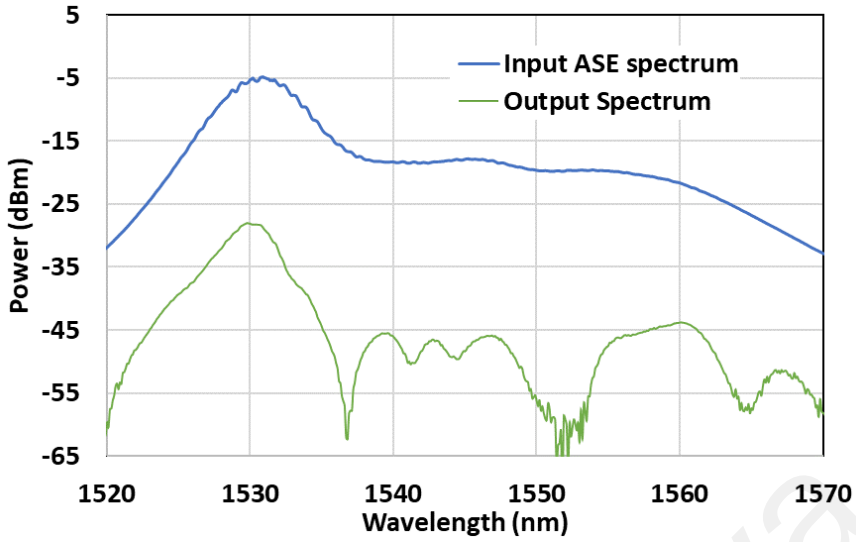

Figure 3.7: The measured input ASE spectrum and transmission spectrum of the SMS structure.

Next, the SMS structure is put inside an oven to investigate the temperature dependence on the SMS' spectral response. The spectral response was investigated over a wide temperature range from 40°C to 100°C. Figure 3.8 shows the measured transmission spectra of the SMS fiber structure at different oven's temperature. Several characteristic peaks and dips were clearly observed in the spectra. With increasing applied temperature, the spectral peak or dip shifted to longer wavelength. Figure 3.9 shows the dip wavelength shift plotted as a function of temperature. It indicates a linear relation with the sensitivity of 0.0183 nm/°C. At temperature above 100°C, no stable peak/dip was observed in the whole spectrum. This behavior seems to be caused by the polarization-dependent spectral fluctuations. This problem might be mitigated by using a polarization scrambler.

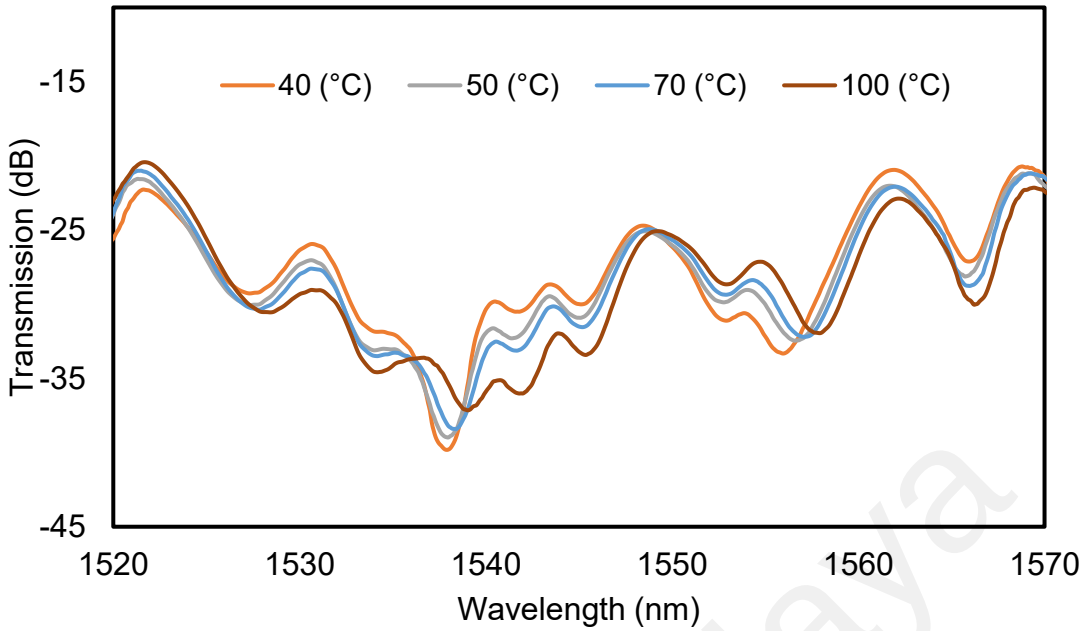

Figure 3.8: Transmission spectra of the SMS structure at various temperatures.

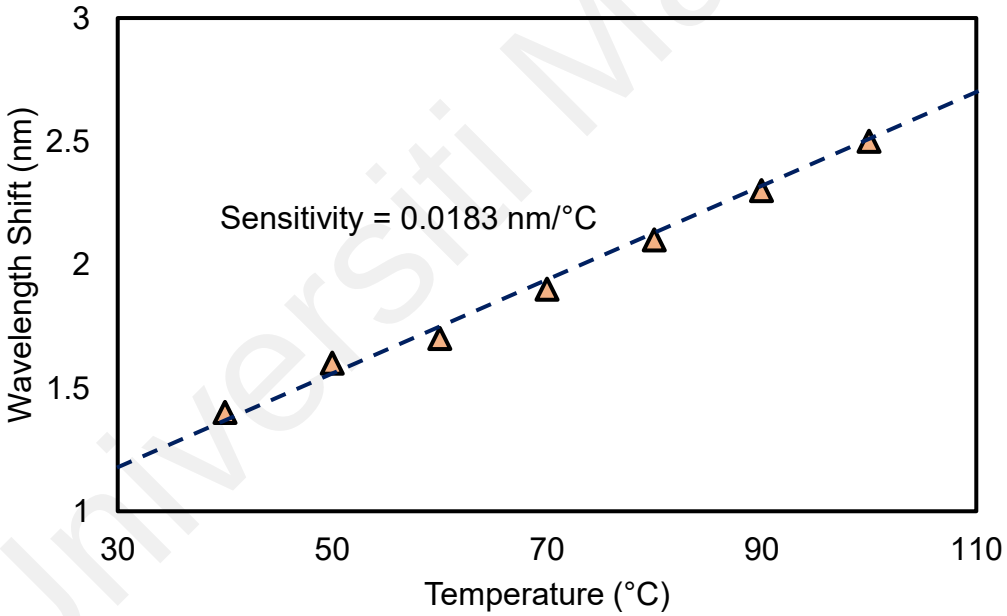

Figure 3.9: Dip wavelength shift vs temperature.

3.3 Preparation of saturable absorber (SA)

Recently, the many new materials have shown their ability to work as passive SA. For example, Jafry et al. demonstrated a passive Q-switched fiber laser erbium-doped fiber laser (EDFL) by using lutetium oxide, which was deposited onto a side-polished fiber as SA (Jafry et al., 2019). In another work, (Al-Hiti et al., 2019) also reported the generation

of Q-switched fiber laser operating at C-band region utilizing Holmium oxide as passive SA. The practical SA device should have great optical properties such as ultrafast response time, appropriate modulation depth, broad saturable absorption, and high damage thresholds while a minimal cost, and ease of manufacture were always vital. This thesis aims to demonstrate a tunable and dual-wavelength Q-switched fiber laser using a passive technique with SA. This section demonstrates the fabrication these Sas (Takahashi et al., 2013).

3.3.1 Preparation of GO SA

In this work, graphene oxide is the key device to achieving Q-switching generation. It functions as a saturable absorber (SA) to modulate the loss or Q-factor of the laser cavity. The SA device is fabricated by embedding a GO material, which was obtained through a electrochemical exfoliation process from graphene flakes into polyvinyl alcohol (PVA) film via a drop-casting method. This method is simple and low-cost. The proposed SA can be operated in a broad wavelength range because of its unselective absorption in 1550 nm region. Figure 3.10 shows the preparation of graphene oxide solution from graphite rods using an electrochemical exfoliation technique. At first, a pair of electrodes (graphite rods) was placed inside electrolyte liquid (1% sodium dodecyl sulphate (SDS) in deionized water) and provided an electrical potential between the electrodes during the exfoliation process. In the experiment, two graphite rods (electrodes) were placed 1 cm apart while applying a constant voltage difference of 20 V. As we applied the electrical potential, the negative ions moved towards an anode and the positive ions moved to the cathode.

This has caused the graphene layers to be removed from the graphite rod through the following chemical reactions:

$$H_2O \rightarrow OH^- + H^+ \quad (3.8)$$

$$CH_3(CH_2)_{11}OSO_3Na \rightarrow CH_3(CH_2)_{11}OSO_3^- + Na^+ \quad (3.9)$$

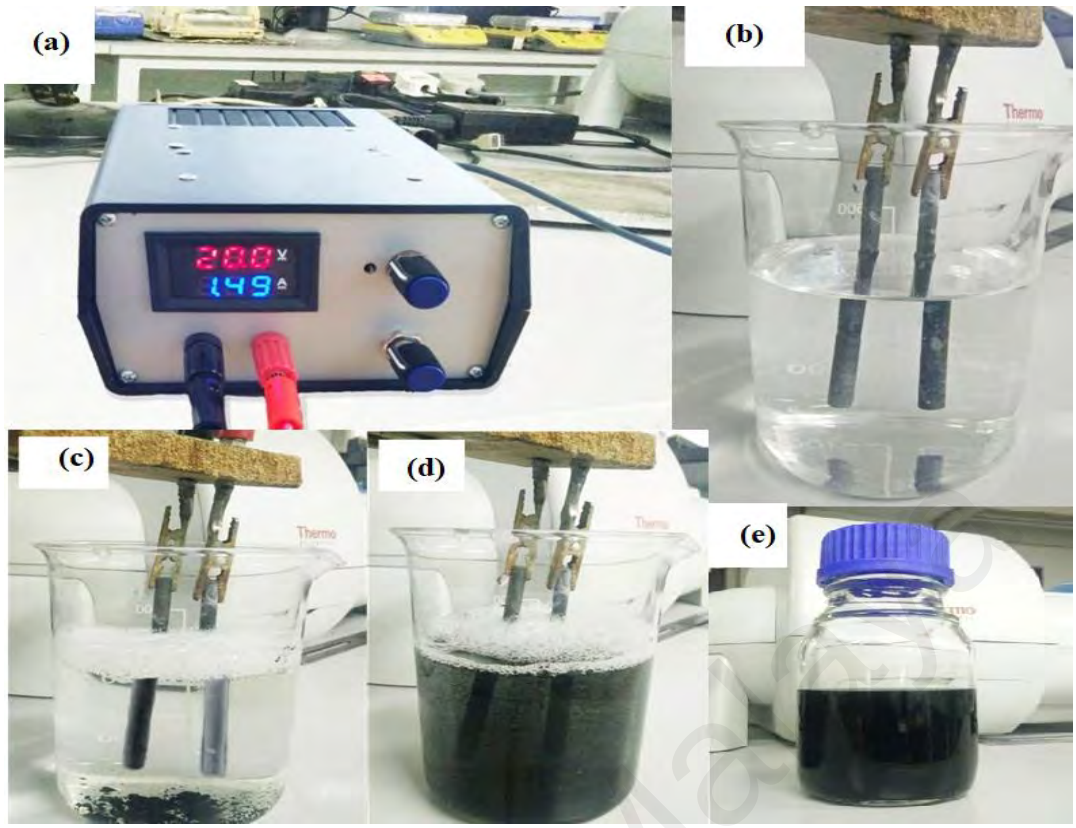

Figure 3.10: Illustrations of the electrochemical exfoliation of graphene from graphite rods. (a) providing 20V potential using a DC power supply, (b) graphite rods as cathode and anode immerse in electrolyte, (c) After several minutes where bubbles were observed at the cathode due to the formation of hydrogen gas (d) after two hours of exfoliation process (e) The graphene suspension obtained after the electrochemical process.

The dodecyl sulphate ions accumulated at the anode and interacted to the surface of the graphite rod. This resulted in the loosening of the graphene layers from the graphite rod (Gao & Huang, 2014). This process was carried out for two about hours to produce a stable graphene suspension, which was then centrifuged for 30 minutes at 3000 rpm to separate large agglomerates. After that, the supernatant portion of the graphene suspension was decanted to obtain a homogeneous graphene oxide solution.

The graphene solution obtained from this process was then mixed with PVA solution to fabricate a SA film via drop casting technique. The PVA solution was prepared by

dissolving 1 g of PVA powder in 120 ml DI water using hot plate stirrer with the aid of magnetic stirrer. From the experiment, it will take around two hours to fully dissolve the PVA in DI water. The mixed solution was poured into a petri dish and dried at room temperature to produce 50 μm thin film. After dry, the thin film was slowly peeled out and the image of the film is shown in Fig. 3.11 (a). Fig. 3.11 (b) shows EDX spectrum of the GO film. It has a carbon content of 57 % wt and an oxygen content of 43% wt. Fig. 3.11 (c) shows the Raman spectrum of the fabricated GO thin film. It clearly shown the D and G peak at position of 1359 cm^{-1} and 1600 cm^{-1}, respectively.

The D peak is obtained due to defect-induced breathing mode of sp^2 rings while the G peak is attributed to the first order scattering of the E_{2g} phonon of sp^2 carbon atoms (Ferrari & Basko, 2013). As observed in the figure, the G peak of the GO is located at a higher frequency (of 1600 cm^{-1}) as compared to graphite (1580 cm^{-1}) and the result is agreed very well with the finding reported by (Kudin et al., 2008). The 2D peak also is observed at 2800 cm^{-1} position. A small piece of the GO film was sandwiched in between two optical fiber ferules, which was locked by a fiber adapter to construct a SA device as shown in Fig. 3.11 (d).

The electrochemical methods usually performed under mild conditions are convenient, controllable, and suitable for mass production. Aside from general advantages, electrochemical exfoliations such as anodic exfoliation and cathodic exfoliation can destroy or weaken the van der Waals forces or electrostatic interactions that bind 2D layers, which can be utilized to exfoliate the bulk layered materials into single-layer or few-layer 2D materials beyond graphene (Yang et al., 2019)

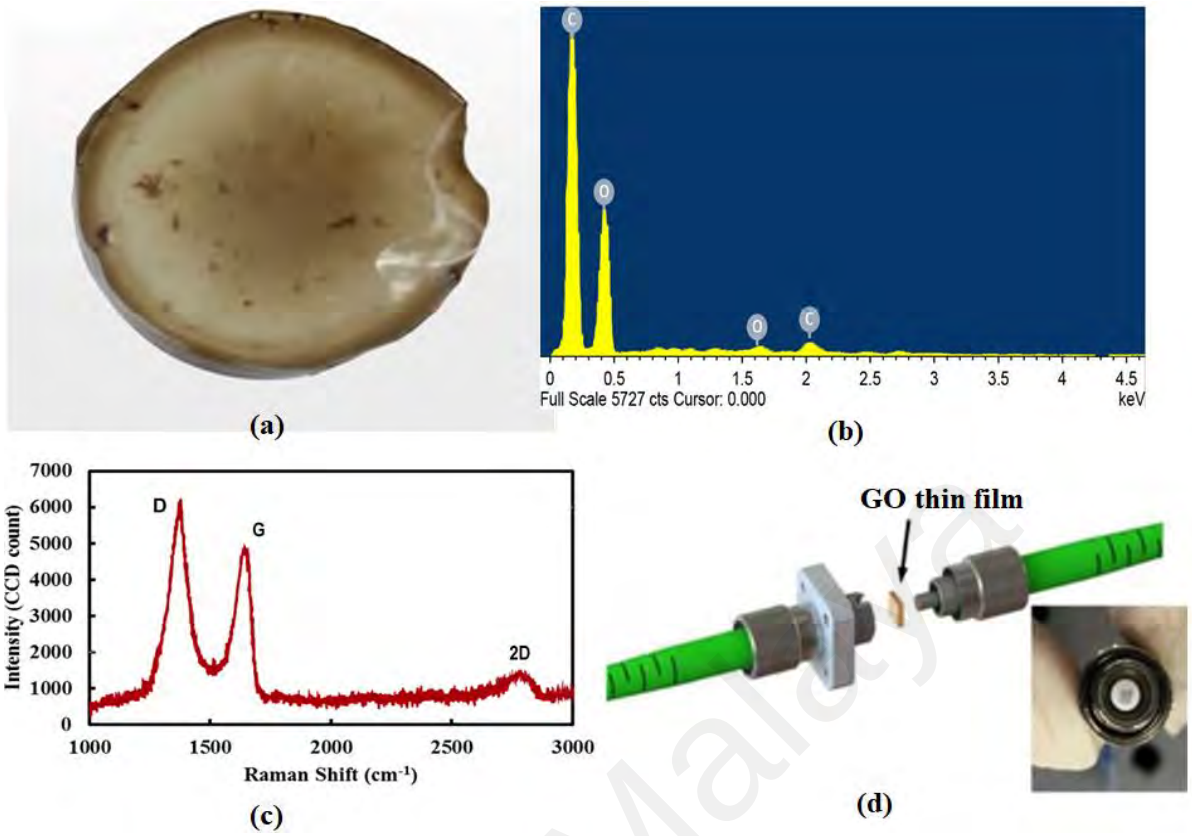

Figure 3.11: (a) The GO PVA thin film obtained after let dry at room temperature (b) EDX profile (c) Raman spectrum (d) The thin film was sandwiched between two ferrules to form a fiber compatible SA device.

3.3.2 Preparation of Al_2O_3 thin film

In this experiment, we fabricated the SA film using a commercially available few-layer Al_2O_3 powder. In the process, the Al_2O_3 powder (with 101.96 g/mol molecular weight) was embedded into Polyvinyl alcohol (PVA) based on a casting method. At first, we prepared the PVA host with the help of magnetically actuated stirrer machine to dissolve 1 g of PVA powder in 120 ml of de-ionized water at room temperature. The stirring was done until all the PVA powder was completely dissolved and the PVA solution become homogenous. Then, 1 mg of Al_2O_3 powder was added into 3 ml of the PVA solution and stirred thoroughly for about 3 hours using the magnetic stirrer. Next, the Al_2O_3 PVA mixture solution was sonicated for 10 minutes inside an ultrasonic bath to ensure the Al_2O_3 material binds with the polymer. The Al_2O_3 PVA solution was then poured and

carefully spread onto a well-covered petri dish. It was then left for at least 48 hours and allowed to dry at room temperature to form Al_2O_3 composite film. The fabrication procedures are summarized and illustrated in Fig. 3.12. The produced Al_2O_3 film has a thickness of about 30 μm.

Figure 3.12: Preparation of Al_2O_3 PVA film.

Figure 3.13 (a) shows the Al_2O_3 nanorods, which were embedded into PVA film as imaged by a Field Emission Scanning Electron Microscope (FESEM). It has a size of about 100 nm. The Al_2O_3 PVA film was then cut into a tiny piece so that it can be attached onto a FC/PC ferrule as shown in Figure 3.13 (b). The ferrule attached with the film was then affixed through a fiber adaptor to another clean ferrule to construct an all-fiber SA

device. The spurious reflections at the interface between the ferrules was reduced with the application of an appropriate amount of index matching gel.

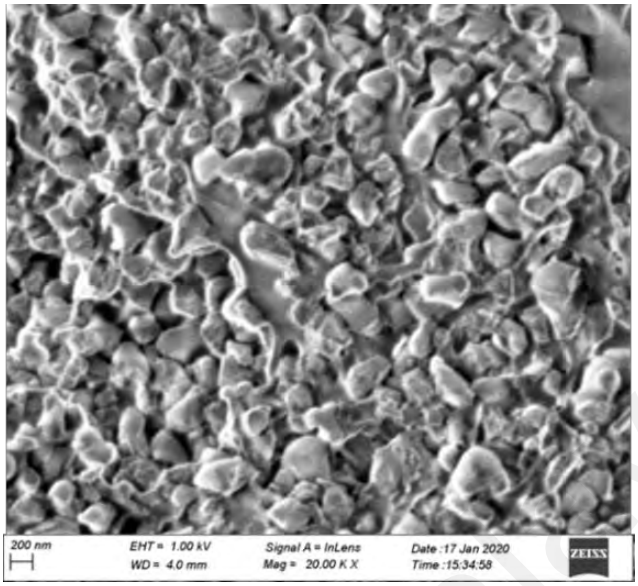

(a)

(b)

Figure 3.13: (a) FESEM image of the Al_2O_3 PVA film, and (b) The image of fabricated film as it was attached onto a fiber ferrule.

3.4 Optical linear and nonlinear characteristics of the prepared SA devices

The linear and nonlinear optical properties of both SA devices were investigated to verify that the fabricated SA devices can be implemented within the laser cavity to generate a stable pulsed laser. At first, the linear absorption characteristic was obtained by transmitting a broadband light from an white light source (WLS) through the SA device as shown in Figure 3.14 (a). The WLS is operating within a wavelength range from

700 nm to 1700 nm. The output light intensity after the SA device was recorded using optical spectrum analyzer (OSA) with resolution of 0.05 nm. The captured spectrum was then recorded for analysis purpose. The purpose of this measurement was to identify whether the SA device can operate within near infrared region.

The nonlinear absorption profile was also obtained by using a balanced twin-detector technique as shown in Figure 3.14 (b). It used a homemade mode-locked Erbium-doped fiber laser (EDFL) as a light source. The EDFL operated at a central wavelength of 1550 nm with a repetition rate of 1 MHz and pulse width of 1 ps. The mode-locked pulses were amplified by using erbium doped fiber amplifier (EDFA) to obtain a sufficient power to saturate the SA material. The intensity of laser light was controlled and varied by using a variable optical attenuator (VOA). The output from the VOA was divided into two using a 3 dB coupler. At one end of the output, it was directly connected to optical power meter (OPM) as a reference. The laser light from another port was transmitted through the SA device before its intensity was measured by another OPM. By gradually varying the input power, a series of optical transmittance with respect to different input intensities had been recorded. Then, the nonlinear transmission profile was estimated by fitting the relation between the optical transmission and the input laser intensity by using the following equation:

$$T(I) = 1 - \Delta T * \exp(-I/I_{sat}) - T_{ns} \quad (3.10)$$

where, T(I) is the transmission rate, ΔT is the saturable absorption, I is the input intensity, I_{sat} is the saturating intensity, and T_{ns} is the non-saturable absorbance.

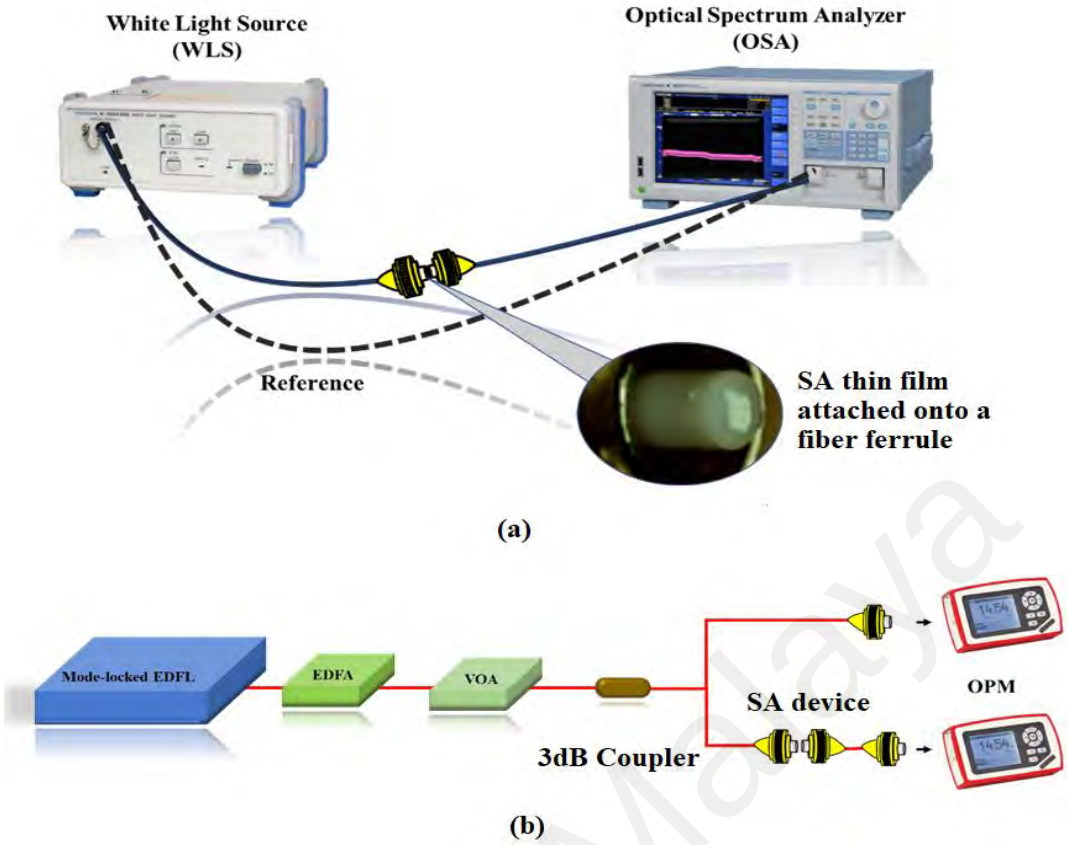

Figure 3.14: The experimental setup for (a) linear absorption and (b) nonlinear absorption measurement.

Figure 3.15 (a) shows the measured linear transmission spectrum for the GO PVA film. It shows an absorption of about 15 % or 0.7 dB at 1550 nm region. The measured nonlinear curve of the GO PVA film is shown in Figure 3.15 (b). It indicates that the film has non-saturable absorption of 35.1%, modulation depth or nonlinear saturable absorption of 24.1% and saturable intensity of 72 MW/cm^2.

The linear absorption spectrum of Al_2O_3 PVA film is shown in Figure 3.16 (a). It is observed that absorption reduces from the visible to the near-infrared band. At 1550 nm region, the absorption loss was around 1.7 dB. The nonlinear transmission of the film was then measured by using a balanced twin-detector technique. Figure 3.16 (b) shows the result, which was obtained by comparing the transmitted power without and with the Al_2O_3 PVA film. As shown in the figure, the modulation depth, saturable intensity, and

non-saturable absorption of the Al_2O_3 PVA film are 3.5%, 0.05 MW/cm2 and 13.5%, respectively. It is worth noting that we have not observed any nonlinear response from pure PVA film, confirming that the saturable absorption property solely originates from Al_2O_3 material.

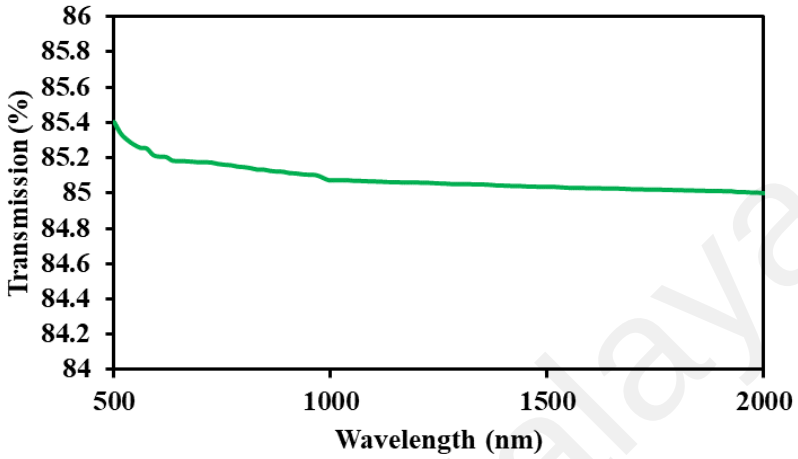

(a)

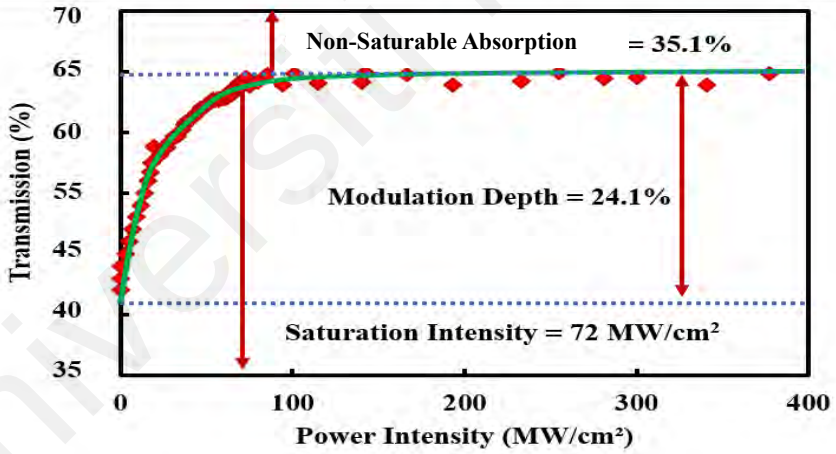

(b)

Figure 3.15: Optical properties of the GO PVA film. (a) linear transmission and (b) nonlinear transmission profile.

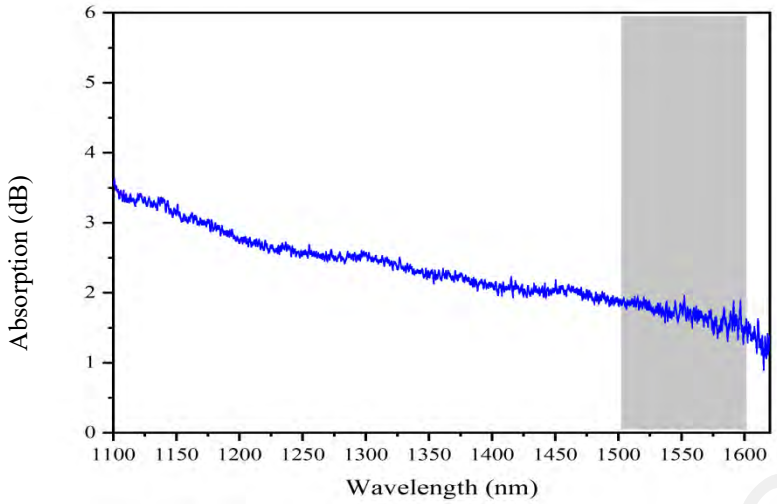

(a)

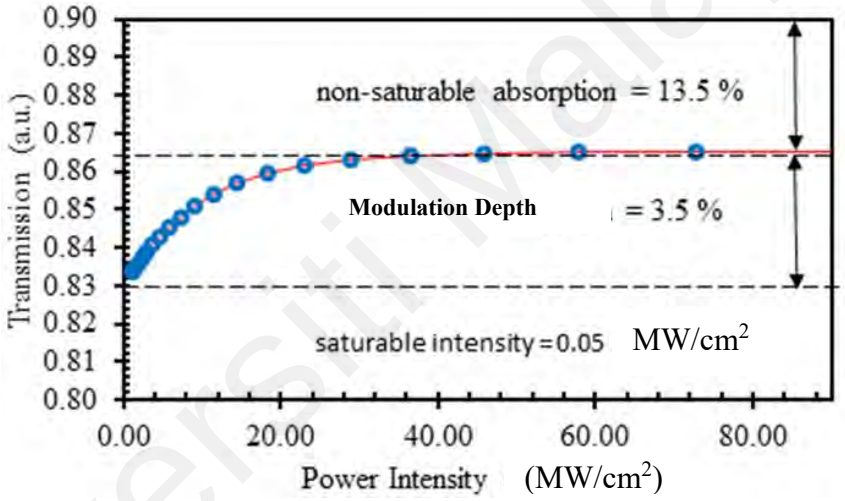

(b)

Figure 3.16: Optical properties of the Al_2O_3 PVA film. (a) linear absorption (b) nonlinear transmission profile.

3.5 Summary

Two fiber optic interferometers: SLM and SMS fiber structure were successfully constructed and characterized. SLM was fabricated by using a 3dB fiber coupler and a fiber loop with PMF. It allows two beams to propagate in counter directions with different polarization states to produce interference, which is sensitive to the change in surrounding temperature. A SMS fiber structure consists of a short section of MMF, which was

fusion- spliced between two SMFs. The mechanism underpinning the operation of an SMS fiber structure is multimode interference and associated self-imaging. SMS structures can be used in temperature sensing. On the other hand, both GO and Al_2O_3, PVA thin films were also successfully fabricated and characterized.

The linear and nonlinear characteristics of these films were also successfully measured and analyzed. The results indicate the potentiality of these SAs to be used in pulse generation. Applying Pauli blocking principle allows stimulated emission to occur which causes pulse laser to produce. The fabrication cost of both SAs is cheap due to the simplicity of the fabrication process, hence reducing the cost of the laser itself. The simple and low-cost fiber lasers are required in many applications including medical diagnostics and environmental sensing. Table 3.1 summarizes the characteristics of the newly developed SA devices.

Table 3.1: Characteristics of both SA thin films

Materials	**Linear absorption**	**Non-saturable absorption**	**Saturable absorption**	**Saturable intensity**
GO	0.7 dB	35.1%	24.1%	72
Al_2O_3	1.7 dB	13.5%	3.5%	0.05 MW/cm^2

CHAPTER 4 : Q-SWITCHED TUNABLE FIBER LASER WITH SAGNAC LOOP MIRROR

4.1 Introduction

Q-switching is one of the techniques that normally use to enable pulsed lasers. It involves a modulation of Q-factor or losses in a laser cavity. Q-factor is defined as the ratio between the energy stored in the gain medium and the losses per oscillation cycle. The lower losses provide the higher Q-factor. During Q-switching operation, laser generation is initially prevented by the low Q-factor as we pump the gain medium. The stored energy in the gain medium is then released as a giant pulses train when lasing is allowed by a high Q-factor. The pulse width of the generated laser is in a range from μs to ns. The time required to replenish the extracted energy between two consecutive pulses is related to the lifetime of the active fiber. The Erbium-doped fiber (EDF) has a typical lifetime of ~ms and thus the repetition rate of the Q-switched fiber laser is usually in a range of kHz. It is lower compared to a mode-locked laser, which normally operates in MHz range.

Q-switched lasers are also capable to produce much higher pulse energy and they are more advantageous in terms of efficiency, cost, and easy implementation, compared to mode-locked lasers. The mode-locked lasers require a careful design of the cavity parameters to create a balance between dispersion and nonlinearity. Q-switched fiber lasers have many potential applications in areas where ultrafast pulses are not necessary, or larger pulses duration are advantageous, such as sensing, material processing, range finding and medical applications (Shi et al., 2014; Vallet et al., 2013; Zajac et al., 2004; McGrath et al., 1998; Gräf et al., 2015).

Wavelength tunability is a highly desired criterion in various applications including sensing and communications. It can be realized by various techniques. Franco et al. reported that wavelength tuning can be obtained through a manipulation of the cavity loss

(Franco et al., 1994). Tunable fiber lasers were also obtained by controlling the output coupling ratio or by using a variable attenuator to manipulate cavity losses (Lin et al., 2006; Guesmi et al., 2014). A tunable Q-switched EDF laser (EDFL) was also reported in recent years by using a tunable filter. Because of the large insertion losses of this narrow bandwidth filter, the Q-switched pulse was only obtained at the relatively high pump threshold power of 132.4 mW (Wang et al., 2015).

Recently, a fiber Sagnac loop mirror (SLM) has found promising applications in many areas such as sensing and fiber lasers. For instance, more recently a stable and tunable Thulium-doped fiber laser (TDFL) based on Sagnac loop was reported by (He et al., 2016) . However, to the best of our knowledge, there are no reports on tunable Q-switched fiber laser using a SLM. In this chapter, a tunable Q-switched EDFL is proposed and demonstrated based on temperature tuning of SLM in figure-of-eight laser configuration using the newly developed passive SA film as a Q-switcher. Two types of SA are explored in this study: graphene oxide and aluminum oxide (Al_2O_3) thin film. (Rizman et al. 2020).

4.2 Passively Q-switched EDFL with Graphene Oxide SA

In this section, a stable passively Q-switched EDFL tunable by Sagnac interferometer operation was described by using a graphene oxide SA as a Q-switcher. By incorporating the GO polymer film into the laser cavity, Q-switching pulses train was obtained and its wavelength operation can be tunable from 1566.3 nm to 1559.3 nm by increasing the temperature of the SLM. The performance of the laser is investigated for two different operating wavelengths. We achieved the Q-switched operation at so much lower threshold pump power compared to ref. (Wang et al., 2015). The threshold pump power depends on many factors including cavity gain and loss. The lower threshold can be expected with a lower cavity loss. It is important to have a low threshold to improve the efficiency of the laser. The proposed fiber laser has 34% lower threshold pump power as compared to work by Wang et al.

4.2.1 Laser configuration

The SA polymer film was constructed from graphene oxide material produced from a commercial graphene flake via an electrochemical exfoliation process as described in the previous chapter. The graphene solution obtained from this process was then mixed with PVA solution to fabricate a SA film via drop casting technique. The mixed solution was poured into a petri dish and dried at room temperature to produce 50 μm thin film. A small piece of the graphene oxide film was sandwiched in between two optical fiber ferules, which was locked by a fiber adapter to construct a SA device.

The SA device was incorporated into an EDFL cavity, which the schematic configuration is shown in Figure 4.1 for Q-switching pulses generation. The set-up was based on figure-of-eight configuration, which was composed of fiber laser ring cavity and a fiber SLM. A ring cavity consisted of a laser diode pump, 980/1550 nm wavelength division multiplexing (WDM) coupler, 2.4 m long EDF, optical isolator, graphene-oxide based SA and an output coupler (90/10). A 980-nm laser diode was employed to pump the EDF through a WDM to produce the light via spontaneous and stimulated emissions at 1550 nm region. The light oscillates in the ring cavity to generate laser. An isolator was set in the ring cavity to ensure the unidirectional propagation of oscillating laser. The EDF gain medium has a core diameter of 4 μm, a numerical aperture (NA) of 0.16 and an erbium ion absorption of 23 dB/m at 980 nm. A fiber SLM interferometer composed of a polarization maintaining fiber (PMF) that was spliced together with the ring cavity through a 2 × 2 3dB coupler to form a figure-of-eight structure. The PMF part of the SLM was put onto a hot plate to change the interference effect inside the SLM and determine the operating wavelength of the Q-switched laser via a temperature tuning. This was realized as the influenced laser light waves were injected back into the ring cavity. An output coupler kept 90% of the oscillating laser light in the cavity and released 10 % of it for various optical measurements.

The wavelength distribution of the laser output light was observed using an optical spectrum analyser (OSA, Yokogawa AQ6370B), while the temporal analysis was done by a digital oscilloscope (GWINSTEK, GDS-3352), coupled with the photodetector (PD, InGaAs). An RF Spectrum Analyzer (RFSA, Anritsu MS2683A) was used to examine the radio frequency (RF) power spectrum in conjunction with an integrated PD. The output power was measured by using a power meter (ILX Lightwave OMM-6810B) combined with a power-head (ILX Lightwave OMH-6727B InGaAs). By this simple and new arrangement, we find that the Q-switched fiber laser output wavelength is tunable by adjusting the SLM filtering effect via temperature tuning.

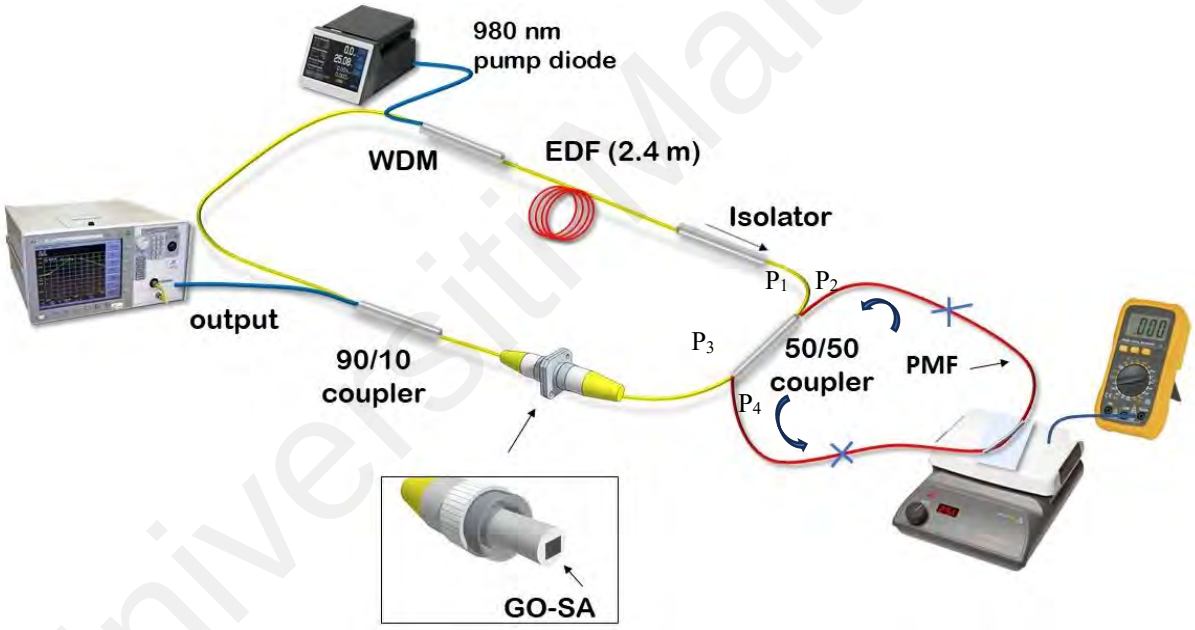

Figure 4.1: Schematic diagram of the Q-switched EDFL with figure-of-eight cavity and GO SA.

4.2.2. Q-switched laser performance

In this work, we employed a SLM with polarization maintaining fiber (PMF) in the proposed tunable Q-switched fiber laser setup to provide spectral filter through the coupling light process between the slow and fast axes of birefringence fiber (PMF) (Sun et al., 2008). In the SLM interferometer, input signal is split into two beams after the 3dB coupler to counter propagate along the loop arm. After propagation in loop, both beams are recombined at the same coupler to produce interference, which provide filtering effect depending on birefringence properties of the cavity. The SLM was used in this work as an interference filter due to its intrinsic advantages such as easy fabrication, flexibility and stability. The tuning of the laser is realized by the change of effective length of the PMF induced by the temperature applied to the fiber.

In the SLM, the input light signal at the 3dB coupler is split into two beams counter-propagating in loop and their polarization states are altered by the temperature. These two beams propagate inside the PMF in opposite direction and thus they experience different phase delay as they recombined at the coupler. The delay is proportional to the product of the PMF length and effective birefringence and thus the mode spacing of the SLM is obtained as follow (Kim, 2004);

$$\Delta\lambda = \frac{\lambda^2}{2|n_s - n_f|L_{PMF}} \tag{4.1}$$

where λ is the operating wavelength, n_s, n_f is the refractive index of the slow and fast birefringence axes of the PMF, respectively and L_{PMF} is the PMF length. As can be seen from the above equation, the spacing of the wavelengths decrease with the increase of the PMF length. The SLM interferometer serves as the wavelength selection component within the ring laser cavity. By tuning the temperature of PMF to effectively change the effective length of the fiber, the operating wavelength of the Q-switched laser shifts to a shorter wavelength.

When the graphene oxide SA device is introduced inside the cavity, a self-started Q-switching pulses are generated when the input pump is increased above the certain threshold pump power. The output spectra of the Q-switching pulses at various temperatures is shown in Figure 4.2 when the pump power is fixed at the Q-switching threshold power. The operating wavelength of the Q-switched laser shifts from 1566.3 nm to 1559.3 nm as the temperature is varied from 30°C to 70°C. At operating wavelength of 1566.3 nm, Q-switched laser self-started as the operating pump power is raised to 77.3 mW and this operation is maintained up to the pump power of 126.5 mW. Figures 4.3 (a) and (b) illustrate the oscillation trace of Q-switched EDFL and single pulse envelop at the threshold pump power of 77.3 mW respectively. At the threshold pump power, the laser produces a typical Q-switching pulse shape with 32.6 μs of distance between pulses, which corresponds to a repetition rate of 30.7 kHz. A single pulse profile at this pump power has full width half maximum (FWHM) of 10.2 μs as shown in Figure 4.3 (b).

To investigate the laser stability, the RF spectrum was measured at the maximum output power using the InGaAs photodiode and an RF spectrum analyzer (Anritsu, MS2683A). Figure 4.3 (c) shows the RF spectrum with a span resolution bandwidth of 600 kHz at 106.8 mW pump power. As shown in inset of Figure 3 (c), the signal-to-noise (SNR) of the Q-switched EDFL is over 40 dB, indicating that the Q-switched pulses operated in a relatively stable regime. The fundamental frequency is 37.0 kHz, corresponding to the frequency of the pulse train. The generation of more than 10 harmonics in the RF spectrum of Figure 4.3(c) further confirms the stability of Q-switching operation.

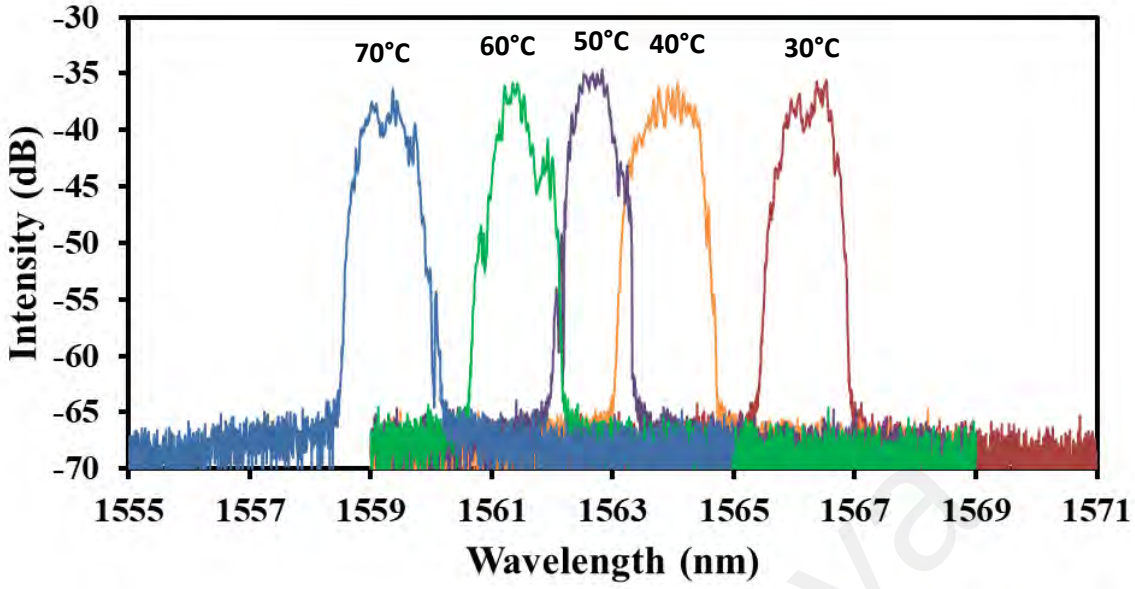

Figure 4.2: Output spectra of the Q-switched EDFL at various temperature applied to PMF.

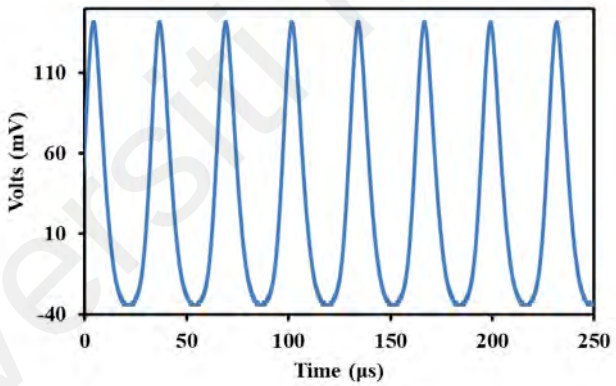

(a)

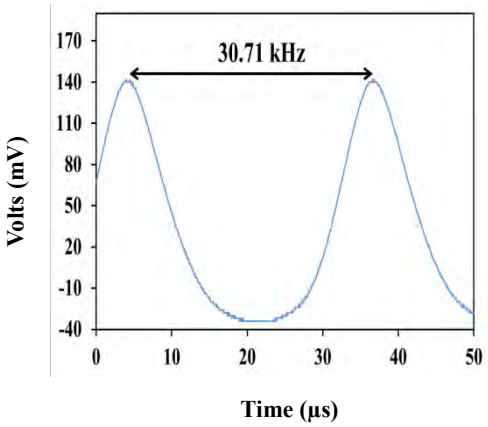

(b)

Figure 4.3, continued.

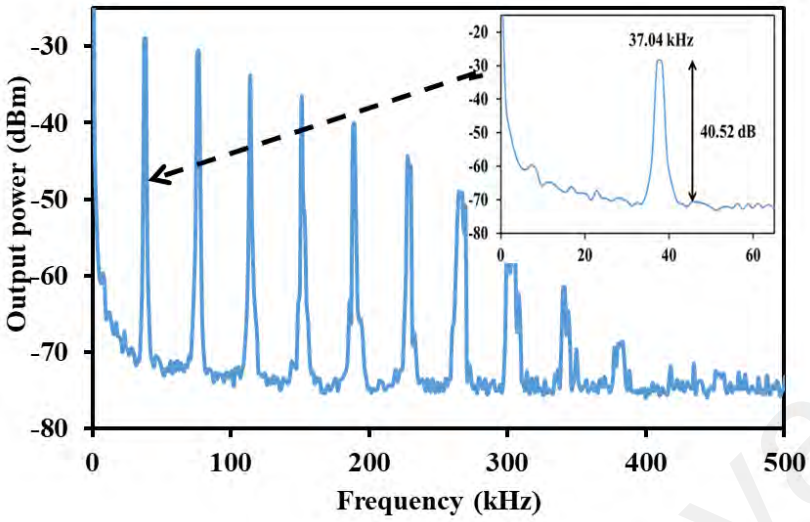

(c)

Figure 4.3: Temporal characteristics of the Q-switched laser at operating wavelength of 1566.3 nm (a) typical pulse train (b) enlarged pulse train (c) RF spectrum. Inset of (c) shows the enlarged RF spectrum at the fundamental frequency.

As the temperature applied onto the PMF is increased, the operating wavelength of the Q-switched laser shifted to a shorter wavelength and the threshold pump power for Q-switching operation is also increased. For instance, at temperature of 60°C, the Q-switched laser operates at 1561.4 nm at the threshold pump power of 116.7 mW. The threshold increases due to insertion loss of the sagnac loop mirror, which increases with the temperature.

The temporal characteristics of the Q-switched EDFL operating at 1561.4 nm is shown in Figure 4.4. Figures. 4.4 (a) and (b) illustrate the pulses train and the corresponding single pulse envelop at the threshold pump power of 116.7 mW, which indicate a typical Q-switching pulse shape. For instance, a distance between pulses of 35.1 µs was obtained, which correspond to repetition rate of 28.5 kHz while a single pulse profile at this pump power has full width half maximum (FWHM) of 8.4 µs. The RF output spectrum with

600 kHz span resolution was measured and illustrated in Fig. 4(c) when the pump power was fixed at 161 mW. The fundamental RF at maximum output pulse of 32.9 kHz was observed to have a signal-to-noise ratio (SNR) of ~40.9 dB, which confirms the stability of the pulse. In the Q-switched trace we observe more than 15 harmonics frequency positioned within 600 kHz span.

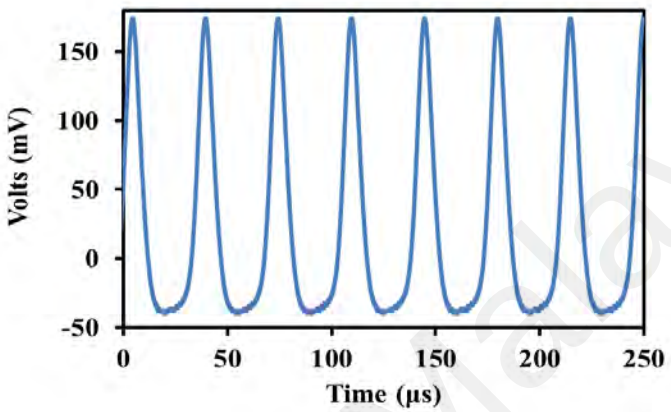

(a)

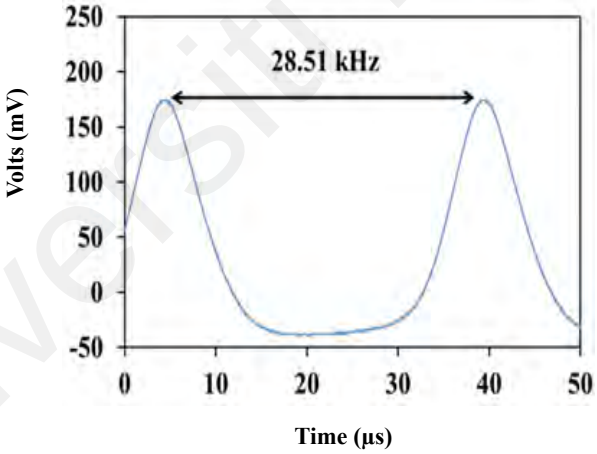

(b)

Figure 4.4, continued.

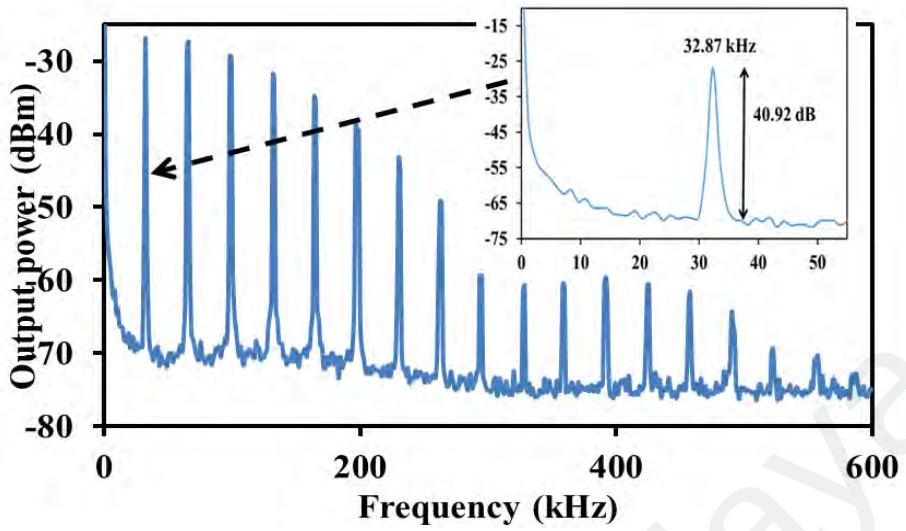

(c)

Figure 4.4: Temporal characteristics of the Q-switched laser at operating wavelength of 1561.4 nm. (a) typical pulse train (b) enlarged pulse train (c) RF spectrum. Inset of (c) shows the enlarged RF spectrum at the fundamental frequency.

Figure 4.5 shows the relationship between repetition rate and pulse width with different input pump power for both operating wavelengths; 1566.3nm and 1561.4 nm. Stable output pulses train with monotonic increment of repetition rate with pump power is observed for both operating wavelengths. For instance, the repetition rate increased from 30.7 kHz to 41.5 kHz as the 980-nm pump power is varied in a range from 77.3 mW to 126.5 mW at operating wavelength of 1566.3 nm. On the other hand, the pulse duration of the 1566.3 nm laser was narrowed or shortened from 10.2 to 7.3 μs with the increment of pump power. The result is a typical characteristic of Q-switching operation.

The average output power and single pulse energy of the Q-switched laser were also measured as a function of the input pump power for both operating wavelengths. The result is shown in Figure 4.6, indicating the increase of pulse energy and output power for both wavelengths with the increment of pump power. Both trends are realized from

the strong modulation of the net gain. The increment of pump power leads to a raise of average output power and shorten the pulse width and hence higher pulse energy is extracted in the Q-switching process. At operating wavelength of 1561.4 nm, the average power increased from 0.46 mW to 0.68 mW, which translates to the slope efficiency of 0.49%. This efficiency is larger compared to the 1566.3 nm laser, which has the efficiency of about 0.28%. This is attributed to the Erbium gain, which is larger at 1561.4 nm region and thus increases the population inversion. On the other hand, the maximum pulse energy of 20.5 nJ is obtained at the pump power of 161.0 mW for 1561.4 nm laser. The Q-switching performance are comparable to the previous works. (Wang et al., 2022)

Meanwhile, it is worthy to note that no mode-locking operation has been observed with the current cavity. It is expected that the mode-locking pulses could also be achieved when the dispersion and SPM parameters of the cavity are optimized. The performance of Q-switched laser could also be improved by further optimizing the SA parameters and the laser cavity design.

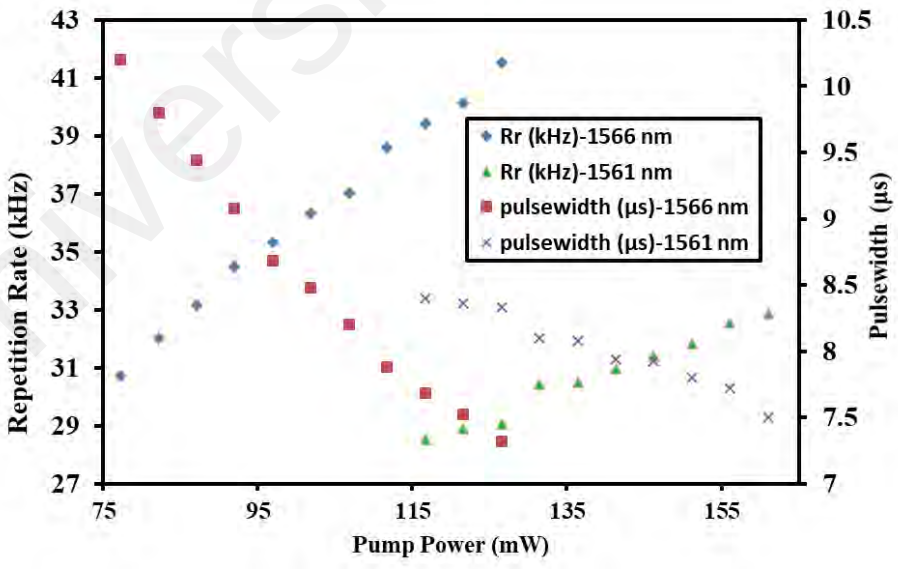

Figure 4.5: Pulse repetition rate(Rr) and pulse width of the GO based Q-switched EDFL against pump.

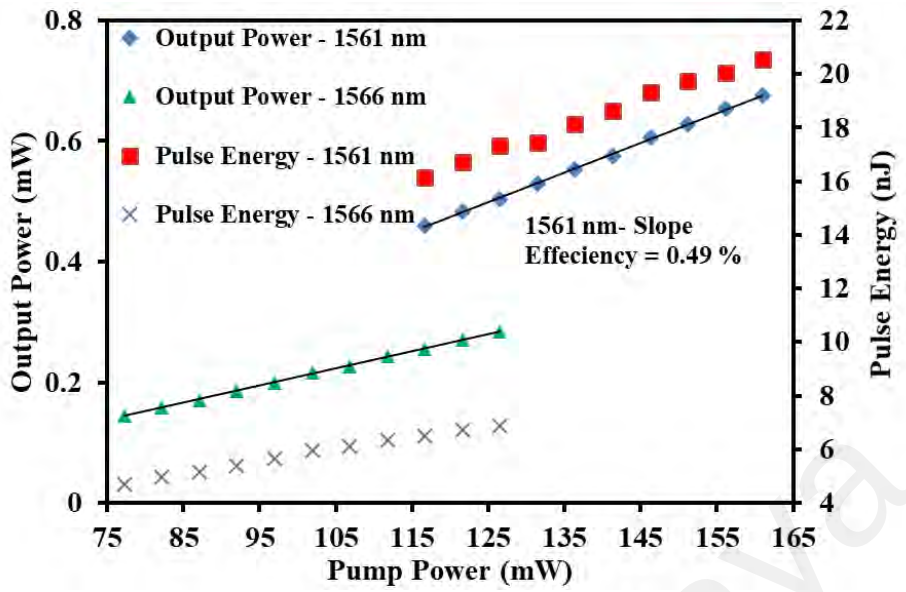

Figure 4.6: Average output power and pulse energy of the GO based Q-switched EDFL against pump.

4.3 Q-switched Tunable Fiber Laser with Aluminum Oxide SA

Despite the recent development in SA technologies, the focus is shifting toward utilizing inexpensive SA. Recently, the utilisation of Al_2O_3 nanoparticles for SA application seems promising as it has unique optical properties such as high nonlinearity in the near-infrared region (Apel et al., 2000). It was also widely employed in medical and industrial applications due to its many advantages in terms of high hardness, transparency, and high stability (Hart, 1990). Compared to other metal such as silver and gold, aluminium offers a broader plasmon resonance band, lower cost, wider availability and has a lower melting point of around 660 °C, which simplifies the fabrication process of nanoparticles.

In this section, a tunable Q-switched EDFL is proposed and demonstrated using a new thin film SA, which was developed based on Al_2O_3 nanoparticles in conjunction with a SLM filter. Besides its ability to function as Q-switcher, Al_2O_3 thin film can also be obtained through an inexpensive and simple preparation process. By inserting the Al_2O_3

polymer film into the proposed figure-of-eight laser cavity, we obtained a stable Q-switching pulses train. The tunability of the operating wavelength of the laser from 1568 nm to 1556 nm can be achieved by varying the applied temperature to the SLM.

4.3.1 Laser Configuration

In this experiment, the SA film was fabricated using a commercially available few-layer Al_2O_3 nanostructures, which were embedded into Polyvinyl alcohol (PVA) based on a casting method. The produced Al_2O_3 PVA thin film has a thickness of about 30 μm and it was cut into a tiny piece so that it can be attached onto a FC/PC ferrule to form a SA device. Figure 4.7 shows the schematic diagram of the experimental setup for the proposed tunable Al_2O_3 based Q-switched EDFL, which was composed of a figure-of-eight ring structure cavity. The ring cavity employed Al_2O_3 film as the SA device while a fiber SLM was used as a tunable filter. A 2.4 m long EDF similar to the previous work was employed in the laser cavity as a gain medium. A 980 nm laser diode pumped the EDF through a WDM coupler to generate laser through the production of amplified spontaneous emission light, which oscillated in the figure-of-eight cavity.

The unidirectional propagation of the oscillating laser in the laser cavity was ensured through the deployment of an optical isolator. The Al_2O_3 film SA device was incorporated into the laser cavity to modulate the loss in the cavity and function as a Q-switcher. A fiber based SLM was constructed by splicing together a piece of PMF with the ring cavity through a 2 × 2 3dB coupler. The combination of SLM and the ring cavity formed a figure-of-eight cavity. The PMF part of the SLM was heated by placing it onto a hot plate to control the interference effect inside the SLM. Furthermore, the changes in the applied temperature tuned the laser operating wavelength.

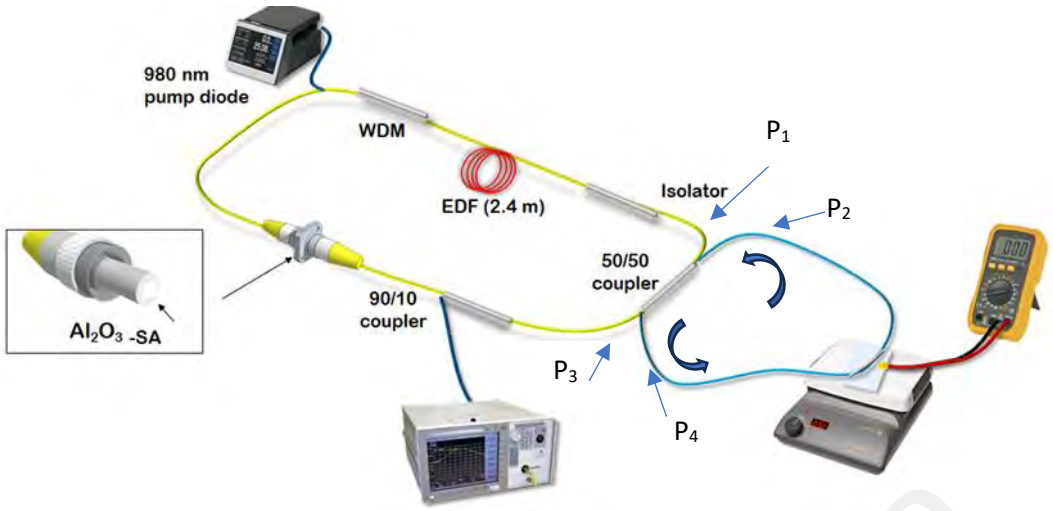

Figure 4.7: Experimental setup of the tunable Q-switched EDFL with Al_2O_3-PVA SA based on a figure-of-eight cavity arrangement.

The output of the laser was tapped out using a 10dB output coupler. This coupler channels 10% of laser light as its the output while permitting 90% of the laser light to oscillate in the ring. The optical spectrum of the output laser was measured using an OSA with a resolution of 0.02 nm. A digital oscilloscope in conjunction with an integrated fast photodetector was used in the analysis of the temporal characteristic of the laser. The electrical spectrum was examined by an RFSA in conjunction with the photodetector. A power meter coupled with an InGaAs powerhead was used for the output laser power measurement.

In the proposed setup, we used the SLM with a temperature tuning ability as an interference filter. It is observed that the operation of the Q-switched fiber laser can be tuned by the varying the applied temperature to the PMF inside the SLM structure. The input signal into the SLM was split using the 3dB coupler, into two beams and counter propagated along the loop arm. After propagating into the loop, they were then recombined and interfered at the same 3 dB coupler. The coupling between the two beams propagating at the slow and fast axes of the birefringence fiber (PMF) provided the filtering effect. The operational wavelength of the laser was governed by the birefringence properties of the cavity, which can be controlled by the temperature (Sun et al., 2008).

The SLM filter has intrinsic advantages of ease of construction, stable and flexible. The tunability of the operational wavelength of the laser can be achieved by varying the applied temperature to the fiber, which affects the PMF's effective length.

4.3.2 Result and discussion

As we incorporated the Al_2O_3 PVA SA device inside the cavity and set the input pump power above a certain threshold power, a self-starting Q-switching pulses train was successfully produced. Figure 4.8 shows the output spectra of the laser at different temperature settings with a fixed pump power at the Q-switching threshold power. The operational wavelength of the laser is tunable from 1568 nm to 1556 nm as the temperature applied to the SLM is varied from 30 °C to 70 °C. This is attributed to the SLM, which functions as a tunable filter in the figure-of-eight resonator. The 3 dB coupler is used to split the input light signal into the SLM into two. These beams are counter-propagated in the loop and their polarization states can be easily changed by the temperature applied to the PMF.

The phase delay for each of the two beams will be different when they recombine at the 3dB coupler since they are propagating in the opposite direction inside the PMF. The delay produces a mode spacing, which is depended on the length of the PMF, and effective birefringence parameter as described in Equation (4.1). It is reported that an increase in the PMF length will cause the mode spacing to decrease (Kim, 2004). As shown in Figure 4.8, the Q-switching operational wavelength shifts with the temperature due to the temperature tuning of PMF. The applied temperature effectively changes the PMF effective length to shift the laser wavelength towards a shorter region.

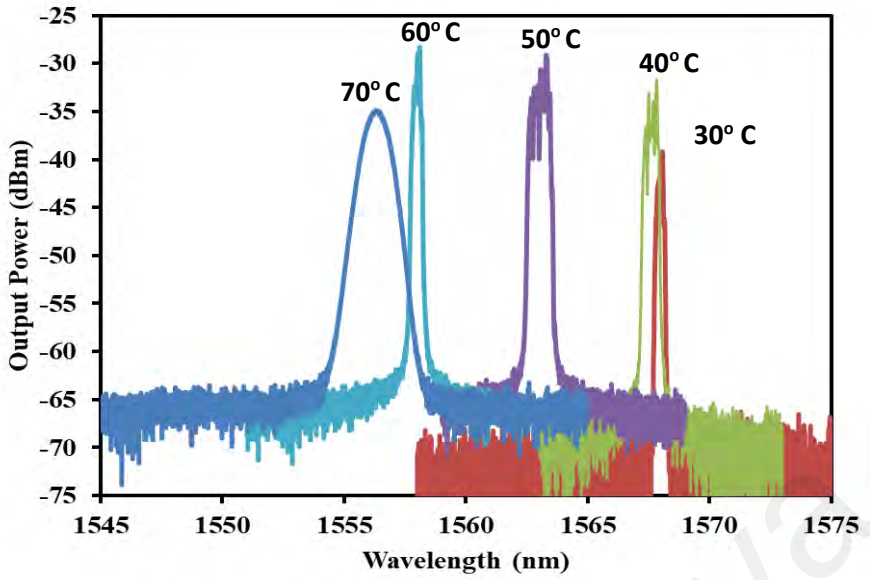

Figure 4.8: Output spectrum of the Q-switched laser at different temperature settings for the SLM.

At first, we fixed the temperature at 30 °C so that the laser operated at 1568 nm wavelength. It was observed that the fiber laser self-started Q-switching pulses at 53 mW threshold pump power and its operation was sustained up to 87 mW pump power. When the temperature was increased, the operating wavelength decreased to a shorter wavelength and the threshold pump power increased. For instance, the Q-switching pulses were obtained within a pump power range from 127 to 171 mW when the operating wavelength was fixed at 1556 nm.

This is most probably due to the SLM's loss which is higher as we increase the temperature applied to the PMF. It is apparent that the operating photon energy of our work (0.81 eV) was much lower than the bandgap of Al_2O_3, the results indicate that sub-bandgap absorption is responsible for the passively Q-switched operation. It is well-known that there is no sub-bandgap absorption in a perfect crystal. However, in a finite system, the sub-bandgap absorption at low photon energies could also be realized which can be attributed to the energy levels within the bandgap that arises from the edge-state.

In our opinion, the sub-bandgap absorption observed in our work is also attributed to the edge-state absorption of the Al_2O_3.

Figures 4.9 (a) and (b) show the temporal and frequency characteristics of the Q-switched laser, respectively when the operating wavelength and pump power were fixed at 1556 nm and 176 mW, respectively. The laser generated a typical Q-switching pulse shape as shown in Figure 4.9 (a). The distance between pulses was 29.36 µs, which corresponds to a repetition rate of 34.06 kHz. Inset of Figure 4.9 (a) shows the corresponding single pulse profile which indicates the full width half maximum (FWHM) of 7.44 µs. Figure 4.9 (b) shows the RF spectrum obtained at 176 mW pump power. It was used to investigate the stability of the laser. A resolution bandwidth span of 600 kHz was used in the RF spectrum measurement. The spectrum shows the fundamental frequency at 34.06 kHz with the signal-to-noise (SNR) of 42.2 dB, which indicates the stability of the Q-switching operation. At least 16 harmonics were generated in the RF spectrum as shown in Figure 4.9 (b).

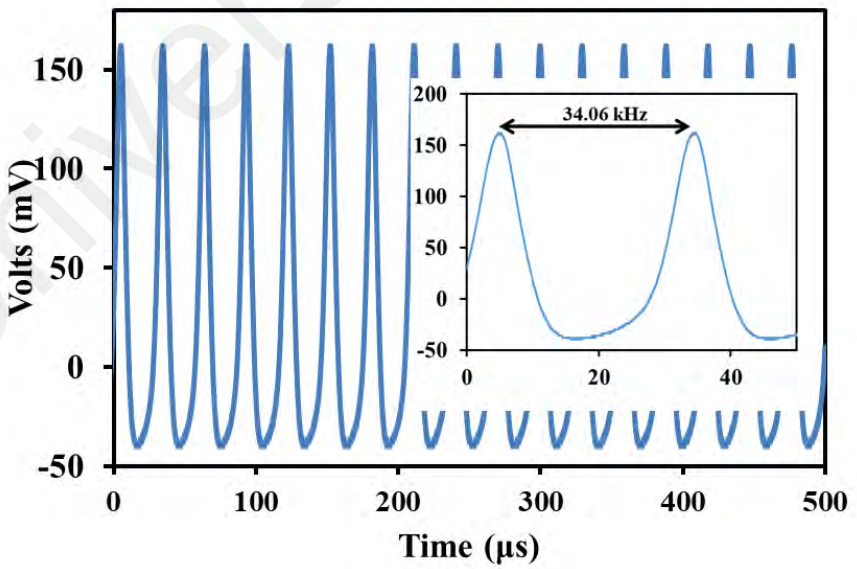

(a)

Figure 4.9, continued.

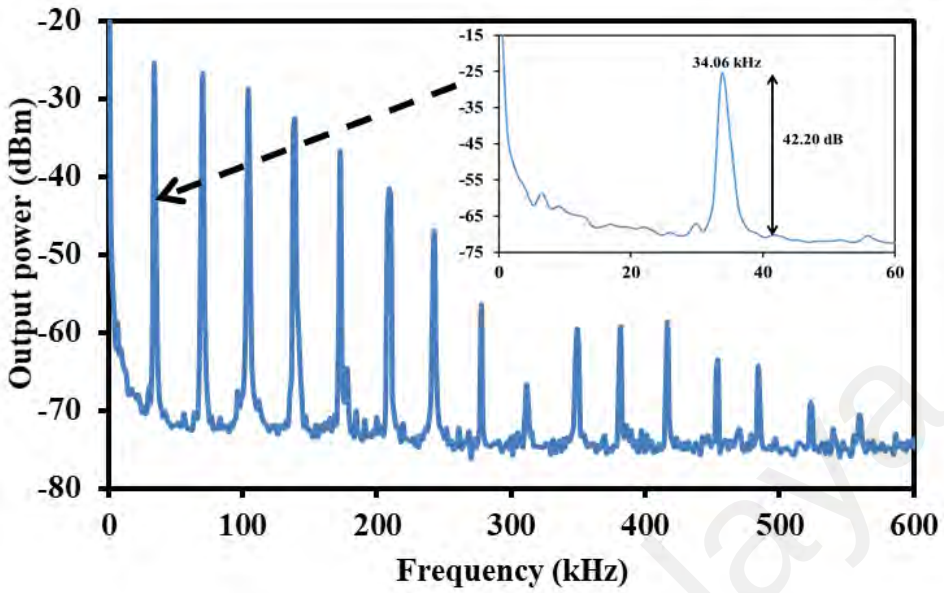

(b)

Figure 4.9: Temporal characteristics at operating wavelength of 1556 nm and pump power of 176 mW (a) typical oscilloscope trace. Inset shows the enlarged pulse train (b) RF spectrum with the inset showing the fundamental frequency in the enlarged RF spectrum.

The temporal and frequency characteristics are presented in Figure 4.10 for operation at 1568 nm. Figure 4.10 (a) illustrates the typical oscilloscope trace at the pump power of 87 mW which indicates a typical Q-switching pulse shape with a 26.25 kHz repetition rate. The distance between pulses is 38.1 μs. Figure 4.10 (b) shows the output RF spectrum with a resolution span of 600 kHz at the pump power of 87 mW. At maximum output pulse, the fundamental frequency of 26.25 kHz was observed with a SNR of ~38.3 dB, which indicates the stability of pulses. More than 18 harmonics frequency can be observed within 600 kHz span.

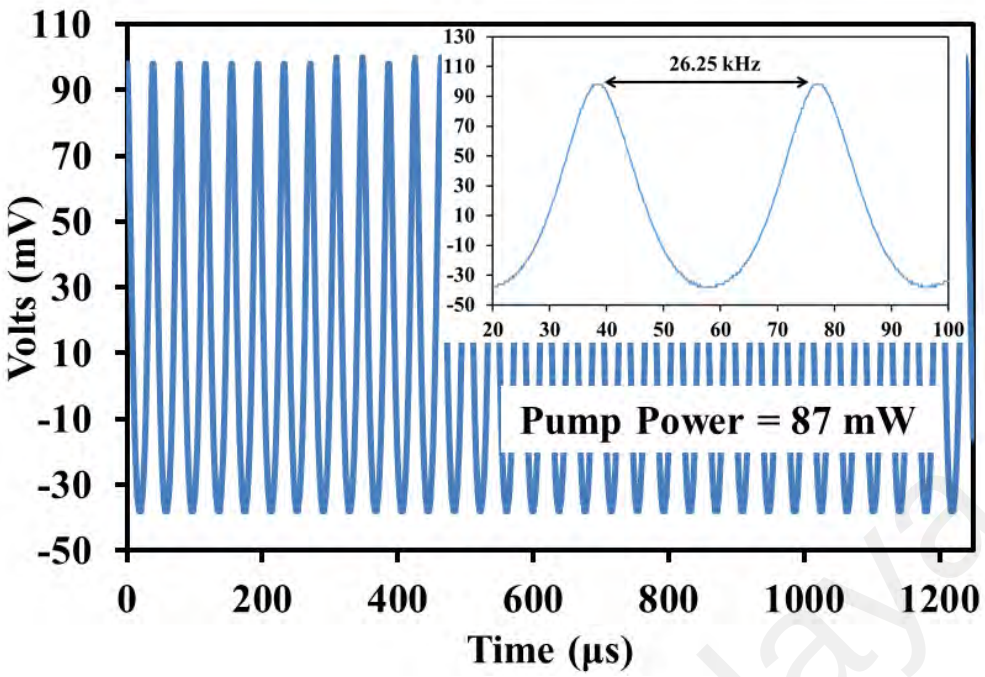

(a)

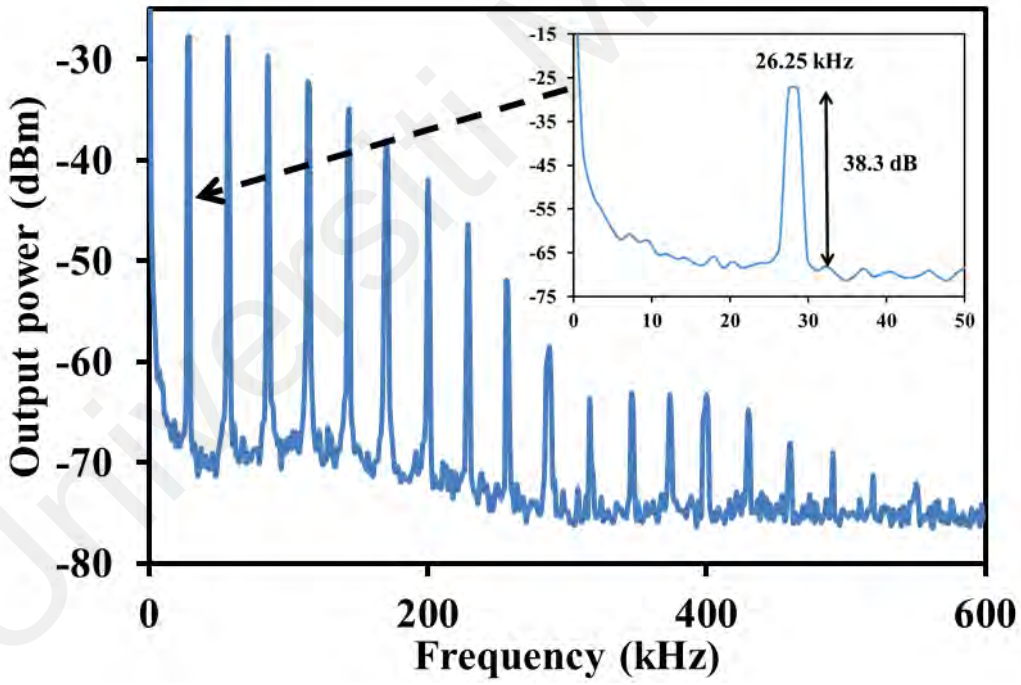

(b)

Figure 4.10: Temporal and frequency characteristics of the Q-switched laser operating at wavelength of 1568 nm when the pump power was 87 mW (a) typical pulse train. Inset shows the enlarged pulse train (b) RF spectrum within 600 kHz span. Inset shows the fundamental frequency at 26.25 kHz in the enlarged spectrum.

The repetition rate and pulse width characteristics were also analyzed for both operating wavelengths; 1556 nm and 1568 nm at various pump power. The result as illustrated in Figure 4.11 indicates that the pulse repetition rate increases linearly with the pump power. For instance, at operating wavelength of 1568 nm, the repetition rate increases from 13.66 kHz at threshold pump power of 53 mW to 26.25 kHz at 87 mW pump power. Conversely, the pulse width decreases exponentially from 18.5 to 14.2 µs with the rise of pump power from 53 mW to 87 mW. This trend is typical for a Q-switched fiber laser.

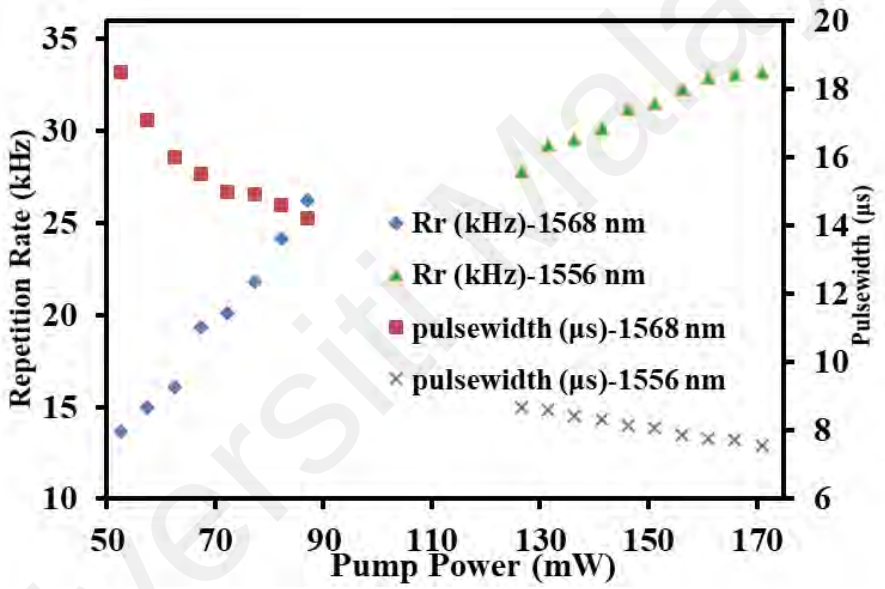

Figure 4.11: The repetition rate(Rr) and pulse width performance with the change of pump power for the proposed Al_2O_3 based laser.

Figure 4.12 presents the average output power and single pulse energy as measured at various pump powers for two different operational wavelengths. As the pump power is increased, the output power and pulse energy increase as well for both wavelengths.

This trend is obtained due to the modulation of the net gain with the pump power. The rise in pump power is causing the average output power to increase and the pulse width to decrease. This indicates that the Q-switching process generated higher pulse energy. At 1556 nm operating wavelength, the laser has an efficiency of 0.59% as can be derived

from the increment of the output power from 0.62 mW to 0.91 mW. However, the 1568 nm laser has slightly higher slope efficiency at about 0.65%. This trend is attributed to the SLM loss, which is larger at the higher temperature of 1556 nm operation and thus slightly reduces the efficiency of the laser. At 171 mW pump power, the maximum pulse energy of 27.4 nJ was obtained for the laser operating at 1556 nm. The performance of the Q-switched laser could be further improved through the optimization of the laser cavity design as well as the SA parameters.

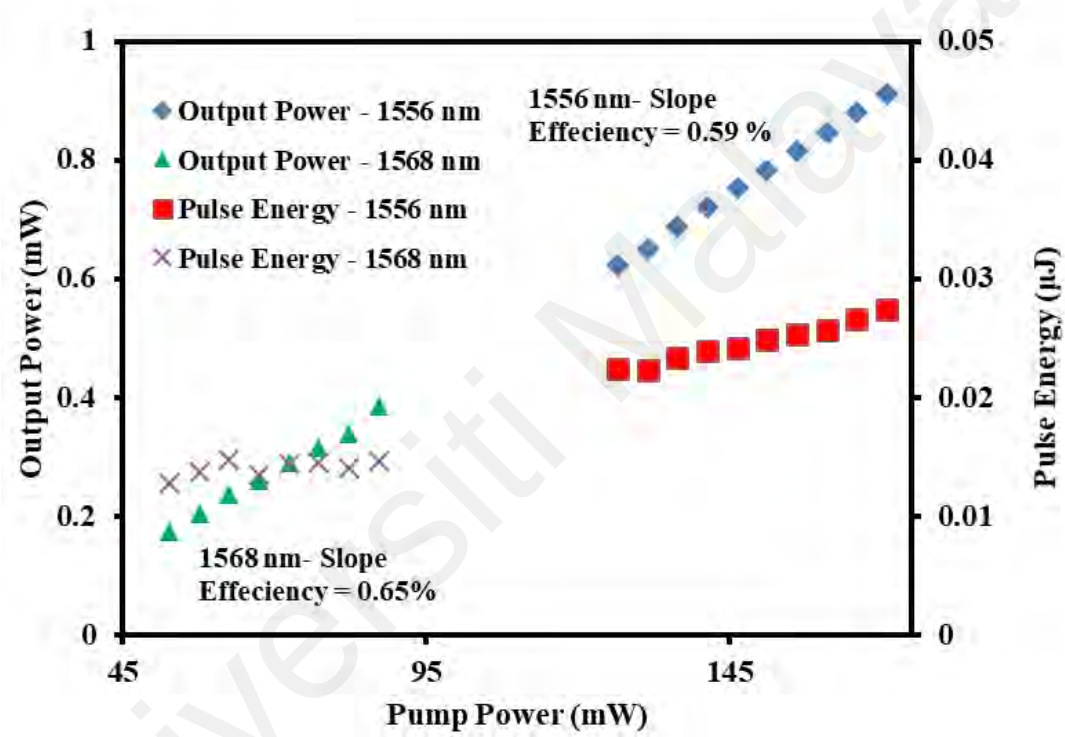

Figure 4.12: The output power and pulse energy agaist pump power for the proposed Al_2O_3 based laser.

In Figure 4.12, the pulse energy for 1568nm has minimal increase compared to the pulse energy at 1556nm. The EDF has a lower gain at longer wavelength. Therefore, the increase of energy is lower at 1568 nm as compared to 1556 nm.

4.4 Summary

Wavelength tunable Q-switched fiber lasers have been successfully demonstrated using Sagnac loop mirror in figure-of-eight laser cavity. At first, a stable passively Q-switched EDFL tunable by Sagnac interferometer operation was described by using a graphene oxide SA as a Q-switcher. By tuning the temperature of SLM from 30ºC to 70ºC, the central wavelength of the Q-switched EDFL could be tuned continuously from 1566.3 nm to 1559.3 nm. At 1566.3 nm operation, the repetition rate increased from 30.7 kHz to 41.5 kHz while pulse width reduced from 10.2 to 7.3 μs as the pump power is varied from the threshold of 77.3 mW to 126.5 mW.

The Q-switching threshold pump power increased while the laser efficiency improved with the increase the temperature. At 1561.4 nm operation, the maximum pulse energy of 20.5 nJ was obtained at pump power of 161.0 mW. A tunable Q-switching pulses train was also successfully realized using Al_2O_3-PVA thin film as a SA in a similar cavity arrangement. By varying the temperature applied to SLM from 30°C to 70°C, it is possible to continuously tune the Q-switched laser operating wavelength from 1568 nm to 1556 nm. At 1556 nm operation, the Q-switching frequency rose from 13.66 kHz to 26.25 kHz while the pulse width shrunk from 18.5 to 14.2 μs with variation of pump power from 53 mW (threshold pump power) to 87 mW. It is found that the Q-switching threshold pump power is higher at higher temperature. As the laser operated at 1568 nm and pump power of 171 mW, the maximum pulse energy obtained was 27.4 nJ.

The laser performance becomes unstable due to the higher temperature fluctuation at higher temperature setting (higher than 70°C). The graphene oxide-based Q-switched laser performed better since the smaller pulse duration and higher repetition rate are obtained. Both Q-switched tunable EDFLs are simple and cost effective and thus they may be useful for various practical applications.

CHAPTER 5: DUAL-WAVELENGTH Q-SWITCHED ERBIUM-DOPED FIBER LASER USING A SMF–MMF–SMF STRUCTURE AND GRAPHENE OXIDE

5.1 Introduction

Dual-wavelength fiber lasers have gained tremendous attentions in recent years for their application in various areas including the generation of Terahertz (THz) signal (Majkić et al., 2014; Li et al, 2019). The THz radiations bring significant value in various applications such as imaging, sensing, manufacturing, military, spectroscopy, and communication (Debus & Bolivar, 2007; Zhang et al., 2013). On the other hand, Erbium-doped fiber (EDF) has been proven to be an outstanding candidate as gain medium for low absorption loss and highly efficient lasing in the near-infrared spectral range. This is attributed to Erbium ions, which has ultra-low quantum defect and high quantum efficiency as it is pumped at 980 nm (Zhang et al, 2020). In addition, EDF possesses broad emission spectrum with high excitation from 1.5 to 1.6 μm, in which the wavelength regions around 1.53 μm and 1.56 μm are the two humps of the emission spectrum (Guo et al., 2021). The gain peak typically occurs at the wavelength region around 1.53 μm, being most pronounced for high excitation levels. Thus, EDF is particularly suitable for generation of dual-wavelength pulses through spectrum filtering.

However, the wide wavelength spacing enlarged by the homogeneous gain broadening can lead to inherent instability of the emitting pulses, which brings trouble to obtain stable multi-wavelength pulse operation due to the mode competition. Many methods have been investigated to stabilize the multi-wavelength fiber lasers, such as via cooling EDF in liquid nitrogen (Yamashita, & Hotate, 1996), inhomogeneous loss mechanisms (Pan et al., 2006), and the four-wave mixing effect (Han et al., 2006), and the polarization hole burning effect (Lian et al., 2017). Furthermore, a nonlinear saturable absorber (SA) device combined with wavelength selectors including fiber Bragg grating (Guo et al., 2021) and

fiber taper (Wang et al., 2016) is an alternative method to realize multi-wavelength operation of pulsed fiber laser. Compared with the wavelength selectors, the fiber-based nonlinear polarization rotating (NPR) technique provides a better way to realize multi-wavelength generation with flexibly controlled birefringence (Zou et al., 2018). Compared to the previous techniques, the single mode fiber–multimode fiber–single mode fiber (SMF–MMF–SMF) structure-based filter is simpler (Zhu et al., 2021). It can provide a higher thermal damage threshold while allowing the pulse generation with higher energy.

Q-switched fiber laser with passive SA has been widely studied to generate short laser pulses for various applications range finding, remote sensing, and medical treatment (Soboh et al., 2021; Xu et al., 2014). Low-dimensional materials have been widely used to modulate the circulating lases recurringly in the laser cavity and generate pulse train in temporal domain (Luo et al., 2010; Ismail et al., 2016; Zhou et al., 2019; Rusdi et al., 2018; Luo et al., 2014). In this chapter, we demonstrate a dual-wavelength Q-switched fiber laser operation using a SMF–MMF–SMF structure and graphene oxide as filter and SA, respectively. The dual-wavelength operation at 1549.6 nm and 1558.6 nm was achieved based on multimode interference effect while the Q-switching operation was achieved due to the saturable absorption effect of graphene oxide. When the pump power is fixed at the maximum power of 225.1 mW, the Q-switched pulse had a repetition rate of 65.3 kHz, together with pulse duration and pulse energy of 2.9 μs and 15.2 nJ, respectively. (Salman et al. 2019; Riehle et al., 1991; Xu et., 2011;)

5.2 Preparation of laser setup

In the experiment, the multimode interference (MMI) filter was fabricated by sequentially fusion splicing of the SMF, a section of 5.1 cm step index MMF, and the SMF, as shown in Fig. 5.1 (a). The SMF has a core/cladding diameter of 9/125 μm while

the MMF has a core/cladding diameter of 50/125 µm. The transmission spectrum of the SMF–MMF–SMF structure was measured to verify this proposed MMI device is suitable as the filter as shown in Fig. 5.2 (b). The MMI device has a wide transmission spectrum from 1520 to 1570 nm. It has several transmission peaks, which are located at 1521 nm, 1531 nm, 1549 nm, 1561nm, and 1569 nm which are beneficial to filter wavelength of light transmission.

(a)

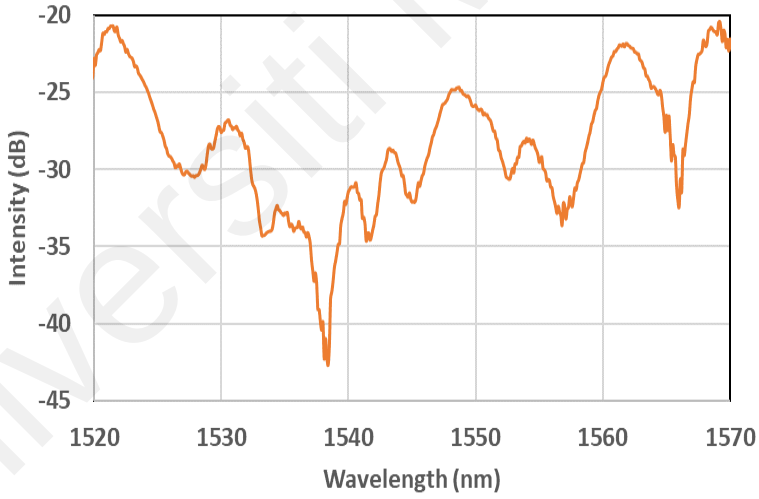

(b)

Figure 5.1: (a) SMF–MMF–SMF structure and (b) its transmission spectrum.

The working principle of SMF–MMF–SMF structure could be explained as follows: when light wave from the first SMF enters step index MMF, it excites transverse modes. Whenever these modes have developed a phase shift that is a multiple of π, it causes interference, and the light wave field is allowed to be coupled into the second SMF. Since

the interference depends on the wavelength and the inverse propagation constants of the transverse modes, such SMF–MMF–SMF structure can be employed as a filter.

The saturable absorber (SA) used in this work is based on graphene oxide (GO) material, which was produced from graphene flakes obtained through an electrochemical exfoliation. During the exfoliation process, a pair of graphite rods was placed inside electrolyte liquid, which was obtained by mixing 1% sodium dedocyl sulphate (SDS) in deionized water. The graphite rod functions as an electrode. An electrical potential was applied between the electrodes, it forces the positive and negative ions to move toward the cathode and anode, respectively. This process removed the graphene layers form the graphite rod and after two hours, a stable graphene suspension can be produced. The graphene suspension was then centrifuged at 3000 rpm for about 30 minutes to split large agglomerates.

The supernatant portion of the graphene suspension was then decanted to get a homogeneous GO solution. The GO solution obtained was then mixed with PVA solution to fabricate a SA film via drop casting technique. The mixed solution was poured into a petri dish and dried at room temperature to produce 50 μm thin film. The GO PVA film was then cut into a small piece so that it can be attached onto a fiber ferrule with the assistance of index matching gel. The ferrule is connected and locked to another fresh ferrule via physical contact adapter to form all fiber SA device. The index matching gel functions to reduce a spurious reflection at the connection.

Fig. 5.2 depicts the experimental setup of the proposed dual-wavelength Q-switched EDFL based on ring cavity using a SMF–MMF–SMF structure and GO SA as a filter and Q-switcher, respectively. A 2.4 m long erbium-doped fibre (EDF) is used as gain medium. It is pumped by a 980 nm laser diode via a wavelength division multiplexer (WDM) to generate an amplified spontaneous emission (ASE) operating at 1550 nm region. A GO SA assembly and MMI filter are integrated inside the ring cavity as a

component to generate the Q-switched dual-wavelength laser. An isolator is used to force a unidirectional light propagation inside the ring cavity and ensure the stability of the Q-switched operation. The optical spectrum, pulse train and electrical spectrum of the output laser from 10% port of output coupler was monitored by an optical spectrum analyzer, oscilloscope, and radio frequency spectrum analyzer (RFSA), respectively. High speed photodetector is used to convert the optical signal to electrical signal for use in oscilloscope and RFSA.

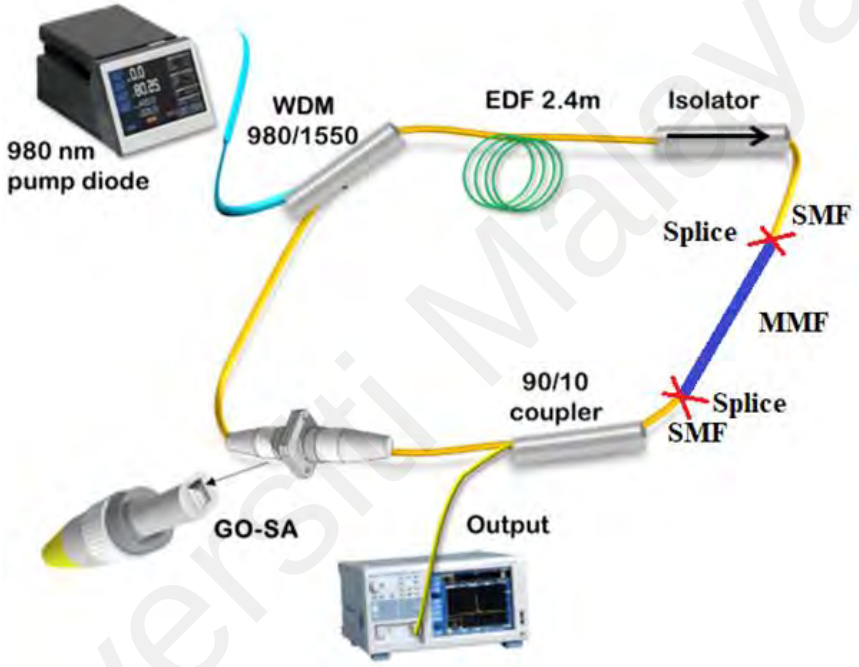

Figure 5.2: Configuration of the dual-wavelength Q-switched laser with GO SA and SMF–MMF–SMF structure.

5.3 Laser performances

Once the pump power is increased to 200.6 mW, the dual-wavelength Q-switched laser was self-started. The Q-switching operation is maintained up to the maximum pump power of 225.1 mW. The output spectrum of the dual-wavelength Q-switched fiber laser at pump power of 225.1 mW is shown in Fig. 5.3. It is observed that the dual wavelengths of outputs are located at 1549.6 nm and 1558.6 nm with a spacing of 9.0 nm. The dual-

wavelength operation was obtained due to the SMF–MMF–SMF structure, which provides spectral filtering effect in the laser cavity. Only two wavelengths are allowed to oscillate due to the gain spectrum of the EDF, which prominent at 1550-1560 nm region due to the high erbium concentration and pumping power in the laser cavity. Without the SA, the laser operates in continuous wave mode.

Fig. 5.4 shows the typical pulse train for the dual-wavelength Q-switched EDFL at 225.1 mW pump power. It was recorded for 1000 µs time span and no significant distortion or fluctuation was observed. The pulse train has repetition rate of 65.27 kHz, corresponding to the time interval of 15.3 µs. The inset of Fig. 5.4 shows the profile of the dual pulse envelop, which indicates the full width half-maximum (FWHM) of 2.9 µs for the output pulses. It has a symmetric temporal profile. The corresponding RF spectrum is also measured as shown in Fig. 5.5 at 225.1 mW pump power. The fundamental frequency is obtained at 65.27 kHz, which is consistent with the oscilloscope data of Fig. 5.4. The signal-to-noise ratio (SNR) is about 45.1 dB, which indicates the high stability of the dual-wavelength operation.

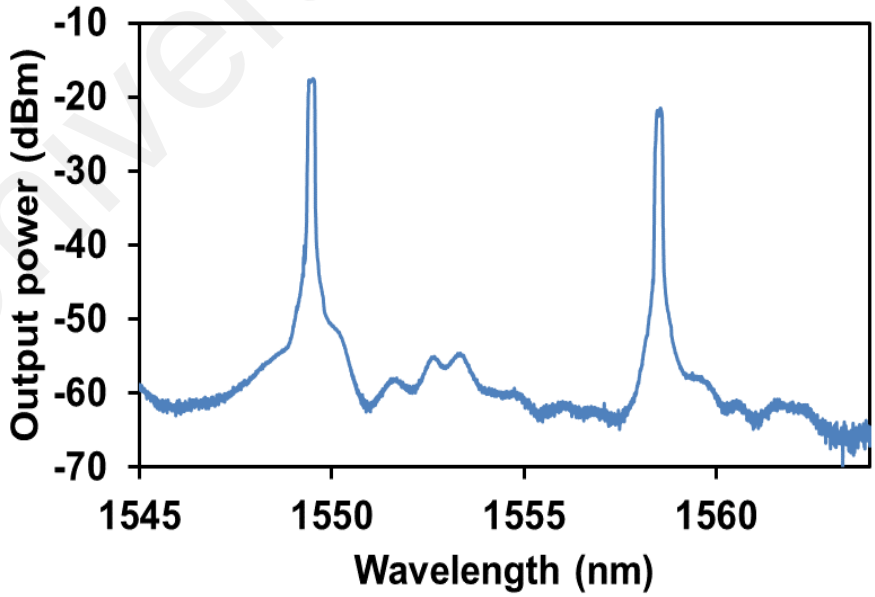

Figure 5.3: Output spectrum of the dual-wavelength Q-switched laser at 225.1 mW pump power.

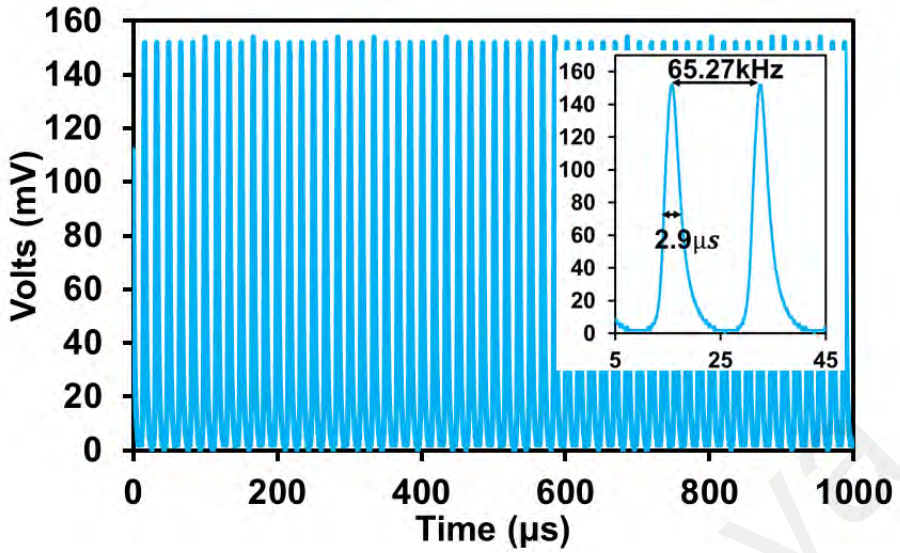

Figure 5.4: Typical pulse train at 225.1 mW pump power. The inset shows the enlarged dual-pulse envelop.

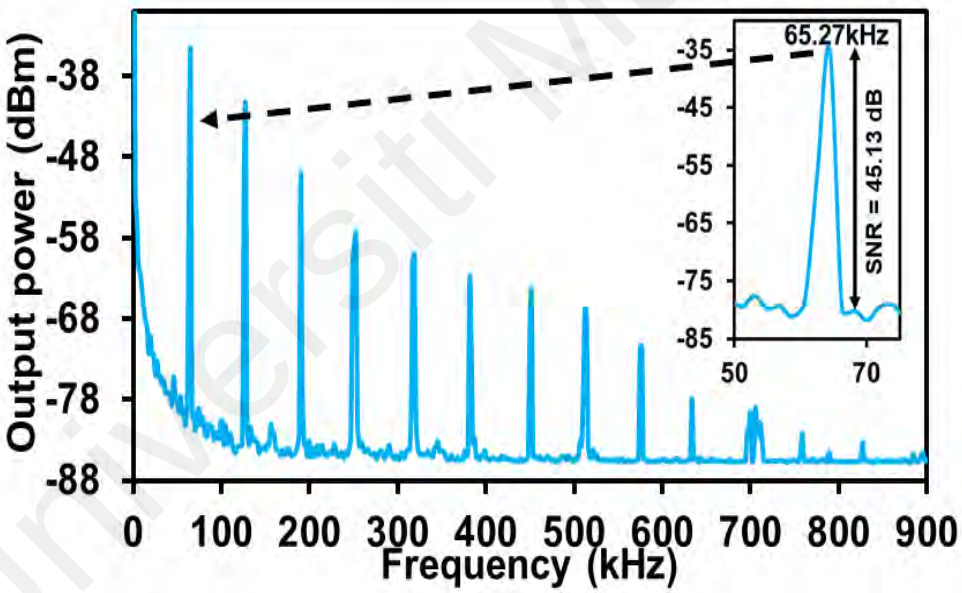

Figure 5.5: RF spectrum at 225.1 mW pump power. The inset shows the fundamental frequency.

Fig. 5. 6 displays the evolution of the repetition rate and pulse width as the pump power is increased from 200.5 to 225.1 mW. When the repetition rate of the Q-switched pulses rises from 59.21 to 65.27 kHz, the pulse duration reduces from 3.3 to 2.9 μs continuously. As the pump power increased, the GO SA is saturated at a higher speed. This is due to the population inversion, which depletes rapidly due to the bleached GO at higher pump

power. Therefore, rising and falling times of the pulses would be reduced, which in turn increases the repetition rate and reduces the pulse width.

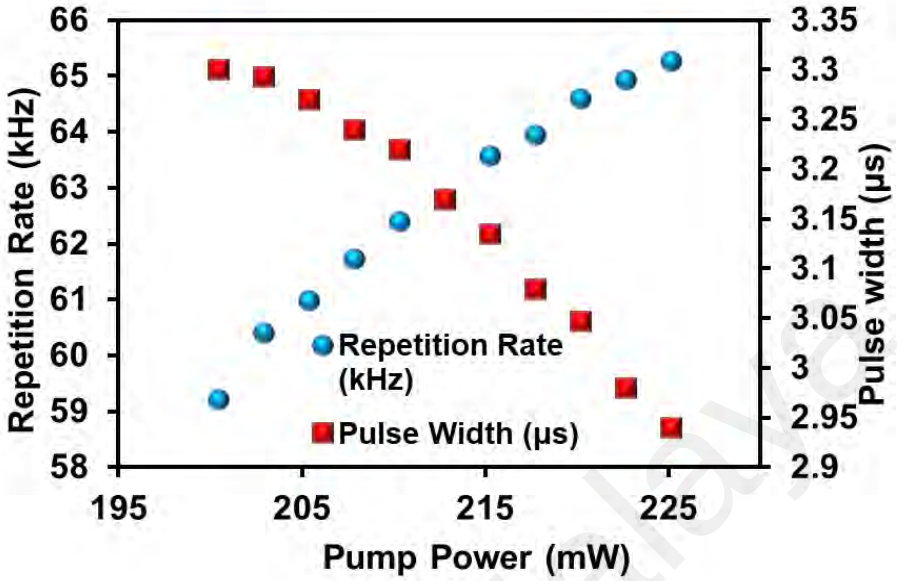

Figure 5.6: Pulse rate and pulse width obtained at different pumping powers.

Fig. 5.7 illustrates the evolution of the average output power and pulse energy with the increase of pump power. The average output power and pulse energy increases from 0.48 to 0.99 mW and from 8.0 to 15.2 nJ, respectively. The slope efficiency of the laser was achieved at 2.06 %, which is relatively low due to the high propagation loss at the SMF-MMF-SMF structure. The population inversion depletes faster due to the bleached GO at the higher pump power. This process reduces the pulse duration, which in turn increases the pulse energy from the Q-switching mechanism. The almost linear output power and pulse energy relations with the pump power prove a stable performance of the fiber laser.

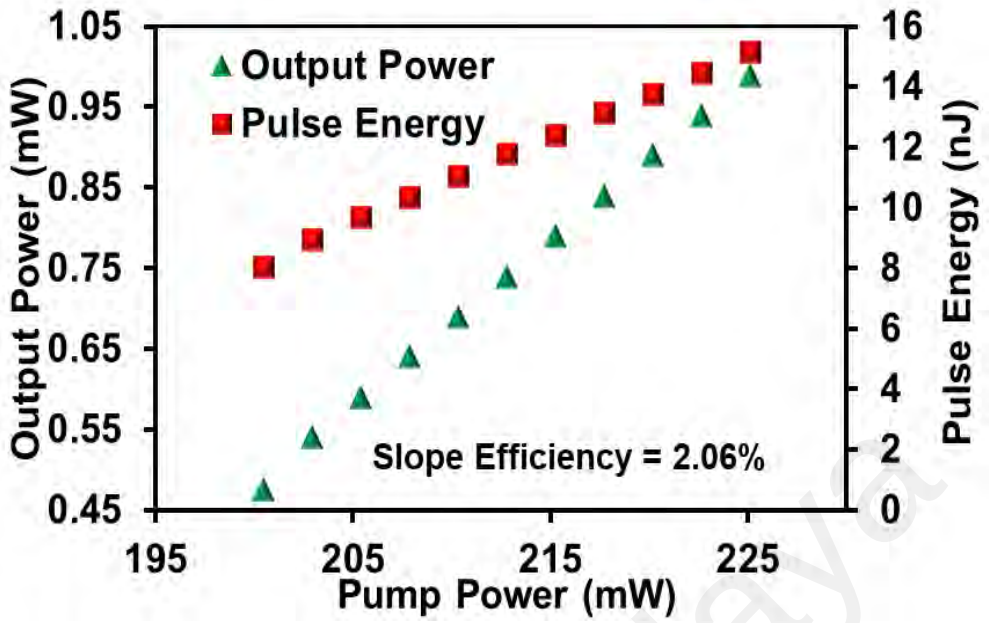

Figure 5.7: Output power and pulse energy obtained at different pumping powers.

5.4 Summary

In summary, a dual-wavelength Q-switched pulse generation was successfully demonstrated in an EDFL cavity using a SMF–MMF–SMF structure based filter and GO SA. The SA was prepared by embedding the GO nanoparticles into PVA. The SA functions to modulate the cavity loss for Q-switching while the MMI filter responsible for dual-wavelength operation. The laser operates at wavelengths of 1549.6 nm and 1558.6 nm. The maximum pulse repetition rate and the shortest pulse width are obtained at 65.27 kHz and 2.9 μs, respectively. At 225.1 mW pump power, the maximum output power and pulse energy were obtained at 0.99 mW and 15.17 nJ, respectively. These results demonstrated that the proposed SMF–MMF–SMF structure has a promising potential to be used as a kind of filter for multi-wavelength laser generation.

CHAPTER 6: CONCLUSION AND FUTURE WORK

6.1 Conclusion

Fiber laser technology has obtained significant interests for many researchers because of their robustness, compact in size and easy to handle compared to the conventional solid-state lasers. They have applications in many areas including telecommunication, micromachining, sensing, medical and military. Most of these applications require the fiber laser to operate in either Q-switching or mode-locking modes. Tunable and multi-wavelength Q-switched fiber lasers have gained tremendous attentions in recent years for their application in various areas including range finding, remote sensing, and medical treatment. The Q-switching can be realized by either active or passive techniques, but passive approach based on saturable absorbers (SAs) are preferable due to their simplicity of design, low cost, compactness, and flexibility.

The SAs act as an optical switch that provides an intensity-dependent transmission without the implementation of expensive and complicated external modulators. Up to date, many materials have been examined and reported as SA such as semiconductor saturable absorber mirror (SESAM), graphene, carbon nanotubes (CNTs), black phosphoros, topological insulators (TIs) and transition metal dichalcogenides (TMDs). These materials, however, have many limitations and thus finding a new material to be used as a high-performance SA has been of great interest in recent years. It is worth mentioning that very little effort has been made to investigate the potential of oxide materials such as graphene oxide (GO) and aluminum oxide (Al_2O_3), which has a simpler fabrication process as a SA. This work was aimed to demonstrate a tunable and dual-wavelength Q-switched fiber laser using a fiber-optic interferometer as a filter and passive SA as a Q-switcher. Two types of fiber-optic interferometer have been explored in this research: sagnac loop mirror (SLM) and single-mode fiber (SMF) – multimode fiber

(MMF) – single-mode fiber (SMF) or SMS structure. The proposed SA and interferometer device were integrated into an Erbium-doped fiber laser (EDFL) cavity for operation in 1.5 region.

Four objectives have been outlined in this research. The first one is to construct and characterize two fiber optic interferometers: SLM and a SMS fiber structure. Both interferometers have been successfully constructed and characterized in Chapter 3. The proposed SLM was fabricated by using a 3dB fiber coupler and a fiber loop with polarization maintaining fiber (PMF). It allows two beams to propagate in counter directions with different polarization states to produce interference, which is sensitive to the change in surrounding temperature. The SMS structure was successfully fabricated using a short section of MMF, which was fusion- spliced between two SMFs. The mechanism underpinning the operation of an SMS fiber structure is multimode interference and associated self-imaging. SMS structure was also demonstrated to function as temperature sensor.

The second objective is to fabricate and characterize two types of SA based on GO and Al_2O_3 thin film for pulse generation. Both GO and Al_2O_3, thin films were successfully fabricated by embedding in PVA thin film to prepare the fiber-compatible SA device as described in Chapter 3. The fabricated SAs were also successfully characterized in terms of FESEM image, Energy Dispersive X-Ray Analysis (EDX), linear and nonlinear absorptions. It was found that GO PVA film exhibits higher modulation depth than the Al_2O_3 film. It has a linear absorption of 0.7 dB, nonlinear absorption of 24.1 %, nonlinear saturable absorption of 35.1 % and saturable intensity of 72 MW/cm^2.

The third objective is to demonstrate tunable Q-switched EDFL based on temperature tuning of SLM in figure-of-eight laser configuration using the newly developed passive SA films. Wavelength tunable Q-switched fiber lasers have been successfully demonstrated using the SLM in figure-of-eight laser cavity as described in Chapter 4.

With a GO PVA thin film-based SA, a stable passively Q-switched EDFL tunable by Sagnac interferometer operation was realized. By tuning the temperature of SLM from 30ºC to 70ºC, the central wavelength of the Q-switched EDFL could be tuned continuously from 1566.3 nm to 1559.3 nm. At 1566.3 nm operation, the repetition rate increased from 30.7 kHz to 41.5 kHz while pulse width reduced from 10.2 to 7.3 μs as the pump power is varied from the threshold of 77.3 mW to 126.5 mW. It was found that the Q-switching threshold pump power increased while the laser efficiency improved with the increase the temperature. A tunable Q-switched EDFL was also obtained by using Al_2O_3-PVA thin film as a Q-switcher in a similar cavity arrangement. By varying the temperature applied to SLM from 30°C to 70°C, it is possible to continuously tune the Q-switched laser operating wavelength from 1568 nm to 1556 nm. Both Q-switched tunable EDFLs are simple and cost effective and thus they may be useful for various practical applications.

The fourth or last objective is to demonstrate a dual-wavelength Q-switched fiber laser operation by using an SMS structure as an interference filter and GO PVA thin film as a SA. A dual-wavelength Q-switched pulse generation has been successfully demonstrated in an EDFL cavity as described in Chapter 5. It used the newly developed GO SA to modulate the cavity loss for Q-switching while the SMS based multimode interferometer filter responsible for dual-wavelength operation. The laser operates at wavelengths of 1549.6 nm and 1558.6 nm. The maximum pulse repetition rate and the shortest pulse width are obtained at 65.27 kHz and 2.9 μs, respectively. At 225.1 mW pump power, the maximum output power and pulse energy were obtained at 0.99 mW and 15.17 nJ, respectively. This finding indicates that the proposed SMS structure has a promising potential to be used as a kind of filter for multi-wavelength laser generation.

This study revealed the promising potential of both GO and Al_2O_3 based SA to be used in pulse generation. The fabrication cost of both SAs is cheap due to the simplicity of the fabrication process, hence reducing the cost of the laser itself. Simple and low-cost fiber lasers are required in many applications including medical diagnostics and environmental sensing. These results verified that all the objectives were fulfilled.

6.2 Recommendation for future work

All four objectives outlined in this study have been successfully implemented. However, the study of both GO and Al_2O_3 based SA can be further explored especially for generating mode-locked pulses. Further work should be devoted to enhancing the performance of the proposed fiber laser in terms of shorting the pulse width, increasing the repetition rate, output power and pulse energy. This can be achieved by addressing a shorter cavity length, higher cavity gain, and improving nonlinear characteristic of the SA films. The loss and nonlinear characteristic of the SA film can be enhanced by optimizing the fabrication technique.

Additionally, a future work should also focus on exploring the developed GO and Al_2O_3 based SA in other wavelength regions such as 1 μm, 2 μm and 3.0 μm using Ytterbium-doped fiber (YDF), Thulium-doped fiber (TDF) and ZBLAN Erbium-doped fiber, respectively, as the active medium. The Q-switched and mode-locked fiber lasers operating in mid-infrared (MIR) region will be a very interesting area to investigate especially for medical applications. Thulium-doped fiber laser (TDFL) and ZBLAN EDFL have gained more interests because of their advantages for application in variety of fields such as military, remote sensing, spectroscopy and medical (Qin et al., 2018). In addition, these lasers operate in eye-safe wavelengths that are suitable for free space applications such as light detection and ranging (LIDAR) and free-space telecommunication system. On the other hand, MIR lasers (operating at wavelength

above 2 μm) are more efficient in absorbing liquid compared to other operating wavelengths of 1.0 um and 1.55 um and thus they are more favorable for use in medical treatment (Traxer et al., 2019).

Table 6.1: Performance Comparison of passively Q-switched fiber lasers with various SAs

Materials	Modulation depth (%)	Saturation intensity (MW/cm^2)	Pulse duration (μs)	Repetition rate (kHz)	SNR (dB)	Pulse energy (nJ)	λ (nm)	wavelength tunability	Reference
FIrpic	12.8	5.5	3.4	39.22 to 87.4	58.36	122.6	1560.4	fixed	S. Salam
MoS_2	-	-	5.02	14.25 to 38.43	37	141.3	1551.4	fixed	M.H.M. Ahmed
WO_3	20	0.04	1.85	29.86 to 56.7	70	142.85	1562.82	fixed	A.S. Al-Hiti
NiO	39	0.025	5.2	19.57 to 52.18	55	31.5	1561.2	fixed	A. Nady
Sb_2Te_3	-	-	0.93	42 to 132	-	152	1559	fixed	J. Bogusławski
BP	-	-	7.04	9.1 to 44.33	50	134	1552.9	fixed	M.H.M. Ahmed
WTe_2	21.4	0.35	1.77	38.39 to 55.56	84.5	18.9	1560.5	fixed	H. Ahmad
Lu_2O_3	10	72	8.47	18.4 to 30.4	40	76	1570	fixed	M.F. Baharom
WSe_2	3.5	-	3.1	4.5 to 49.6	-	33.2	1560	fixed	B. Chen
Ti_2AlC_6	6.3	31.2	4.88	16.14 to 27.45	-	22.58	1560.4	fixed	J. Lee
Si	20.1	5.78	2.32	11.1 to 58.7	-	-	1550	fixed	G. Liu
P_3HT	11	80.45	3.79	62.97 to 78.63	55.23	15	1562	fixed	F.S.M. Samsamnun
Eu_2O_3	20	10	3.6	60.1 to 68.6	57	162	1568	fixed	N.F. Zulkipli
CuO	3.5	3.3	2.6	69 to 83	59.5	66	1560	fixed	S.A. Sadeq
Al_2O_3	-	-	2.8	57.8 to 81	-	56.7	1560	fixed	S.K.M. Al-Hayali
Turmeric	23	0.16	0.725	58.21 to 90.09	80	150.96	1566.69	fixed	A.S. Al-Hiti
Al_2O_3 (SLM)	3.5	0.05	18.5 to 14.2	13.66 to 26.25	38.3	27.4	1568 to 1556	tunable (30 - 70°C)	This work
GO (SLM)	24.1	72	10.2 to 7.3	30.7 to 41.5	40.9	20.5	1566.3 to 1559.3	tunable (30 - 70°C)	This work

Table 6.1 shows the comparison of various saturable absorbers with the saturable absorbers used in this work. The table gives information regarding Modulation depth, Saturation intensity, pulse duration, repetition rate, Signal Noise Ratio (SNR), pulse energy, wavelength (λ) and wavelength tunability with reference to work done by Al-Hiti et al. (2021). The Q-switching performance is comparable to the previous work on fixed wavelength. There is not much work on tunable laser in literatures which shows the novelty of this work.

Suggestion for future and further work, the focus should be given to enhance the performance for both Sagnac Loop Mirror (SLM) and Single mode-Multimode-Single mode (SMS) interference filter.

REFERENCE

Adachi, S. & Koyamada, Y. (2002) *Analysis and design of Q-switched erbium-doped fiber lasers and their application to OTDR.* Journal of lightwave technology, 20(8): p. 1506.

Addanki, S., Amiri, I.S., & Yupapin, P. (2018) Review of optical fibers-introduction and applications in fiber lasers. Results in Physics, 10: p. 743-750.

Ahmad, H., Hissah Saedoon Albaqawi., Norazreina Yusoff., Yi, C, W. (2020) 56 nm wide- band tunable Q-switched erbium doped fiber laser with tungsten ditelluride (WTe 2) saturable absorber, Sci. Rep. 10 (1) 1–10.

Ahmad, H., Soltani, S., & Thambiratnam, K. (2019) *Q-switched erbium-doped fiber laser with molybdenum disulfide (MoS2) nanoparticles on D-shaped fiber as saturable absorber.* Journal of Nonlinear Optical Physics & Materials, 2019. 28(03): p. 1950026.

Ahmad, H., Lee, C., Mohd Afiq Ismail., Zainal Abidin Ali., Siti Aisyah Reduan., Ruslan, N, E., ... Sulaiman Wadi Harun. (2016) *Zinc oxide (ZnO) nanoparticles as saturable absorber in passively Q-switched fiber laser.* Optics Communications, 2016. 381: p. 72-76.

Ahmad, H., Siti Aisyah Reduan., Ruslan, N, E., Lee, C., Zulkifli, M, Z., Kavintheran Thambiratnam. (2019) *Tunable Q-switched erbium-doped fiber laser in the C-band region using nanoparticles (TiO2).* Optics Communications, 2019. 435: p. 283-288.

Ahmed, M, H, M., Ali, N, M., Salleh, Z, S., Rahman, A, A., Sulaiman Wadi Harun., Mazani Manaf., ... Hamzah Arof. (2015) *Q-switched erbium doped fiber laser based on single and multiple walled carbon nanotubes embedded in polyethylene oxide film as saturable absorber.* Optics & Laser Technology, 65: p. 25-28.

Ahmed, M, H, M., Noha Mustafa Ali., Salleh, Z, S., Rahman, A, A., Sulaiman Wadi Harun., Mazani Manaf., .. Hamzah Arof. (2017) Mechanically exfoliated 2D nanomaterials as saturable absorber for Q-switched erbium doped fiber laser, Indian J. Phys. 91 (10) 1259–1264.

Ahmed, M. H. M., Al-Masoodi, A. H. H., Latiff, A. A., Arof, H., Harun, S. W. (2017) Mechanically exfoliated 2D nanomaterials as saturable absorber for Q-switched erbium doped fiber laser, Indian J. Phys. 91 (10) 1259–1264.

Al-Hayali, S, K, M., Mohammed, D, Z., Khaleel, W, A., Al-Janabi, A. (2017) Aluminum oxide nanoparticles as saturable absorber for Cband passively Q-switched fiber laser, Appl. Opt. 56 (16), 4720–4726.

Al-Hiti, A, S., Al-Masoodi, A., Hamzah Arof., Wong, W, R., Sulaiman Wadi Harun. (2020) Tungsten tri-oxide (WO3) film absorber for generating Qswitched pulses in erbium laser, J. Mod. Opt. 67 (4) 374–382.

Al-Hiti, A, S., Al-Masoodi, A, H, H., Wong, W, R., Yasin, M., Al-Masoodi, A, H, H., Harun, S, W. (2021) "Nanosecond passively Q-switched fiber laser in the 1.5 μm region using turmeric saturable absorber", Optics & Laser Technology (vol. 139), 106971, ISSN 0030-3992

Al-Hiti, A. S., Rahman, M. F. A., Harun, S. W., Yupapin, P., & M. Yasin, (2019) Holmium oxide thin film as a saturable absorber for generating Q-switched and mode-locked erbium-doped fiber lasers, Optical Fiber Technology, Volume 52, 101996, ISSN 1068-5200

Apel, O., Mann, K., & Marowsky, G., (2000) Appl. Phys. A 71,593–596.

Aziz, N., Latiff, A., Lokman, M., Hanafi, E., Harun, S, W., (2017) *Zinc oxide-based Q-switched erbium-doped fiber laser.* Chinese Physics Letters, 2017. 34(4): p. 044202.

Babu, P., Seo, H, J., Jang, K, H., Balakrishnaiah, R., Jayasankar, C, K., ... Lavin,V (2007) Optical spectroscopy, 1.5 μm emission, and upconversion properties of Er 3+-doped metaphosphate laser glasses. Journal of the Optical Society of America B, 24(9): p. 2218-2228.

Baharom, M, F., Rahman, M, F, A., Latiff, A, A., Wang, P., Arof, H., Harun, S, W. (2019) Lutetium oxide film as a passive saturable absorber for generating Q-switched fiber laser at 1570 nm wavelength, Opt. Fiber Technol. 50, 82–86.

Bai, X., Mou, C., Xu, L., Wang, S., Pu, S., & Zeng, X. (2016) *Passively Q-switched erbium-doped fiber laser using Fe3O4-nanoparticle saturable absorber.* Applied Physics Express, 2016. 9(4): p. 042701.

Balling, P. & Schou, J. (2013) Femtosecond-laser ablation dynamics of dielectrics: basics and applications for thin films. Reports on Progress in Physics, 76(3): p. 39.

Boetti, N. G., Diego, P., Edoardo, C.G., Joris, L., Davide, J., & Daniel, M., (2017) "Highly Doped Phosphate Glass Fibers for Compact Lasers and Amplifiers: A Review" Applied Sciences 7, no. 12: 1295. https://doi.org/10.3390/app7121295

Bogue, R. (2018) *Sensing with terahertz radiation: A review of recent progress.* Sensor Review, ISSN 0260-2288

Bogusławski, J., Sobon, G., Tarnowski, K., Zybala, R., Mars, K., Mikula, A., .. Sotor, J. (2016) All-polarization-maintaining-fiber laser Q-switched by evanescent field interaction with Sb 2 Te 3 saturable absorber, Opt. Eng. 55 (8) 081316.

Bonaccorso, F. & Sun, Z. P. (2014) Solution processing of graphene, topological insulators and other 2d crystals for ultrafast photonics. Optical Materials Express, 4(1): p. 63-78.

Chen, B; Zhang, X., Guo, C., Wu, K., Chen, J., Wang, J. (2016) Tungsten diselenide Q-switched erbium-doped fiber laser, Opt. Eng. 55 (8) 081306.

Chen, H., Babin, F., Leblanc, M., Schinn, G, W., (2003) *Widely tunable single-frequency erbium-doped fiber lasers.* IEEE Photonics Technology Letters, 15(2): p. 185-187.

Chen, Y., Jiang, G., Chen, S., Guo, Z., Yu, X., Zhao, C., ... Fan, D (2015) Mechanically exfoliated black phosphorus as a new saturable absorber for both Q-switching and Mode-locking laser operation. Optics Express, 23(10): p. 12823-12833.

Chen, Y., Zhao, C., Chen, S., Du, J., Tang, P., ... Tang, D., (2013) *Large energy, wavelength widely tunable, topological insulator Q-switched erbium-doped fiber laser.* IEEE Journal of Selected Topics in Quantum Electronics, 20(5): p. 315-322.

Chiavaioli, F., Gouveia, C. A., Jorge, P. A., & Baldini, F. (2017). Towards a uniform metrological assessment of grating-based optical fiber sensors: From refractometers to biosensors. *Biosensors, 7*(2), 23.

Choi, S.Y., Rotermund, F., Jung, H., Oh, K., & Yeom, D, I., (2009) *Femtosecond mode-locked fiber laser employing a hollow optical fiber filled with carbon nanotube dispersion as saturable absorber.* Optics Express, 2009. 17(24): p. 21788-21793

Chraplyvy, A., & Tkach, R. (1993) What is the actual capacity of single-mode fibers in amplified lightwave systems? J IEEE Photonics Technology Letters, 5(6): p. 666-668.

Chu, Z., Liu, J., Guo, Z., Zhang, H., (2016) *2 μm passively Q-switched laser based on black phosphorus.* Optical Materials Express, 6(7): p. 2374-2379.

Csencsits, R., Lemaire, P, J., Nelson, K, T., & Walker, K, L (1988) Low-loss silica optical waveguides. Google Patents.

Culshaw, B. (2005) The optical fibre Sagnac interferometer: an overview of its principles and applications. Measurement Science and Technology, 17(1): p. R1.

Debus, C., & Bolivar, P,H., (2007) Frequency selective surfaces for high sensitivity terahertz sensing [J] Applied Physics Letters, 91(18): 184102.

Dong, X., Tam, H.Y., & Shum, P. (2007) Temperature-insensitive strain sensor with polarization-maintaining photonic crystal fiber based Sagnac interferometer. Applied physics letters, 90(15): p. 151113.

Dong, Z., Li, H, P., Xia, H, D., Liu, Y., Wang, Z, G., & Chen, Y, F (2012) Passively Q-switched erbium-doped fiber laser using a graphene saturable absorber. in Asia Communications and Photonics Conference. Optical Society of America.

Dubey, A.K. & Yadava, V. (2008) Laser beam machining - A review. International Journal of Machine Tools & Manufacture, 48(6): p. 609-628.

Eberle, T., Steinlechner, S., Bauchrowitz, J., Händchen, V., Vahlbruch, H., ... Schnabel, R (2010) Quantum enhancement of the zero-area sagnac interferometer topology for gravitational wave detection. Physical review letters, 104(25): p. 251102.

Einstein, A., (1917) *The Quantum Theory of Radiation*.

Ferrari, A. C., & Basko, D. M. (2013). Raman spectroscopy as a versatile tool for studying the properties of graphene. Nature Nanotechnology, 8(4), 235–246.

Franco, P., Midrio, M., Tozzato, A., Romagnoli, M., & Fontana, F. (1994). Characterization and optimization criteria for filterless erbium-doped fiber lasers. Journal of the Optical Society of America B, 11(6), 1090.

Fu, H. Y., Tam, H. Y., Shao, L.-Y., Dong, X., Wai, P. K. A., Lu, C., & Khijwania, S. K. (2008). Pressure sensor realized with polarization-maintaining photonic crystal fiber-based Sagnac interferometer. Applied Optics, 47(15), 2835.

Fu, H. Y., Tam, H. Y., Shao, L.-Y., Dong, X., Wai, P. K. A., Lu, C., & Khijwania, S. K. (2008). Pressure sensor realized with polarization-maintaining photonic crystal fiber-based Sagnac interferometer. Applied Optics, 47(15), 2835.

Gao, W., Huang, R., (2014) Thermomechanics of monolayer graphene: Rippling, thermal expansion and elasticity, Journal of the Mechanics and Physics of Solids, Volume 66, Pages 42-58, ISSN 0022-5096,

Goel, A. (2008) *Clinical applications of Q-switched NdYAG laser.* Indian Journal of Dermatology, Venereology, and Leprology, 74(6): p. 682.

Goldberg, D.J. (1993) *Benign pigmented lesions of the skin: treatment with the Q-switched ruby laser.* The Journal of dermatologic surgery and oncology, 19(4): p. 376-379.

Graf, S., Staupendahl, G., Krämer, A., & Müller, F, A (2015) High precision materials processing using a novel Q-switched CO2 laser. Optics and Lasers in Engineering, 66: p. 152-157.

Guesmi, K., Meng, Y., Niang, A., Mouchel, P., Salhi, M., Bahloul, F., Attia, R., & Sanchez, F., (2014) "1.6 μm emission based on linear loss control in a Er:Yb doped double-clad fiber laser," Opt. Lett., vol. 39(22), 6383–6386.

Guo, S., Zhang, A. and Pan, H. (2021) Passively Q-switched fiber laser with single and double wavelength switching based on parallel FBGs [J] Optik, 241: 166973.

Han, Y.G., Tran, T.V.A. & Lee, S.B., (2006) Wavelength-spacing tunable multiwavelength erbium-doped fiber laser based on four-wave mixing of dispersion-shifted fiber [J] Optics letters, 31(6): 697-699.

Haris, H., et al. (2017) *Passively Q-switched Erbium-doped and Ytterbium-doped fibre lasers with topological insulator bismuth selenide (Bi2Se3) as saturable absorber.* Optics & Laser Technology, 88: p. 121-127.

Hart, L. D., (1990) Alumina Chemicals Science and Technology Handbook.

Hasan, T., Sun, Z., Wang, F., Bonaccorso, F., Tan, P, H., Rozhinn, A, G., & Ferrari, A, C (2009) Nanotube–polymer composites for ultrafast photonics. Advanced Materials, 21(38-39): p. 3874-3899.

Hatta, A. M., Semenova, Y., & Farrell, G. (2013). Performance evaluation of an all-fiber ratiometric wavelength monitor system using edge filters based on sms fiber structures. Microwave and Optical Technology Letters, 55(7), 1645–1649.

He, W., Zhu, L., Dong, M., & Luo, F., (2016) "Tunable and switchable thulium-doped fiber laser utilizing Sagnac loops incorporating two-stage polarization maintaining fibers," Optical Fiber Technology, 29, 65-69.

Hecht, J. (2019) *The Remarkable Fiber Optic Vision Of Charles Kao.* Optics and Photonics News, 30(3): p. 26-33.

Hussain, S.A. (2019) Discovery of Several New Families of Saturable Absorbers for Ultrashort Pulsed Laser Systems. Scientific Reports, 9(1): p. 19910.

Ismail, E, I., Kadir, N, A., Latiff, A, A., Ahmad, H., & Harun, S, W., (2016) Black phosphorus crystal as a saturable absorber for both a Q-switched and mode-locked erbium-doped fiber laser (J) RSC advances, 6(76): 72692-72697.

Ismail, M., Ahmad. F., Harun. S., Arof. H., Ahmad. H., (2013) *A Q-switched erbium-doped fiber laser with a graphene saturable absorber.* Laser Physics Letters, 2013. 10(2): p. 025102.

Jafry, A. A. A., Kasim, N., Munajat, Y., Yusoff, R. A. M., Rusdi, M. F. M., Mahyuddin, M. B. H., … Apsari, R. (2019). Passively Q-switched erbium-doped fiber laser utilizing lutetium oxide deposited onto D-shaped fiber as saturable absorber. Optik, 193, 162972.

Jiang, L., Wang, A, D., Li, B., Cui, T, H., & Lu, Y, F (2018) Electrons dynamics control by shaping femtosecond laser pulses in micro/nanofabrication: modeling, method, measurement and application. Light-Science & Applications, 7: p. 27.

Juodkazis, S., Mizeikis, V., & Misawa, H. (2009) Three-dimensional microfabrication of materials by femtosecond lasers for photonics applications. Journal of Applied Physics, 106(5): p. 14.

Kang, H., Lee, B., Kim, H., Shin, D., Kim, J., Palade, V., ... Jain, L. (2003). *A Study on Performance Evaluation of the Liveness Detection for Various Fingerprint Sensor Modules*. 1245-1253

Kang, Z., Liu, M., Li, Z., Li, S., Jia, Z., Liu, C., . . . Qin, G. (2018). Passively Q-switched erbium doped fiber laser using a gold nanostars based saturable absorber. *Photonics Research, 6*(6), 549-553.

Kaushik, S., Pandey, A., Tiwari, U. K., & Sinha, R. K. (2018). A label-free fiber optic biosensor for Salmonella Typhimurium detection. Optical Fiber Technology, 46, 95–103.

Keiser, G. (2006). Optical Communications Essentials. (pp. 19–44).

Keller, U. (2003) Recent developments in compact ultrafast lasers. Nature, 424: p. 831.

Keller, U., Weingarten, K, J., Kartner, F, X., Kopf, D., Braun, B., ... Aus der Au, J (1996) Semiconductor saturable absorber mirrors (SESAM's) for femtosecond to nanosecond pulse generation in solid-state lasers. Ieee Journal of Selected Topics in Quantum Electronics, 2(3): p. 435-453.

Keller, U., Weingarten, K, J., Kartner, F, X., Kopf, D., Braun, B., Jung, I, D., ... Aus der Au, J (1996) "Semiconductor saturable absorber mirrors (SESAM's) for femtosecond to nanosecond pulse generation in solid-state lasers," in IEEE Journal of Selected Topics in Quantum Electronics, vol. 2, no. 3, pp. 435-453,

Kim, C., (2004) "Tunable Multiwavelength fiber lasers Based on novel Fiber-Optic Components," Section 3, UMI Baltimore, Maryland, USA.

Kim, C., (2004) Section 3, UMI Baltimore, Maryland, USA.

Kim, C., (2004) "Tunable Multiwavelength fiber lasers Based on novel Fiber-Optic Components," Section 3, UMI Baltimore, Maryland, USA.

Kudin, K. N., Ozbas, B., Schniepp, H. C., Prud'homme, R. K., Aksay, I. A., & Car, R. (2008). Raman Spectra of Graphite Oxide and Functionalized Graphene Sheets. Nano Letters, 8(1), 36–41.

Lee, B.-H., Eom, J.-B., Park, K.-S., Park, S.-J., & Ju, M.-J. (2010). Specialty Fiber Coupler: Fabrications and Applications. Journal of the Optical Society of Korea, 14(4), 326–332. doi:10.3807/josk.2010.14.4.326

Lee, B. H., Kim, Y. H., Park, K. S., Eom, J. B., Kim, M. J., Rho, B. S., & Choi, H. Y. (2012). Interferometric Fiber Optic Sensors. Sensors, 12(3), 2467–2486.

Lee, J., Kwon, S., Lee, J, H., (2019) Ti 2 AlC-based saturable absorber for passive Q-switching of a fiber laser, Opt. Mater. Express 9 (5) 2057–2066.

Li, S., Yin, Y., Ran, G., Ouyang, Q., Chen, Y., Tokurakawa, M., Lewis, E., Harun, S.W. and Wang, (2019) P. Dual-wavelength mode-locked erbium-doped fiber laser based on tin disulfide thin film as saturable absorber [J] Journal of Applied Physics, 125(24): 243104.

Li, X., Wang, Y., Wang, Y., Zhao, W., Yu, X., Sun, Z., ... Wang, Q, J (2014) Nonlinear absorption of SWNT film and its effects to the operation state of pulsed fiber laser. Optics express, 22(14): p. 17227-17235.

Li, X., Yu, Q., Zhou, X., Zhang, Y., Lv, L., & Zhao, Y., (2023) Magnetic sensing technology of fiber optic interferometer based on magnetic fluid: A review, Measurement, Volume 216, 112929, ISSN 0263-2241,

Lian, Y., Ren, G., Zhu, B., Gao, Y., Jian, W., Ren, W., & Jian, S., (2017) Switchable multiwavelength fiber laser using erbium-doped twin-core fiber and nonlinear polarization rotation [J] Laser Physics Letters, 14(5): 055101.

Lin, G.-R., Chang, J, Y., Liao, Y, S., Lu, H, H., (2006) *L-band erbium-doped fiber laser with coupling-ratio controlled wavelength tunability.* Optics Express, 14(21): p. 9743-9749.

Lin, G.-R., Chang, J.-Y., Liao, Y.-S., & Lu, H.-H. (2006). L-band erbium-doped fiber laser with coupling-ratio controlled wavelength tunability. Optics Express, 14(21), 9743.

Liu, G., Lyu, Y., Li, Z., Wu, T., Yuan, J., Yue, X., .. Fu, S. (2020) Q-switched erbium-doped fiber laser based on silicon nanosheets as saturable absorber, Optik 202, 163692.

Liu, W., Liu, M., Yang, Y, O., Hou, H., Lei, M., & Wei, Z (2018) CVD-grown MoSe2 with high modulation depth for ultrafast mode-locked erbium-doped fiber laser. Nanotechnology, 29(39): p. 394002.

Liu, Y., Liu. J., & Chen. W., (2011) *Fiber laser sensing system and its applications.* Photonic Sensors, 1(1): p. 43-53.

Liu, Y., Liu, J., & Chen, W. (2011) *Eye-safe, single-frequency pulsed all-fiber laser for Doppler wind lidar.* Chinese Optics Letters, 9(9): p. 090604.

Liu, Y., Liu, B., Feng, X., Zhang, W., Zhou, G., ... Dong, X (2005) High-birefringence fiber loop mirrors and their applications as sensors. Applied optics, 2005. 44(12): p. 2382-2390.

Lou J, Wang Y, Tong L., (2014) Microfiber Optical Sensors: A Review. Sensors. 14(4):5823-5844. https://doi.org/10.3390/s140405823

Luo, Z., Huang, Y., Zhong, M., Li, Y., Wu, J., Xu, B., ... Weng, J. (2014) 1-, 1.5-, and 2-μm fiber lasers Q-switched by a broadband few-layer MoS_2 saturable absorber [J]. Journal of Lightwave Technology, 32(24):4077-

Luo, Z., Zhou, M., Weng, J., Huang, G., Xu, H., Ye, C., & Cai Z., (2010) Graphene-based passively Q-switched dual-wavelength erbium-doped fiber laser [J]. Optics letters, 35(21):3709-3711

Maiman, T.H. (1960) *Stimulated Optical Radiation in Ruby.* Nature, 187: p. 493.

Majkić, A., Zgonik, M., Petelin, A., Jazbinšek, M., Ruiz, B., Medrano, C., & Günter, P (2014) *Terahertz source at 9.4 THz based on a dual-wavelength infrared laser and quasi-phase matching in organic crystals OH1.* Applied Physics Letters, 105(14): p. 141115.

Majkić, A., Zgonik, M., Petelin, A., Jazbinšek, M., Ruiz, B., Medrano, C. & Günter, P., (2014) Terahertz source at 9.4 THz based on a dual-wavelength infrared laser and quasi-phase matching in organic crystals OH1 [J] Applied Physics Letters, 105(14): 141115.

Mao, D., Zhang, S., Wang, Y., Gan, X., Zhang, W., Mei, T., ...Zhao, J (2015) WS 2 saturable absorber for dissipative soliton mode locking at 1.06 and 1.55 μm. Optics express, 23(21): p. 27509-27519.

McGrath, A. J., Munch, J., Smith, G., & Veitch, P., (1998), pp.5706-5709
Gräf, S., Staupendahl, G., Krämer, A, & Müller, F,A., (2015) "High precision materials processing using a novel Q-switched CO2 laser," Optics and Lasers in Engineering, 66, 152-157.

Milani, A., et al. (2019) Handbook of Graphene, Volume 3: Graphene-Like 2D Materials.

Mittleman, D.M. (2017) *Perspective: Terahertz science and technology.* Journal of Applied Physics, 122(23): p. 230901.

Mizuno, T. et al, (2017) *Development of the laser altimeter (LIDAR) for Hayabusa2.* Space Science Reviews, 208(1): p. 33-47.

Mohd Arif Mohd Sarjidan., F.S.M.Samsamnun., Nur Farhanah Zulkipli., Abd Majid W.H., Muhammad Abdul Khudus., Ahmad Shuhaimi., & Afiq Arif Aminuddin Jafry. (2020) Poly (3-hexylthiophene-2, 5-diyl) regioregular (P3HT) thin film as saturable absorber for passively Q-switched and mode-locked erbiumdoped fiber laser, Opt. Fiber Technol. 54, 102073.

Moon, D.S., Kim, B, H., Sun, G., Han, Y, G., Han, W, T., & Chung, Y (2007) The temperature sensitivity of Sagnac loop interferometer based on polarization maintaining side-hole fiber. Optics Express, 15(13): p.7962-7967

Muanenda, Y., Oton, C. J., & Di Pasquale, F. (2019). Application of Raman and Brillouin Scattering Phenomena in Distributed Optical Fiber Sensing. Frontiers in Physics, 7. doi:10.3389/fphy.2019.00155

Nady, A., Ahmed, M, H, M., Anas Abdul Latif., Numan, A., Ooi, R., Sulaiman Wadi Harun. (2017) Nickel oxide nanoparticles as a saturable absorber for an all-fiber passively Q-switched erbium-doped fiber laser, Laser Phys. 27 (6) 065105.

Ngo, N.Q & Binh, L, N (2018) Ultra-fast fiber lasers: principles and applications with MATLAB® models. CRC Press.

Nikodem, M.P., et al. (2008) *Actively mode-locked fiber laser using acousto-optic modulator*. in *16th Polish-Slovak-Czech Optical Conference on Wave and Quantum Aspects of Contemporary Optics*. International Society for Optics and Photonics. **QC**

Niu, K., Sun, R., Chen, Q., Man, B., & Zhang, H (2018) Passively mode-locked Er-doped fiber laser based on SnS 2 nanosheets as a saturable absorber. Photonics Research, 6(2): p. 72-76.

Nizamani, B., Jafry, A, A, A., Khudus, M, I, M, A., Memon, F, A., Shuhaimi, A., Kasim, N., ... Harun, S, W (2020) Indium tin oxide coated D-shape fiber as a saturable absorber for generating a dark pulse mode-locked laser. Chinese Physics Letters, 37(5): p. 054202.

Niziev, V., Chang, R., & Nesterov, A. (2006) Generation of inhomogeneously polarized laser beams by use of a Sagnac interferometer. Applied Optics, 2006. 45(33): p. 8393-8399.

Nur Farhanah Zulkipli., Afiq Arif Aminuddin Jafry., Retna Apsari., Samsamnun, F, S, M., Batumalay, M., Muhammad Abdul Khudus., .. Sulaiman Wadi Harun. (2020) Generation of Q-switched and mode-locked pulses with Eu2O3 saturable absorber, Opt. Laser Technol. 127, 106163.

Okhotnikov, O., Grudinin, A. & Pessa, M. (2004) *Ultra-fast fibre laser systems based on SESAM technology: new horizons and applications.* New journal of physics, 6(1): p. 177.

Pan, S., Lou, C. and Gao, Y., (2006) Multiwavelength erbium-doped fiber laser based on inhomogeneous loss mechanism by use of a highly nonlinear fiber and a Fabry- Perot filter [J] Optics Express, 14(3): 1113-1118.

Paschotta, R. (2008) Field guide to laser pulse generation. Vol. 14. 2008: SPIE press Bellingham.

Popa, D., Sun, Z., Hasan, T., Torrisi, F., Wang, F., & Ferrari, A. C., (2011). Graphene Q-switched, tunable fiber laser. Applied Physics Letters, 98(7), 073106.

Qi, Y., Kang, Z., Sun, J., Ma, L., Jin, W., Lian, Y., & Jian, S., (2016) Wavelength-switchable fiber laser based on few-mode fiber filter with core-offset structure, Optics & Laser Technology, Volume 81, P 26-32, ISSN 0030-3992,

Qin, Z., Hai, T., Xie, G., Ma, J., Yuan, P., Qian, L., Li, L., Zhao, L., & Shen, D., (2018) "Black phosphorus Q-switched and mode-locked mid-infrared Er:ZBLAN fiber laser at 3.5 μm wavelength," Opt. Express 26, 8224-8231

Rao, Y, J., (2006) Recent progress in fiber-optic extrinsic Fabry–Perot interferometric sensors, Optical Fiber Technology, Volume 12, Issue 3, P 227-237, ISSN 1068-5200,

Reyes-Vera, E., Cordeiro, C.M., & Torres, P. (2017) *Highly sensitive temperature sensor using a Sagnac loop interferometer based on a side-hole photonic crystal fiber filled with metal.* Applied optics, 56(2): p. 156-162.

Riehle, F., Kisters, Th., Witte, A., Helmcke, J., & Bord\'e, C, J., (1991) "Optical Ramsey spectroscopy in a rotating frame: Sagnac effect in a matter-wave interferometer". Phys. Rev. Lett. Vol. 67(2). p177-180

Rizman, Z, I., Zulkipli, N, F., Arof, H., Yasin, M., Harun, S, W., (2020). Q-switched and tunable wavelength fiber laser utilizing nickel oxide saturable absorber and sagnac loop mirror filter. Infrared Physics & Technology, 109, 103433

Rusdi, M, F, M., Mahyuddin, M, B, H., Latiff, A, A., Ahmad, H., & Harun, S, W., (2018) Q-switched erbium-doped fiber laser using cadmium selenide coated onto side-polished d-shape fiber as saturable absorber [J]. Chinese Physics Letters, *35*(10): 104201.

Sadeq, S, A., Al-Hayali, S, K., Sulaiman Wadi Harun., Al-Janabi, A. (2018) Copper oxide nanomaterial saturable absorber as a new passive Q-switcher in erbium-doped fiber laser ring cavity configuration, Results Phys. 10, 264–269.

Sakimoto, T., Rosenblatt, M.I., & Azar, D.T. (2006) *Laser eye surgery for refractive errors.* The Lancet, 367(9520): p. 1432-1447.

Salam, S., Al-Masoodi, A,H,H., Al-Hiti, A, S., Al-Masoodi, Ab, H, H., Wang, P., Wong, W, R., & Harun, S, W. (2019) FIrpic thin film as saturable absorber for passively Q-switched and mode-locked erbium-doped fiber laser, Opt. Fiber Technol. 50 256–262.

Salam, S., Wong, W, R., Al-Masoodi, A, H, H., & Harun, S, W (2019) High-energy Q-switched ytterbium-doped all-fiber laser with tris-(8-hydroxyquinoline) aluminum as saturable absorber. Optical Materials Express, 9(8): p. 3215-3225.

Salman, Ali A., Al-Janabi., A Hadi. (2019). Multiwavelength Q -switched erbium-doped fibre laser-based aluminum nanoparticles saturable absorber and sagnac loop filter. Laser Physics, 29(6), 065103–.

Shah, S. & Alster, T.S. (2010) Laser Treatment of Dark Skin An Updated Review. American Journal of Clinical Dermatology, 11(6): p. 389-397.

Shao, L.-Y., Luo, Y., Zhang, Z., Zou, X., Luo, B., Pan, W., & Yan, L. (2015). Sensitivity-enhanced temperature sensor with cascaded fiber optic Sagnac interferometers based on Vernier-effect. Optics Communications, 336, 73–76.

Shao, L.-Y., Zhang, X,P., He, H., Zhang, Z., Zou, X., ... Yan, L (2016) Optical fiber temperature and torsion sensor based on Lyot-Sagnac interferometer. Sensors, 16(10): p. 1774.

Shi, W. et al., (2014) *Fiber lasers and their applications.* Applied optics, 53(28): p. 6554-6568.

Shi, W., Fang, Q., Zhu, X., Norwood, R. A., & Peyghambarian, N. (2014). Fiber lasers and their applications [invited]. Applied optics, 53(28), 6554-6568.

Shiner, B. (2016) *Fiber lasers continue to gain market share in material processing applications.* Manuf. Eng., 156: p. 79-85.

Snitzer, E. (1966) Glass lasers. Proceedings of the IEEE, 54(10): p. 1249-1261.

Soares, M.S., Vidal, M., Santos, N.F., Costa, F.M., Marques, C., Pereira, S.O., & Leitao, C., (2021) Immunosensing Based on Optical Fiber Technology: Recent Advnaces. Biosensors (Basel). Aug;11(9):305. doi: 10.3390/bios11090305. PMID: 34562895; PMCID: PMC8472567.

Soboh, R, S., Al-Masoodi, A. H., Erman, F, N., Al-Masoodi, A, H., Nizamani, B., Arof H, Yasin, M., & Harun, S, W., (2021) Lawsone dye material as potential saturable absorber for Q-switched erbium doped fiber laser [J]. Optical Fiber Technology, 64: 102537.

Sobon, G., Sotor, J., Jagiello, J., Kozinski, R., Librant, K., ... Abramski, K, M (2012) Linearly polarized, Q-switched Er-doped fiber laser based on reduced graphene oxide saturable absorber. Applied Physics Letters, 101(24): p. 4.

Soldano, L.B., & Pennings, E.C. (1995) Optical multi-mode interference devices based on self-imaging: principles and applications. Journal of lightwave technology, 13(4): p. 615-627.

Soltanian, M., Ahmad, H., Khodaie, A., Amiri, I, S., Ismail, M, F., & Harun, S, W (2015) A stable dual-wavelength Thulium-doped fiber laser at 1.9 μm using photonic crystal fiber. Scientific reports, 5(1): p. 1-8.

Sotor, J., Sobon, G., Kowalczyk, M., Macherzynski, W., Paletko, P., & Abramski, K, M (2015) Ultrafast thulium-doped fiber laser mode locked with black phosphorus. Optics letters, 40(16): p. 3885-3888.

Spühler, G.J., Pashotta, R., Fluck, R., Braun, B., Moser, M., ... Keller, U (1999) Experimentally confirmed design guidelines for passively Q-switched microchip lasers using semiconductor saturable absorbers. Journal of the Optical Society of America B, 16(3): p. 376-388.

Sugioka, K., & Cheng, Y. (2014) *Ultrafast lasers—reliable tools for advanced materials processing.* Light: Science & Applications, 3(4): p. e149-e149.

Sun, G., Moon, D. S., Lin, A., Han, W., & Chung, Y., (2008) Optics Express, 16, 3652.

Sun, G., Moon, D.S., Lin, A., Han, W., & Chung, Y., (2008) "Tunable Multiwavelength Fiber Laser Using a Comb Filter Based on ErbiumYtterbium Co-doped Polarization Maintaining Fiber Loop Mirror," Optics Express, 16(6), 3652-3658.

Takahashi, M., Ueda, W., Goto, N., & Yanagiya, S., (2013). "Saturable Absorption by Vertically Inserted or Overlaid Monolayer Graphene in Optical Waveguide for All- Optical Switching Circuit," IEEE Photonics Journal, vol. 5, no. 5, pp. 6602109-6602109

Tian, K., Xin, Y., Yang, W., Geng, T., Ren, J., Fan, Y, X., ... Wang, P (2017) *A curvature sensor based on twisted single-mode–multimode–single-mode hybrid optical fiber structure.* Journal of Lightwave Technology, 35(9): p. 1725-1731.

Travagnin, M. (2001) Effects of Pauli blocking on semiconductor laser intensity and phase noise spectra. Physical Review A, 64(1): p. 013818.

Traxer, Olivier & Keller, E. (2019) Thulium fiber laser: the new player for kidney stone treatment? A comparison with Holmium: YAG laser. World Journal of Urology. 38. 10.1007/s00345-019-2654-5

Tünnermann, A., Schreiber, T., & Limpert, J. (2010) Fiber lasers and amplifiers: an ultrafast performance evolution. Applied optics, 49(25): p. F71-F78.

Vallet, M., Barreaux, J., Romanelli, M., Pillet, G., Thévenin, J., Wang, L., & Brunel, M. (2013). Lidar–radar velocimetry using a pulse-to-pulse coherent rf-modulated Q-switched laser. Applied Optics, 52(22), 5402.

Wang, J., Cai, Z., Xu, P., Du, G., Wang, F., Ruan, S., ... Hasan, T (2015) Pulse dynamics in carbon nanotube mode-locked fiber lasers near zero cavity dispersion. Optics express, 23(8): p. 9947-9958.

Wang, L., Li, X., Wang, C., Luo, W., Feng, T., ... Zhang, H (2019) Few-Layer Mxene Ti3C2Tx (T=F, O, Or OH) for Robust Pulse Generation in a Compact Er-Doped Fiber Laser. ChemNanoMat, 5(9): p. 1233-1238.

Wang, P., Zhu, C., (2022) Passively Q-Switched and Mode-Locked Fiber Laser Based on a Zeolitic Imidazolate Framework-67 Saturable Absorber. Frontiers in Physics Vol. 10, ISSN 2296-424X

Wang, Q., Farrell, G., & Yan, W. (2008) Investigation on single-mode–multimode–single-mode fiber structure. Journal of Lightwave Technology, 26(5): p. 512-519.

Wang, Q., Farrell, G., & Yan, W. (2008) "Investigation on Single-Mode–Multimode–Single-Mode Fiber Structure," J. Lightwave Technol. 26, 512-519.

Wang, X., Zhao, N., Liu, H., Tang, R., Zhu, Y., Xue, J., ... Xu, W (2015) *Experimental investigation on Q-switching and Q-switched mode-locking operation in gold nanorods-based erbium-doped fiber laser.* Chinese Optics Letters, 13(8): p. 081401.

Wang, X., Zhao, N., Liu, H., Tang, R., Zhu, Y., Xue, J., ... Xu, W., (2015) "Experimental investigation on Q-switching and Q-switched mode-locking operation in gold nanorods-based erbium doped fiber laser," Chin. Opt. Lett., 13(8), 081401.

Wang, Y., Li, J., Zhai, B., Hu, Y., Mo, K., Lu, R. & Liu, Y. (2016) Tunable and switchable dual-wavelength mode-locked Tm 3+-doped fiber laser based on a fiber taper [J] Optics express, 24(14): 15299-15306.

Wu, Q., Semenova, Y., Wang, P., & Farrell, G (2011) High sensitivity SMS fiber structure based refractometer–analysis and experiment. Optics express, 19(9): p. 7937-7944.

Wu, Q., Qu, Y., Liu, J., Yuan, J., Wan, S, P., ... Farrell, G (2020) Singlemode-multimode-singlemode fiber structures for sensing applications—A review. IEEE Sensors Journal, 21(11): p. 12734-12751.

Xu, B., Tang, W., Sun, W., Wang, J., Jiang, K., .. Xia, W., (2022) Watt-level high-stability all-solid-state passively Q-switched laser based on germanene nanosheets. Frontiers in Physics Vol. 10. ISSN 2296-424X

Xu, J, L., Li, X, L., He, J, L., Hao, X, P., Wu, Y, Z., Yang, Y., & Yang, K, J., (2011) Performance of large-area few-layer graphene saturable absorber in femtosecond bulk laser. Applied Physics Letters, 99(26), 261107–.

Xu, X., Zhai, J., Li, L., Chen, Y., Yu, Y., Zhang, M., Ruan, S., & Tang, Z., (2014) Passively mode-locking erbium-doped fiber lasers with 0.3 nm Single-Walled Carbon Nanotubes [J] Scientific reports, 4(1): 6761.

Yamashita, S., & Hotate, K., (1996) Multiwavelength erbium-doped fibre laser using intracavity etalon and cooled by liquid nitrogen [J] Electronics Letters, 32 (14): 1298-1299.

Yang, Y., Yang, S., Li, C., & Lin, X (2019) Passively Q-switched and mode-locked Tm-Ho co-doped fiber laser using a WS2 saturable absorber fabricated by chemical vapor deposition. Optics & Laser Technology, 111: p. 571-574.

Yue, W., Wang, Y, X., Xiong, C, D., Wang, Y, W., & Qiu, Q (2013) Intensity noise of erbium-doped fiber laser based on full quantum theory. Journal of the Optical Society of America B, 30(2): p. 275-281.

Zajac, A., Skorczakowski, M., Swiderski, J., & Nyga, P. (2004). Electrooptically Q-switched mid-infrared Er:YAG laser for medical applications. Optics Express, 12(21), 5125.

Zhang, J.J., Zhang, X.S., Li, L., Wu, S.H., Yin, H., Liu, X. & Gong, X.K., (2020) Enhanced mid-infrared emission of non-oxide erbium doped fluorochloride glass [J] Optoelectronics Letters, 16(5): 360-364.

Zhang, L., Ren, G.J. & Yao, J.Q., (2013) A new photonic crystal fiber gas sensor based on evanescent wave in terahertz wave band: design and simulation [J] Optoelectronics Letters, 9(6): 438-440.

Zhang, P., et al., (2021) *Bismuth-doped fiber Q-switcher in erbium-doped fiber laser cavity.* Microwave and Optical Technology Letters, 2021. 63(8): p. 2214-2218.

Zhou, C., Zou, H., Li, M., Sun, C., Ren D., & Li Y., (2018) Fiber optic surface plasmon resonance sensor for detection of E. coli O157:H7 based on antimicrobial peptides and AgNPs-rGO. Biosens Bioelectron ;117:347-353. doi: 10.1016/j.bios.2018.06.005. Epub 2018 Jun 5. PMID: 29935488.

Zhou, Y., Zhang, R., Chen, P., Liu, Y., Fang, Y., Wang, T., ... Liao, M., (2019) Passively Q-switched and mode-locked ytterbium fiber laser with Bi_2S_3 nanowire [J]. Laser Physics, 29(5):055101

Zhu, Y., Zheng, J., Deng, H., Yuan, L., Deng, S. & Teng, C., (2021) Refractive index and temperature measurement by cascading macrobending fiber and a sealed alternated SMF-MMF structure [J] Optics Communications, 485: 126738.

Zou, C., Huang, Q., Wang, T., Yan, Z., AlAraimi, M., Rozhin, A. & Mou, C., (2018) Single/dual-wavelength switchable bidirectional Q-switched all-fiber laser using a bidirectional fiber polarizer [J] Optics Letters, 43(19): 4819-4822.

Zuikafly, S, N, F., Ahmad, H., Ismail, M, F., Abdul Rahman, M, A, Yahya, W, J., Abu Husain, N., ... Ahmad, F., (2023) Dual Regime Mode-Locked and Q-Switched Erbium-Doped Fiber Laser by Employing Graphene Filament–Chitin Film-Based Passive Saturable Absorber. Micromachines 2023, 14, 1048.

Zulkipli, N.F., et al., (2020) *Q-switching pulses generation with samarium oxide film saturable absorber.* Microwave and Optical Technology Letters, 2020. 62(3): p. 1049-1055.

Zu, P., Chan, C, C., Koh, G, W., Lew, W, S., Jin, Y., ... Dong, X (2014) Enhancement of the sensitivity of magneto-optical fiber sensor by magnifying the birefringence of magnetic fluid film with Loyt-Sagnac interferometer. Sensors and Actuators B: Chemical, 191: p. 19-23.